



Oxidation of phenanthrene in soil washing effluent by photogenerated hydroxyl and sulfate radicals

Yufang Tao

► To cite this version:

Yufang Tao. Oxidation of phenanthrene in soil washing effluent by photogenerated hydroxyl and sulfate radicals. Theoretical and/or physical chemistry. Université Clermont Auvergne [2017-2020], 2020. English. NNT : 2020CLFAC080 . tel-03411371

HAL Id: tel-03411371

<https://theses.hal.science/tel-03411371>

Submitted on 2 Nov 2021

HAL is a multi-disciplinary open access archive for the deposit and dissemination of scientific research documents, whether they are published or not. The documents may come from teaching and research institutions in France or abroad, or from public or private research centers.

L'archive ouverte pluridisciplinaire **HAL**, est destinée au dépôt et à la diffusion de documents scientifiques de niveau recherche, publiés ou non, émanant des établissements d'enseignement et de recherche français ou étrangers, des laboratoires publics ou privés.

ED SF n° d'ordre :

UNIVERSITE CLERMONT AUVERGNE
ECOLE DOCTORALE DES SCIENCES FONDAMENTALES

THESE

présentée pour obtenir le grade de

DOCTEUR D'UNIVERSITE

Spécialité : Chimie théorique, physique, analytique

Par **Yufang TAO**

**OXIDATION OF PHENANTHRENE IN SOIL WASHING EFFLUENT BY
PHOTOGENERATED HYDROXYL AND SULFATE RADICALS**

Soutenance le « 25/11/2020 », devant la commission d'examen

suivante :

Présidente:

Vanessa PREVOT, DR CNRS, Université Clermont Auvergne, France

Rapporteuses :

Zhihui AI, Pr., Central China Normal University, Wuhan, Chine

Alessandra BIANCO-PREVOT, Pr., Université de Turin, Italie

Examineurs:

Hui ZHANG, Pr., Université de Wuhan, Chine

Marcello BRIGANTE, Pr., Université Clermont Auvergne, France

Directeur :

Gilles MAILHOT, DR CNRS, Université Clermont Auvergne, France

Acknowledgement

I would like to thank gratefully to my supervisors Prof. Gilles. MAILHOT, Prof. Marcello BRIGANTE and Prof. Hui ZHANG for giving me the chance to conduct the thesis work. It is my great pleasure to work with all of them and I learned a lot of thing from them.

I'm sincerely grateful to Prof. Feng Wu for his precious advice and kind help for me to work in the team of photochemistry of Université Clermont Auvergne.

I would also like to thank Engineer Guillaume VOYARD for giving me technical supports for the experiments of this thesis.

I wish to express my gratitude to Prof. Vanessa PREVOT (DR CNRS, Université Clermont Auvergne, France), Zhihui AI (Central China Normal University, China), Alessandra BIANCO-PREVOT (Université de Turin, Italy) for their acceptance to be part of thesis jury.

I also wish to thank all my colleagues in Advanced Oxidation Lab of Wuhan University and Institut de Chimie de Clermont-Ferrand of Université Clermont Auvergne for their kindness help.

Thank for the fund support of China Scholarship Council (CSC) affiliated with the Ministry of Education of P.R. China.

Finally, I would especially like to thank my parents and my husband for always been there with encouragement.

Table of contents

List of Abbreviations.....	I
List of Figures.....	II
List of Tables.....	V
Abstract.....	VI
Chapter 1 Introduction.....	1
1.1 Background.....	2
1.2 Research goals and objective	5
1.3 Structure of the thesis.....	5
Chapter 2 Literature review	17
2.1 Polycyclic aromatic hydrocarbons (PAHs)	18
2.1.1 PAHs pollution in soil	18
2.1.2 Sources and hazards of PAHs	19
2.1.3 Properties of PAHs – case of phenanthrene (PHE).....	20
2.2 Surfactant aided soil washing (SW) processes	21
2.3 Advanced oxidation processes (AOPs) for SW effluent treatment.....	23
2.3.1 Hydroxyl radical (HO [•]) based AOPs	23
2.3.2 Sulfate radical (SO ₄ ^{•-}) based AOPs	27
Chapter 3 Phenanthrene decomposition in soil washing effluents using UVB/H₂O₂ and UVB/PS.....	47
3.1 Introduction.....	48
3.2 Materials and methods	49
3.2.1 Chemicals.....	49
3.2.2 Preparation of the mimic and real SW solutions.....	49
3.2.3 Irradiation experiments	50

3.2.4 Analytic methods	51
3.3 Results and discussion	53
3.3.1 Comparison of UVB activation of H ₂ O ₂ and PS.....	53
3.3.2 Effect of oxidant concentration.....	56
3.3.3 Effect of initial pH	58
3.3.4 Effect of inorganic anions- chloride.....	59
3.3.5 Effect of inorganic anions- bicarbonate	63
3.3.6 Effect of inorganic anions- nitrate	65
3.3.7 Treatment of real SW effluent.....	67
3.3.8 Economic comparison.....	69
3.4 Conclusion	70
Chapter 4 Oxidation of phenanthrene in soil washing effluent by photo-Fenton process using Fe(III)-citric acid complex.....	78
4.1 Introduction.....	79
4.2 Materials and methods	80
4.2.1 Chemicals.....	80
4.2.2 Experimental procedures and irradiation setup.....	81
4.2.3 Analytical methods.....	81
4.3 Results and discussion	83
4.3.1 Physicochemical and photochemical properties of Fe(III)-CA	83
4.3.2 Comparison of PHE oxidation under various systems	85
4.3.3 PHE oxidation using different ligands chelated Fe(III) complexes.....	90
4.3.4 Effect of Fe(III)/CA molar ratio.....	93
4.3.5 Effect of Fe(III)-CA concentration	94
4.3.6 Effect of H ₂ O ₂ concentration	95
4.3.7 Effect of initial solution pH	99

4.3.8 Radicals scavenging tests.....	102
4.4 Conclusion	103
Chapter 5 Phenanthrene degradation in soil washing effluent by Fe(III)-EDDS photoactivation of persulfate	109
5.1 Introduction.....	110
5.2 Experimental details.....	111
5.2.1 Chemicals.....	111
5.2.2 Preparation of the synthetic SW effluent	112
5.2.3 Irradiation experiments and degradation kinetics	112
5.2.4 Laser flash photolysis	114
5.2.5 Competition kinetic.....	115
5.3 Results and discussion	115
5.3.1 PHE degradation under various systems.....	115
5.3.2 Effect of Fe(III)-EDDS	120
5.3.3 Effect of PS concentrations.....	122
5.3.4 Effect of Fe(III)/EDDS ratio	124
5.3.5 Effect of TW80 concentration.....	125
5.3.6 Effect of chloride ions addition.....	127
5.3.7 Radical species involvement.....	130
5.4 Conclusions.....	132
Chapter 6 General conclusion and perspectives	138
6.1 General conclusion.....	139
6.2 Perspectives.....	140
Publications	142

List of Abbreviations

AOPs	Advance oxidation processes
CA	Citric acid
CF	Chloroform
CMC	Critical micellar concentration
DDE	Dichlorodiphenyldichloroethylene
DDT	Dichlorodiphenyltrichloroethane
EDDS	Ethylenediamine disuccinic acid
EDTA	Ethylenediaminetetraacetic acid
HOCs	Hydrophobic organic compound
HPAA	4-hydroxyphenylacetic acid
HPLC	High performance liquid chromatography
NTA	Nitrilotriacetic acid
PAHs	Polycyclic aromatic hydrocarbons
PDS	Peroxydisulfate
PHE	Phenanthrene
PMS	Peroxymonosulfate
POD	Peroxidase from horseradish
PS	Persulfate
PYR	Pyrene
SR-AOPs	$\text{SO}_4^{\bullet-}$ based advance oxidation processes
SW	Soil washing
TBA	Tert-butanol
TW80	Tween 80

List of Figures

Figure 2-1 Sources of PAHs and their threats on human health.....	20
Figure 2-2 Molecular structure of persulfates.....	28
Figure 3-1 Schematic representation of the experimental setup	51
Figure 3-2 Absorption spectra of H ₂ O ₂ (5 mM), PS (5 mM), PHE (10 mg L ⁻¹ in 0.5 g L ⁻¹ of TW80) and emission spectrum of the adopted UVB lamps.	52
Figure 3-3 Degradation of PHE in the presence of TW80 in different systems. Inserts are the corresponding pseudo-first order rate constants	54
Figure 3-4 Influence of oxidant concentration on the photo-degradation of PHE. Inserts are the corresponding pseudo first order rate constants. (a) UVB/H ₂ O ₂ ; (b) UVB/PS	57
Figure 3-5 Influence of initial solution pH on the photo-degradation of PHE. Inserts are the corresponding pseudo first order rate constants. (a) UVB/H ₂ O ₂ ; (b) UVB/PS	59
Figure 3-6 Influence of Cl ⁻ concentration on the photo-degradation of PHE. (a) UVB/H ₂ O ₂ at pH = 3.3 ± 0.1; (b) UVB/PS at pH = 3.3 ± 0.1; (c) UVB/H ₂ O ₂ at pH = 7.1 ± 0.1; (d) UVB/PS at pH = 7.1 ± 0.1; (e) UVB/H ₂ O ₂ at pH = 8.6; (f) UVB/PS at pH = 8.6. Inserts are the corresponding first-order rate constants	63
Figure 3-7 Influence of HCO ₃ ⁻ concentration on the photo-degradation of PHE. (a) UVB/H ₂ O ₂ ; (b) UVB/PS. Inserts are the corresponding first-order rate constants	64
Figure 3-8 Influence of NO ₃ ⁻ concentration on the photo-degradation of PHE. (a) UVB/H ₂ O ₂ at pH 3.3 ± 0.1; (b) UVB/PS at pH 3.3 ± 0.1; (c) UVB/H ₂ O ₂ at different pH; (d) UVB/PS at different pH. Inserts are the corresponding first-order rate constants.....	67

Figure 3-9 Degradation of PHE with three real SW effluents in different systems.....	69
Figure 3-10 The electrical energy consumption for UVB, UVB/H ₂ O ₂ and UVB/PS for PHE degradation with both simulated and real SW effluents.....	70
Figure 4-1 Absorption spectra of Fe(III)-CA (0.5 mM), H ₂ O ₂ (5 mM), PHE (10 mg L ⁻¹ in 0.5 g L ⁻¹ of TW80) and emission spectrum of the adopted UVB tubes.....	82
Figure 4-2 UV-vis absorption spectra of: (a) complexes with different Fe(III)/CA ratios, inset is the absorbance at 250 and 313 nm; (b) spectra of Fe(III)-CA in dark with time	85
Figure 4-3 UV-vis absorption spectra evolution of 0.5 mM Fe(III)-CA under the adopted UVB irradiation	85
Figure 4-4 (a) Degradation of PHE in different systems; (b) H ₂ O ₂ consumption in UVB/H ₂ O ₂ /Fe(III)-CA system and Fe species variation in different systems	88
Figure 4-5 (a) Degradation of PHE; (b) H ₂ O ₂ consumption and Fe species variation in different systems	90
Figure 4-6 Degradation of PHE using different organic ligand chelated Fe(III) complexes	91
Figure 4-7 (a) Fe species variation and (b) H ₂ O ₂ consumption in systems using different organic ligands	92
Figure 4-8 Effect of Fe(III)/CA molar ratio on PHE degradation.....	94
Figure 4-9 Effect of Fe(III)-CA concentration on (a) PHE oxidation and (b) the variation of pseudo first order rate constants of PHE decay	95
Figure 4-10 Effect of H ₂ O ₂ concentration on PHE oxidation in (a) the UVB/H ₂ O ₂ /Fe(III)-CA system; (b) UVB/H ₂ O ₂ system; (c) PHE removal in UVB/H ₂ O ₂ and UVB/H ₂ O ₂ /Fe(III)-CA systems.....	99
Figure 4-11 Effect of initial solution pH on (a) PHE oxidation in the UVB/H ₂ O ₂ /Fe(III)- CA system; (b) PHE removal in UVB/H ₂ O ₂ and UVB/H ₂ O ₂ /Fe(III)-CA systems	

.....	101
Figure 4-12 PHE degradation in different systems at $\text{pH} = 4.5 \pm 0.1$	102
Figure 4-13 Free radicals scavenging tests for PHE oxidation.....	103
Figure 5-1 Absorption spectra of Fe(III)-EDDS (0.5 mM), $\text{S}_2\text{O}_8^{2-}$ (5 mM) and 90 μM of PHE in 0.5 g L ⁻¹ of TW80. Emission spectrum of the adopted irradiation lamps with a maximum wavelength centred at 365 nm.	113
Figure 5-2 Solubility of PHE using different concentrations of TW80.....	116
Figure 5-3 (a) Degradation of PHE and (b) degradation of Fe(III)-EDDS in different systems.....	118
Figure 5-4 (a) Degradation of PHE in different systems at initial $\text{pH} 7.0 \pm 0.2$; (b) Influence of initial pH on photo degradation of PHE in aqueous solution of TW80, insert are the removal percentages of PHE as a function of pH	120
Figure 5-5 Influence of Fe(III)-EDDS concentration (a) on the degradation of PHE and (b) removal percentages of PHE	121
Figure 5-6 Effect of PS dose on PHE oxidation in the (a) UV/PS system; (b) UV/PS/Fe(III)-EDDS system; (c) PHE removal percentage in UV/PS and UV/PS/Fe(III)-EDDS systems	124
Figure 5-7 Degradation of PHE using different concentrations of Fe(III) in the presence of 0.5 mM of EDDS.....	125
Figure 5-8 Influence of TW80 concentration on (a) photo degradation of PHE and (b) the pseudo first-order rate constants of PHE oxidation	127
Figure 5-9 Influence of Cl^- concentration for photodegradation of PHE in TW80 aqueous solution.....	129
Figure 5-10 Free radical scavenging tests of photo degradation of PHE	131

List of Tables

Table 2-1 Main characteristics of phenanthrene	21
Table 2-2 Examples of SW solution treatment by HO [•] based AOPs	27
Table 2-3 Examples of SW solution treatment by SO ₄ ^{•-} based AOPs.....	31
Table 3-1 Pseudo-first-order rate constants and half-lives for PHE oxidation in the UVB, UVB/H ₂ O ₂ and UVB/PS systems	54
Table 3-2 Initial and final pH in UVB/H ₂ O ₂ and UVB/PS systems	58
Table 3-3 Composition of SW effluent samples (in µg L ⁻¹).....	68
Table 4-1 First order rate constants of PHE decay with different H ₂ O ₂ concentrations	97
Table 5-1 Second order rate constants (M ⁻¹ s ⁻¹) of TW80 and PHE with different radicals determined using LFP and competition kinetic method.....	126

Abstract

Soil contamination by toxic pollutants, especially by the recalcitrant hydrophobic organic compounds (HOCs) is a matter of significant public, scientific and regulatory concerns worldwide. Polycyclic aromatic hydrocarbons (PAHs) are typical representatives of HOCs being detected in the contaminated soil due to their ubiquitous occurrence, long-term persistence and low solubility in water. Surfactant-enhanced *ex-situ* soil washing (SW) has been proposed as a promising technology for elimination of PHE from contaminated soils due to its high extraction efficiency and low remediation cost. Nevertheless, the SW process generates a large amount of effluent containing soil pollutants and surfactant, which should be further treated with appropriate methods for the complete elimination of soil pollutants. In the past few decades, hydroxyl radical (HO^\bullet) or sulfate radical ($\text{SO}_4^{\bullet-}$) based AOPs have been extensively investigated for the treatment of contaminants in water under UV irradiation. However, the investigation on PAHs decomposition in SW effluent by UV light-based AOPs is pretty limited. In this dissertation, the oxidation of the model PAHs compound phenanthrene (PHE) in surfactant Tween 80 (TW80) aided SW effluent has been investigated using HO^\bullet and/or $\text{SO}_4^{\bullet-}$ radicals produced in the photochemical processes. The decomposition efficiencies are evaluated, and the oxidation mechanism, the effect of co-existing species are elucidated. The main content and results consist of:

(1) The degradation of PHE in mimic and real SW effluents using UVB light assisted activation of hydrogen peroxide (H_2O_2) and persulfate (PS) oxidation processes was investigated. The results revealed the oxidation efficiency was greatly impacted by oxidant concentration while the initial solution pH has little influence on PHE decomposition. The effect of inorganic anions (Cl^- , HCO_3^- and NO_3^-) on the PHE degradation efficiency was evaluated under various experimental conditions. Chloride

was found to play different roles in the two activation systems. The influence of bicarbonate in UVB/PS for PHE elimination was negligible, while an inhibition effect was observed for UVB/H₂O₂ system. Nitrate inhibited the PHE degradation in both UVB/H₂O₂ and UVB/PS processes. Application of the two activation processes on real SW effluents indicated that up to 85.0 % of PHE degradation could be reached under 6h UVB irradiation with PS. Finally, energy consumption in the two AOPs was compared and UVB/PS was suggested to be more cost-effective process than UVB/H₂O₂.

(2) Fe(III)-CA was employed in the photo-Fenton processes to remove PHE from mimic SW solution. The introduction of Fe(III)-CA strongly intensified PHE oxidation when compared with photo-Fenton process using traditional iron ions, and Fe(III)-CA was more efficient than other Fe(III) organic complexes. PHE decay obey a two-stage profile and the oxidative degradation rates of the two stages and total removal efficiencies of PHE were mainly impacted by Fe(III)/CA ratio, Fe(III)-CA dosage, H₂O₂ concentration, and initial pH. According to the radical scavenging tests, HO[•] was the dominant active species though O₂^{•-} was also involved in the photo-Fenton process.

(3) The oxidation of PHE in mimic SW effluent was performed by enhanced activation of PS using Fe(III)-EDDS complexes under simulated solar light irradiation. The presence of Fe(III)-EDDS pronouncedly enhanced PHE photo-oxidation with PS, and PHE kinetic showed two different decay steps. The influence of initial solution pH on PHE degradation could be neglected. The rise of PS concentration increased the oxidation efficiency of PHE while higher TW80 dosage exhibited stronger inhibition of PHE degradation. The concentration of Fe(III)-EDDS evidently affected PHE oxidation and the optimal concentration was 0.5 mM. The effect of chloride on PHE oxidation was evaluated and it was found that the presence of chloride significantly

enhanced PHE decomposition. The second-order rate constants of the generated radicals with PHE and TW80 in solution were determined. Quenching experiments were conducted to explore PHE degradation mechanism and $\text{SO}_4^{\bullet-}$ radical was proved to be dominantly responsible for PHE degradation.

Keywords: Hydroxyl radical; Sulfate radical; Polycyclic aromatic hydrocarbons (PAHs); Soil washing effluent; Photo-Fenton process.

Chapter 1 Introduction

1.1 Background

Soil pollution by recalcitrant organic compounds has been one of the major environmental concern of the worldwide (Brombal et al., 2015; Kuppusamy et al., 2017; Panagos et al., 2013). Polycyclic aromatic hydrocarbons (PAHs), as one of the most widely distributed classes of soil organic contaminants, are ubiquitous hydrophobic organic compounds (HOCs) with the characteristics of persistency, recalcitrance and potential mutagenicity, carcinogenicity or teratogenicity (Bortey-Sam et al., 2014; Cachada et al., 2012; Yang et al., 2014a). Plenty investigations and trials of PAHs contaminated soil remediation concentrated on *in situ* electrokinetic remediation (Alcántara et al., 2010; Boulakradeche et al., 2015; Pazos et al., 2010) and bioremediation (Bacosa and Inoue 2015; Kadri et al., 2017; Lors et al., 2012), including phytoremediation (Lu et al., 2019a; Petrová et al., 2017). However, those remediation technologies generally hold the drawbacks of time consumption or inefficiency (Gan et al., 2009a). As a consequence, *ex situ* soil washing (SW) as a promising technique for remediation of PAHs contaminated soils has received increasing attention (Peng et al., 2011; Von Lau et al., 2014). To enhance the washing efficiency of PAHs, facilitating agents especially various surfactants are widely used in the SW processes (Lamichhane et al., 2017b; Peng et al., 2011). Thereupon, the mixture of surfactant and soil pollutant generate during the SW processes, which should be further treated with appropriate technologies to thoroughly decompose the soil pollutant and to reuse the surfactant. In the previous work, the biological method (Gharibzadeh et al., 2016), selective adsorption (Li et al., 2014; Zheng et al., 2018; Zhou et al., 2013) and advanced oxidation processes (AOPs) (Mousset et al., 2014b; Zhang et al., 2011) have been applied for treatment of SW effluent. However, biological method bears the drawbacks of long duration and low efficiency, while adsorption possess potential risks since the

contaminants could not be completely decomposed. In this case, AOPs have been developed to the most commonly applied technology for PAHs and various surfactant involved SW effluent treatments.

AOPs, based on generation of highly active species such as hydroxyl radical (HO^\bullet) and sulfate radical ($\text{SO}_4^{\bullet-}$), have been extensively applied as effective and promising techniques for decomposition of recalcitrant and hazardous organic compounds such as pharmaceuticals (Ao and Liu 2017; Zhang et al., 2015), pesticides (Chen et al., 2018a; Luo et al., 2015), dyes (Bilińska et al., 2016; Yuan et al., 2014), phenolic compounds (Fang et al., 2017; Huang et al., 2018a) and personal care products (Abdelmelek et al., 2011; Dhaka et al., 2017) in water and PAHs (Choi et al., 2014; Gan and Ng 2012; Usman et al., 2012b), herbicides (Chen et al., 2018b; Villa et al., 2010), polychlorinated biphenyls (PCBs) (Ahmad et al., 2011; Tang et al., 2015) in soils. Among the AOPs, UV/ H_2O_2 and photo-Fenton oxidation are typical HO^\bullet ($E^0 = 1.8\text{--}2.7\text{ V}$) based processes using H_2O_2 as the precursor. H_2O_2 could be activated by UV light (Yu and Barker 2003a) or iron (Brand et al., 1998a; Pignatello et al., 2006) to yield HO^\bullet radical to oxidize organic compounds.

Photo-Fenton oxidation processes have been extensively employed as effective technologies for decomposition of various organic compounds (Elmolla and Chaudhuri 2011; Farré et al., 2006; Mailhot et al., 2002a; Miró et al., 2013; Primo et al., 2008; Sirtori et al., 2011) due to the simplicity of the technique and nontoxic reagents involvement. However, the application of traditional photo-Fenton implies the disadvantages including the operating condition in a narrow pH range (2.8–3.5) (Clarizia et al., 2017) due to the formation of precipitation of iron oxyhydroxides. To prevent the precipitation and broadening the application range of pH, polycarboxylates or aminopolycarboxylates such as ethylenediaminetetraacetic acid (EDTA),

ethylenediamine disuccinic acid (EDDS), citrate acid (CA), nitrilotriacetic acid (NTA) have been introduced in the photo-Fenton processes (De Luca et al., 2014; Miralles-Cuevas et al., 2014; Wu et al., 2015; Zhang et al., 2006). Polycarboxylates and aminopolycarboxylates can complex iron ions and absorb UV-vis light to undergo photochemical reactions leading to the formation of Fe^{2+} (Clarizia et al., 2017).

The involvement of iron complexing agents can avoid the cost of removing acidification and neutralization phases and open tremendous opportunities to employ photo-Fenton processes at near neutral pH (Clarizia et al., 2017; De la Cruz et al., 2012). AOPs based on $\text{SO}_4^{\bullet-}$ (SR-AOPs) using persulfate (PS) as the precursor have aroused increasing interest in the AOPs research community since $\text{SO}_4^{\bullet-}$ possess higher redox potential ($E^0 = 2.5\text{-}3.1\text{ V}$) and it exhibits longer lifetime than HO^{\bullet} (Wacławek et al., 2017a; Yang et al., 2020). Similar to H_2O_2 , PS can be activated by UV light (Mark et al., 1990b) or transition metals such as iron (Fordham and Williams 1951) to generate strong oxidative $\text{SO}_4^{\bullet-}$ for decomposition of organics (Bu et al., 2016; Liu et al., 2016b; Wang and Wang 2018; Wang et al., 2019b; Xie et al., 2015).

To enhance regeneration of Fe^{2+} and accelerate the efficiency of the iron activated PS systems, similar to the photo-Fenton processes, chelating agents are involved for the decomposition of organic contaminants (Liang et al., 2004; Niu et al., 2012; Wu et al., 2015). Although iron complexing agents have been widely investigated in the homogenous PS activation and photo-Fenton processes for various contaminants in aqueous solution, the application of those catalysts for decomposition of PAHs in surfactant aided SW effluents are pretty limited.

In this PhD work, UV activation of different oxidants and various complexing agents modified photo-Fenton and photo-activated PS processes were studied for treatment of SW effluents contaminated by surfactant and PAH. This work aimed at providing more

knowledge on application of photo generated $\text{SO}_4^{\bullet-}$ and HO^\bullet for organic oxidation and providing novel proposals for PAHs polluted SW effluent treatments.

1.2 Research goals and objective

The objective of this work was to reach the oxidation of the model soil pollutant phenanthrene (PHE) in the nonionic surfactant Tween 80 (TW80) aided SW effluent. The effects of reaction parameters on oxidation performance were evaluated and the oxidation mechanism was elucidated. To meet the objective, the following specific goals for every individual system are defined:

1. To investigate the performance of PHE oxidation in mimic and real SW effluent by UVB/ H_2O_2 and UVB/PS processes, and to evaluate the effect of reaction parameters and coexisting inorganic anions on the oxidation efficiency of PHE.
2. To study the photo-oxidation of PHE in the mimic SW effluent by Fe(III)-citric acid modified photo Fenton process. The influence of operating parameters and the cycle of $\text{Fe}^{3+}/\text{Fe}^{2+}$ were investigated. The reaction mechanism during photo-Fenton oxidation was elucidated.
3. To reach the degradation of PHE in synthetic SW effluent by photo activation of PS using Fe(III)-EDDS complex. The second order rate constants of generated radicals with PHE and TW80 were measured. The reactivity and selectivity of different radicals towards PHE were assessed and the parameters affecting the oxidation efficiency were investigated.

1.3 Structure of the thesis

This thesis is composed of 6 chapters.

Chapter 1 is an introduction, including background information of soil pollutants and soil washing and hydroxyl radical and sulfate radical based advanced oxidation processes (AOPs). Research objectives are also introduced.

Chapter 2 presents a review of recent work related to this study. Three parts are described:

2.1 Polycyclic aromatic hydrocarbons (PAHs)

2.2 Surfactant aided soil washing (SW) processes

2.3 Advanced oxidation processes (AOPs) for SW effluent treatment

Chapter 3 is entitled “Phenanthrene degradation in soil washing effluents by UVB/H₂O₂ and UVB/PS”. The degradation of PHE in mimic and real soil washing effluents by UVB activation of hydrogen peroxide and persulfate was investigated. PHE removals by different systems of UVB, UVB/H₂O₂ and UVB/PS were compared. The effects of initial pH, oxidant dosage and inorganic anions (Cl⁻, HCO₃⁻/CO₃²⁻ and NO₃⁻) on the PHE decomposition were investigated. The feasibility of treatment of three real soil washing effluent by the three processes was also evaluated. Finally, the energy consumption of treatment both the mimic and real soil washing effluents by the involved processes was analyzed.

This chapter is already published in Chemosphere (Phenanthrene decomposition in soil washing effluents using UVB activation of hydrogen peroxide and peroxydisulfate Y. TAO, O. MONFORT, M. BRIGANTE, H. ZHANG, G. MAILHOT, Chemosphere, 2021, 263, 127996).

Chapter 4 is entitled “Oxidation of phenanthrene in soil washing effluent by photo-Fenton process using Fe(III)-citric acid complex”. In this system, PHE oxidation in soil washing effluent was performed by Fe(III)-citric acid (CA) complex assisted photo

Fenton process. The effects of the ratio of Fe(III) to CA, concentrations of Fe(III)-CA and H₂O₂, solution pH on PHE removal were investigated. Furthermore, PHE photo-oxidation mechanism was elucidated with Fe(III)/Fe(II) cycle and H₂O₂ decomposition detections and also with radical scavenging experiments.

Chapter 5 is entitled “Phenanthrene degradation in soil washing effluent by Fe(III)-EDDS photoactivation of persulfate”. In this system, the performance of PHE elimination using Fe(III)-EDDS photoactivation of persulfate was investigated. Different physicochemical parameters such as PS and Fe(III)-EDDS concentrations, solution pH were studied. The second-order rate constants of the generated radicals with pollutants in solution were identified. Finally, the selectivity and reactivity of different radicals towards PHE oxidation were analyzed by radical scavenging experiments.

This chapter is already published in Chemosphere (Phenanthrene degradation using Fe(III)-EDDS photoactivation under simulated solar light: A model for soil washing effluent treatment Y. TAO, H. ZHANG, M. BRIGANTE, G. MAILHOT, Chemosphere, 2019, 236, 124366.).*

Finally, the thesis manuscript ends with **Chapter 6** entitled “General conclusions and perspectives”

References

- Abdelmelek, S.B., Greaves, J., Ishida, K.P., Cooper, W.J., Song, W., 2011. Removal of pharmaceutical and personal care products from reverse osmosis retentate using advanced oxidation processes. *Environmental Science & Technology* 45 (8), 3665-3671.
- Ahmad, M., Simon, M.A., Sherrin, A., Tuccillo, M.E., Ullman, J.L., Teel, A.L., Watts,

- R.J., 2011. Treatment of polychlorinated biphenyls in two surface soils using catalyzed H₂O₂ propagations. *Chemosphere* 84 (7), 855-862.
- Alcántara, M., Gómez, J., Pazos, M., Sanromán, M., 2010. Electrokinetic remediation of PAH mixtures from kaolin. *Journal of Hazardous Materials* 179 (1-3), 1156-1160.
- Ao, X., Liu, W., 2017. Degradation of sulfamethoxazole by medium pressure UV and oxidants: peroxymonosulfate, persulfate, and hydrogen peroxide. *Chemical Engineering Journal* 313, 629-637.
- Bacosa, H.P., Inoue, C., 2015. Polycyclic aromatic hydrocarbons (PAHs) biodegradation potential and diversity of microbial consortia enriched from tsunami sediments in Miyagi, Japan. *Journal of Hazardous Materials* 283, 689-697.
- Bilińska, L., Gmurek, M., Ledakowicz, S., 2016. Comparison between industrial and simulated textile wastewater treatment by AOPs – Biodegradability, toxicity and cost assessment. *Chemical Engineering Journal* 306, 550-559.
- Bortey-Sam, N., Ikenaka, Y., Nakayama, S.M., Akoto, O., Yohannes, Y.B., Baidoo, E., Mizukawa, H., Ishizuka, M., 2014. Occurrence, distribution, sources and toxic potential of polycyclic aromatic hydrocarbons (PAHs) in surface soils from the Kumasi Metropolis, Ghana. *Science of The Total Environment* 496, 471-478.
- Boulakradeche, M.O., Akretche, D.E., Cameselle, C., Hamidi, N., 2015. Enhanced electrokinetic remediation of hydrophobic organics contaminated soils by the combination of non-ionic and ionic surfactants. *Electrochimica Acta* 174, 1057-1066.
- Brand, N., Mailhot, G., Bolte, M., 1998. Degradation photoinduced by Fe (III): method of alkylphenol ethoxylates removal in water. *Environmental Science & Technology* 32 (18), 2715-2720.

- Brombal, D., Wang, H., Pizzol, L., Critto, A., Giubilato, E., Guo, G., 2015. Soil environmental management systems for contaminated sites in China and the EU. Common challenges and perspectives for lesson drawing. *Land Use Policy* 48, 286-298.
- Bu, L., Shi, Z., Zhou, S., 2016. Modeling of Fe (II)-activated persulfate oxidation using atrazine as a target contaminant. *Separation and Purification Technology* 169, 59-65.
- Cachada, A., Pato, P., Rocha-Santos, T., da Silva, E.F., Duarte, A., 2012. Levels, sources and potential human health risks of organic pollutants in urban soils. *Science of The Total Environment* 430, 184-192.
- Chen, L., Cai, T., Cheng, C., Xiong, Z., Ding, D., 2018a. Degradation of acetamiprid in UV/H₂O₂ and UV/persulfate systems: a comparative study. *Chemical Engineering Journal* 351, 1137-1146.
- Chen, L., Hu, X., Yang, Y., Jiang, C., Bian, C., Liu, C., Zhang, M., Cai, T., 2018b. Degradation of atrazine and structurally related s-triazine herbicides in soils by ferrous-activated persulfate: Kinetics, mechanisms and soil-types effects. *Chemical Engineering Journal* 351, 523-531.
- Choi, K., Bae, S., Lee, W., 2014. Degradation of pyrene in cetylpyridinium chloride-aided soil washing wastewater by pyrite Fenton reaction. *Chemical Engineering Journal* 249, 34-41.
- Clarizia, L., Russo, D., Di Somma, I., Marotta, R., Andreozzi, R., 2017. Homogeneous photo-Fenton processes at near neutral pH: a review. *Applied Catalysis B: Environmental* 209, 358-371.
- De la Cruz, N., Giménez, J., Esplugas, S., Grandjean, D., De Alencastro, L., Pulgarin, C., 2012. Degradation of 32 emergent contaminants by UV and neutral photo-

- fenton in domestic wastewater effluent previously treated by activated sludge. *Water Research* 46 (6), 1947-1957.
- De Luca, A., Dantas, R.F., Esplugas, S., 2014. Assessment of iron chelates efficiency for photo-Fenton at neutral pH. *Water Research* 61, 232-242.
- Dhaka, S., Kumar, R., Khan, M.A., Paeng, K.-J., Kurade, M.B., Kim, S.-J., Jeon, B.-H., 2017. Aqueous phase degradation of methyl paraben using UV-activated persulfate method. *Chemical Engineering Journal* 321, 11-19.
- Elmolla, E.S., Chaudhuri, M., 2011. Combined photo-Fenton–SBR process for antibiotic wastewater treatment. *Journal of Hazardous Materials* 192 (3), 1418-1426.
- Fang, C., Lou, X., Huang, Y., Feng, M., Wang, Z., Liu, J., 2017. Monochlorophenols degradation by UV/persulfate is immune to the presence of chloride: illusion or reality? *Chemical Engineering Journal* 323, 124-133.
- Farré, M.J., Doménech, X., Peral, J., 2006. Assessment of photo-Fenton and biological treatment coupling for Diuron and Linuron removal from water. *Water Research* 40 (13), 2533-2540.
- Fordham, J., Williams, H.L., 1951. The persulfate-iron (II) initiator system for free radical polymerizations¹. *Journal of The American Chemical Society* 73 (10), 4855-4859.
- Gan, S., Lau, E., Ng, H., 2009. Remediation of soils contaminated with polycyclic aromatic hydrocarbons (PAHs). *Journal of Hazardous Materials* 172 (2-3), 532-549.
- Gan, S., Ng, H.K., 2012. Modified Fenton oxidation of polycyclic aromatic hydrocarbon (PAH)-contaminated soils and the potential of bioremediation as post-treatment. *Science of The Total Environment* 419, 240-249.

- Gharibzadeh, F., Kalantary, R.R., Nasser, S., Esrafil, A., Azari, A., 2016. Reuse of polycyclic aromatic hydrocarbons (PAHs) contaminated soil washing effluent by bioaugmentation/biostimulation process. *Separation and Purification Technology* 168, 248-256.
- Huang, W., Bianco, A., Brigante, M., Mailhot, G., 2018. UVA-UVB activation of hydrogen peroxide and persulfate for advanced oxidation processes: efficiency, mechanism and effect of various water constituents. *Journal of Hazardous Materials* 347, 279-287.
- Kadri, T., Rouissi, T., Brar, S.K., Cledon, M., Sarma, S., Verma, M., 2017. Biodegradation of polycyclic aromatic hydrocarbons (PAHs) by fungal enzymes: A review. *Journal of Environmental Sciences* 51, 52-74.
- Kuppusamy, S., Thavamani, P., Venkateswarlu, K., Lee, Y.B., Naidu, R., Megharaj, M., 2017. Remediation approaches for polycyclic aromatic hydrocarbons (PAHs) contaminated soils: Technological constraints, emerging trends and future directions. *Chemosphere* 168, 944-968.
- Lamichhane, S., Krishna, K.B., Sarukkalige, R., 2017. Surfactant-enhanced remediation of polycyclic aromatic hydrocarbons: a review. *Journal of Environmental Management* 199, 46-61.
- Li, H., Qu, R., Li, C., Guo, W., Han, X., He, F., Ma, Y., Xing, B., 2014. Selective removal of polycyclic aromatic hydrocarbons (PAHs) from soil washing effluents using biochars produced at different pyrolytic temperatures. *Bioresource Technology* 163, 193-198.
- Liang, C., Bruell, C.J., Marley, M.C., Sperry, K.L., 2004. Persulfate oxidation for in situ remediation of TCE. II. Activated by chelated ferrous ion. *Chemosphere* 55 (9), 1225-1233.

- Liu, Y., He, X., Fu, Y., Dionysiou, D.D., 2016. Kinetics and mechanism investigation on the destruction of oxytetracycline by UV-254 nm activation of persulfate. *Journal of Hazardous Materials* 305, 229-239.
- Lors, C., Damidot, D., Ponge, J.-F., Périé, F., 2012. Comparison of a bioremediation process of PAHs in a PAH-contaminated soil at field and laboratory scales. *Environmental Pollution* 165, 11-17.
- Lu, H., Wang, W., Li, F., Zhu, L., 2019. Mixed-surfactant-enhanced phytoremediation of PAHs in soil: Bioavailability of PAHs and responses of microbial community structure. *Science of The Total Environment* 653, 658-666.
- Luo, C., Ma, J., Jiang, J., Liu, Y., Song, Y., Yang, Y., Guan, Y., Wu, D., 2015. Simulation and comparative study on the oxidation kinetics of atrazine by UV/H₂O₂, UV/HSO₅⁻ and UV/S₂O₈²⁻. *Water Research* 80, 99-108.
- Mailhot, G., Sarakha, M., Lavedrine, B., Caceres, J., Malato, S., 2002. Fe (III)-solar light induced degradation of diethyl phthalate (DEP) in aqueous solutions. *Chemosphere* 49 (6), 525-532.
- Mark, G., Schuchmann, M.N., Schuchmann, H.-P., von Sonntag, C., 1990. The photolysis of potassium peroxodisulphate in aqueous solution in the presence of tert-butanol: a simple actinometer for 254 nm radiation. *Journal of Photochemistry and Photobiology A: Chemistry* 55 (2), 157-168.
- Miralles-Cuevas, S., Oller, I., Pérez, J.S., Malato, S., 2014. Removal of pharmaceuticals from MWTP effluent by nanofiltration and solar photo-Fenton using two different iron complexes at neutral pH. *Water Research* 64, 23-31.
- Miró, P., Arques, A., Amat, A., Marin, M., Miranda, M., 2013. A mechanistic study on the oxidative photodegradation of 2, 6-dichlorodiphenylamine-derived drugs: Photo-Fenton versus photocatalysis with a triphenylpyrylium salt. *Applied*

- Catalysis B: Environmental 140, 412-418.
- Mousset, E., Oturan, N., Van Hullebusch, E.D., Guibaud, G., Esposito, G., Oturan, M.A., 2014. Treatment of synthetic soil washing solutions containing phenanthrene and cyclodextrin by electro-oxidation. Influence of anode materials on toxicity removal and biodegradability enhancement. *Applied Catalysis B: Environmental* 160, 666-675.
- Niu, C.-G., Wang, Y., Zhang, X.-G., Zeng, G.-M., Huang, D.-W., Ruan, M., Li, X.-W., 2012. Decolorization of an azo dye Orange G in microbial fuel cells using Fe (II)-EDTA catalyzed persulfate. *Bioresource Technology* 126, 101-106.
- Panagos, P., Van Liedekerke, M., Yigini, Y., Montanarella, L., 2013. Contaminated sites in Europe: review of the current situation based on data collected through a European network. *Journal of Environmental and Public Health* 2013.
- Pazos, M., Rosales, E., Alcántara, T., Gómez, J., Sanromán, M., 2010. Decontamination of soils containing PAHs by electroremediation: a review. *Journal of Hazardous Materials* 177 (1-3), 1-11.
- Peng, S., Wu, W., Chen, J., 2011. Removal of PAHs with surfactant-enhanced soil washing: influencing factors and removal effectiveness. *Chemosphere* 82 (8), 1173-1177.
- Petrová, Š., Rezek, J., Soudek, P., Vaněk, T., 2017. Preliminary study of phytoremediation of brownfield soil contaminated by PAHs. *Science of The Total Environment* 599, 572-580.
- Pignatello, J.J., Oliveros, E., MacKay, A., 2006. Advanced oxidation processes for organic contaminant destruction based on the Fenton reaction and related chemistry. *Critical Reviews in Environmental Science and Technology* 36 (1), 1-84.

- Primo, O., Rivero, M.J., Ortiz, I., 2008. Photo-Fenton process as an efficient alternative to the treatment of landfill leachates. *Journal of Hazardous Materials* 153 (1-2), 834-842.
- Sirtori, C., Zapata, A., Gernjak, W., Malato, S., Lopez, A., Agüera, A., 2011. Solar photo-Fenton degradation of nalidixic acid in waters and wastewaters of different composition. Analytical assessment by LC–TOF-MS. *Water Research* 45 (4), 1736-1744.
- Tang, X., Hashmi, M.Z., Zeng, B., Yang, J., Shen, C., 2015. Application of iron-activated persulfate oxidation for the degradation of PCBs in soil. *Chemical Engineering Journal* 279, 673-680.
- Usman, M., Faure, P., Ruby, C., Hanna, K., 2012. Application of magnetite-activated persulfate oxidation for the degradation of PAHs in contaminated soils. *Chemosphere* 87 (3), 234-240.
- Villa, R.D., Trovó, A.G., Nogueira, R.F.P., 2010. Soil remediation using a coupled process: soil washing with surfactant followed by photo-Fenton oxidation. *Journal of Hazardous Materials* 174 (1-3), 770-775.
- Von Lau, E., Gan, S., Ng, H.K., Poh, P.E., 2014. Extraction agents for the removal of polycyclic aromatic hydrocarbons (PAHs) from soil in soil washing technologies. *Environmental Pollution* 184, 640-649.
- Waclawek, S., Lutze, H.V., Grübel, K., Padil, V.V., Černík, M., Dionysiou, D.D., 2017. Chemistry of persulfates in water and wastewater treatment: a review. *Chemical Engineering Journal* 330, 44-62.
- Wang, S., Wang, J., 2018. Trimethoprim degradation by Fenton and Fe (II)-activated persulfate processes. *Chemosphere* 191, 97-105.
- Wang, S., Wu, J., Lu, X., Xu, W., Gong, Q., Ding, J., Dan, B., Xie, P., 2019. Removal

- of acetaminophen in the Fe^{2+} /persulfate system: Kinetic model and degradation pathways. *Chemical Engineering Journal* 358, 1091-1100.
- Wu, Y., Bianco, A., Brigante, M., Dong, W., de Sainte-Claire, P., Hanna, K., Mailhot, G., 2015. Sulfate radical photogeneration using Fe-EDDS: influence of critical parameters and naturally occurring scavengers. *Environmental Science & Technology* 49 (24), 14343-14349.
- Xie, P., Ma, J., Liu, W., Zou, J., Yue, S., Li, X., Wiesner, M.R., Fang, J., 2015. Removal of 2-MIB and geosmin using UV/persulfate: contributions of hydroxyl and sulfate radicals. *Water Research* 69, 223-233.
- Yang, L., He, L., Xue, J., Ma, Y., Xie, Z., Wu, L., Huang, M., Zhang, Z., 2020. Persulfate-based degradation of perfluorooctanoic acid (PFOA) and perfluorooctane sulfonate (PFOS) in aqueous solution: Review on influences, mechanisms and prospective. *Journal of Hazardous Materials*, 122405.
- Yang, W., Lang, Y., Li, G., 2014. Cancer risk of polycyclic aromatic hydrocarbons (PAHs) in the soils from Jiaozhou Bay wetland. *Chemosphere* 112, 289-295.
- Yu, X.-Y., Barker, J.R., 2003. Hydrogen peroxide photolysis in acidic aqueous solutions containing chloride ions. II. Quantum yield of $\text{HO}\cdot(\text{Aq})$ radicals. *The Journal of Physical Chemistry A* 107 (9), 1325-1332.
- Yuan, R., Wang, Z., Hu, Y., Wang, B., Gao, S., 2014. Probing the radical chemistry in UV/persulfate-based saline wastewater treatment: kinetics modeling and byproducts identification. *Chemosphere* 109, 106-112.
- Zhang, C., Wang, L., Wu, F., Deng, N., 2006. Quantitation of Hydroxyl Radicals from Photolysis of Fe (III)-Citrate Complexes in Aerobic Water (5 pp). *Environmental Science and Pollution Research* 13 (3), 156-160.
- Zhang, R., Sun, P., Boyer, T.H., Zhao, L., Huang, C.-H., 2015. Degradation of

- pharmaceuticals and metabolite in synthetic human urine by UV, UV/H₂O₂, and UV/PDS. *Environmental Science & Technology* 49 (5), 3056-3066.
- Zhang, Y., Wong, J., Liu, P., Yuan, M., 2011. Heterogeneous photocatalytic degradation of phenanthrene in surfactant solution containing TiO₂ particles. *Journal of Hazardous Materials* 191 (1-3), 136-143.
- Zheng, X., Lin, H., Tao, Y., Zhang, H., 2018. Selective adsorption of phenanthrene dissolved in Tween 80 solution using activated carbon derived from walnut shells. *Chemosphere* 208, 951-959.
- Zhou, W., Wang, X., Chen, C., Zhu, L., 2013. Removal of polycyclic aromatic hydrocarbons from surfactant solutions by selective sorption with organo-bentonite. *Chemical Engineering Journal* 233 (11), 251-257.

Chapter 2 Literature review

2.1 Polycyclic aromatic hydrocarbons (PAHs)

Polycyclic aromatic hydrocarbons (PAHs), a group of semi-volatile, chemically stable and hydrophobic organic compounds, consist of two or more linear, angular or cluster fused aromatic rings (Wilson and Jones 1993). Although several hundred different combinations of PAHs exist in the environment, only 28 compounds were identified as hazardous contaminants and 16 of those were listed as priority control pollutants by the US Environmental Protection Agency (US EPA) (Gan et al., 2009b; Yan et al., 2004). According to the molecular structure, PAHs can be categorized as low molecular weight (LMW) with 2-3 rings and high molecular weight (HMW) PAHs with 4-7 rings (Duan et al., 2015).

2.1.1 PAHs pollution in soil

PAHs are ubiquitous contaminants in the environment and soil pollution by PAHs has been one of the major environmental concern of the worldwide (Kuppusamy et al., 2017; Wilson and Jones 1993). In Europe, PAHs contaminants contribute to 10.9% of soil contaminations (Panagos et al., 2013). Among 1408 hazardous waste sites that are targeted for long-term federal cleanup activities identified by the US Environmental Protection Agency (US EPA), at least 42.6% of the sites have been found to be polluted with PAHs (Duan et al., 2015). In China, according to the report of the first National Soil Pollution Survey released by Ministry of Environmental Protection (MEP) and Ministry of Land and Resources (MLR), soil contamination by PAHs is particularly severe in the case of mining areas and 33.4% of soils does not meet national requirements (Brombal et al., 2015). Another report of overall contamination status of surface soil by PAHs in China revealed that from > 6000 surface soil samples, the proportions of heavily contaminated, contaminated, weakly contaminated soil samples were 21.4%, 11.9% and 49.5%, respectively (Zhang and Chen 2017). PAHs are

generally being found at sites associated with coking plants, wood preserving, petroleum and gas production industries (Kuppusamy et al., 2017; Wilson and Jones 1993). PAHs are persistent contaminants with half-lives ranging from several months to decades due to their hydrophobicity and recalcitrance (McKay et al., 1992; Wild et al., 1990). Concentration of PAHs at contaminated sites varying from dozens to tens of thousands of mg kg^{-1} soil according to the types of polluted sites (Kuppusamy et al., 2017).

2.1.2 Sources and hazards of PAHs

The main sources of PAHs in the environment include natural processes and anthropogenic activities. Natural sources of PAHs are emissions from combustion processes in forest and bush fires, spillage of petroleum and volcanic eruptions (Kaushik and Haritash 2006; Makkar and Rockne 2003). Anthropogenic activities include combustion or pyrolysis of biomass, fossil fuels or fossil fuel derived products such as coke, petroleum, gas and coal tar, vehicle emissions, soil waste incineration, petroleum refining, petroleum and waste water discharges (Haritash and Kaushik 2009; Rahmanpoor et al., 2014; Wolska et al., 2012).

PAHs can be bio-accumulated by food chains and exert health threats on human bodies. The effect of PAHs on human health depends mainly on the duration and route of exposure, exposure concentrations and toxicity associated with categories of PAHs. Exposure to high levels of PAHs can lead to acute symptoms including irritation of the eyes, mucous membranes and skin, vomiting, nausea etc (Hussein and Mona 2016; Warshawsky 2001). Long-term exposure to PAHs potentially results in chronic health hazards such as neurasthenia, bone marrow dysfunction, organs (kidney, liver, lung etc) damage and skin inflammation (Diggs et al., 2011; Wu et al., 2011). Embryotoxic effect during pregnancy and suppression of immune reactions have also been reported with

exposure to high concentrations of PAHs (Burchiel and Luster 2001; Wassenberg and Di Giulio 2004). Moreover, PAHs can also potentially pose carcinogenicity, teratogenicity, and genotoxicity to human body (Armstrong et al., 2004; Edwards et al., 2010; Gamboa et al., 2008; Man et al., 2013). The sources of PAHs and their threats on human health are summarized in Figure 2-1 (Dudhagara et al., 2016).

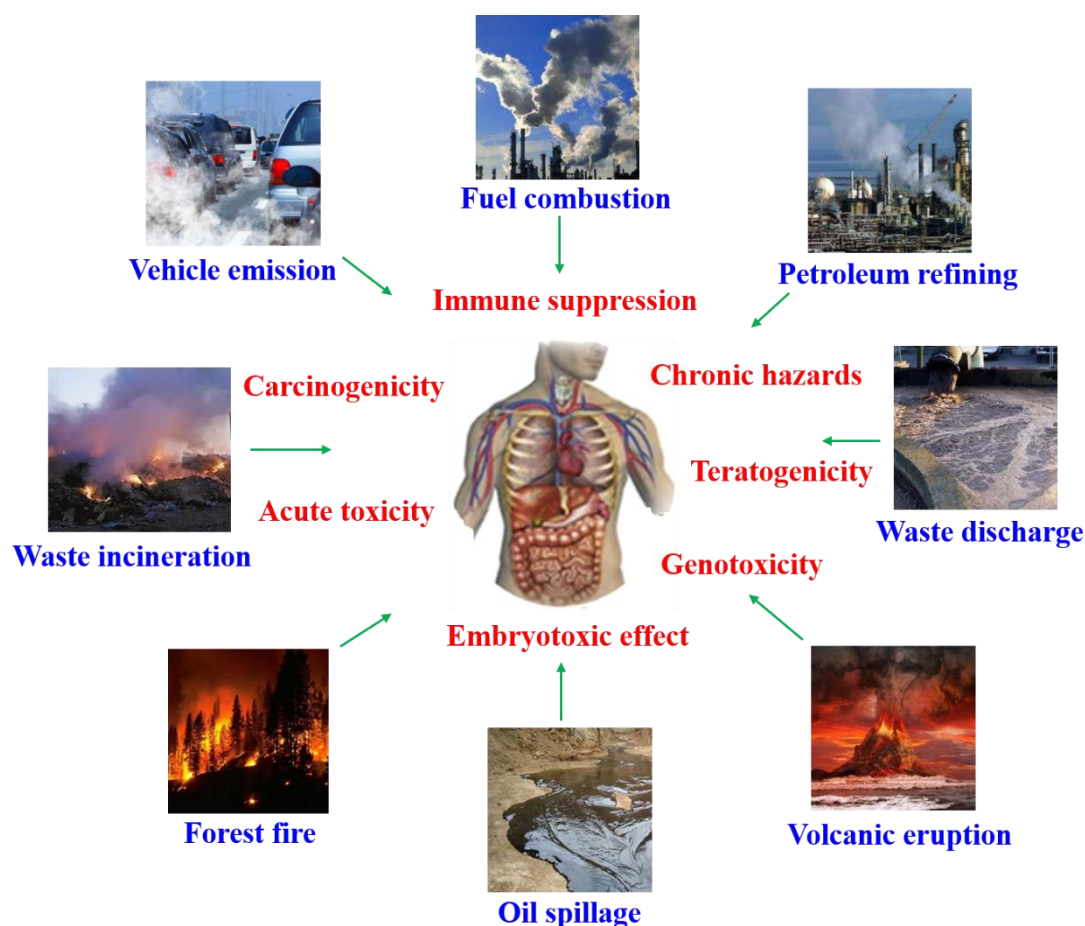


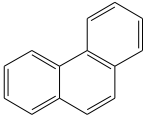
Figure 2-1 Sources of PAHs and their threats on human health

2.1.3 Properties of PAHs – case of phenanthrene (PHE)

PAHs are characterized with low solubility in water, high melting and boiling points and low vapor pressure (Haritash and Kaushik 2009). PAHs pollutants exhibit poor water solubility properties and the solubility decrease almost linearly with increase in molecular weight. With an increase in molecular mass, the melting point and boiling point of PAHs increase and the vapor pressure decreases (Patnaik 2007). Phenanthrene

(PHE) is a typical representative of PAH and its main characteristics is listed in Table 2-1 (Kadri et al., 2017; Wang et al., 2007). PHE is a LMW PAH and it is composed of three benzene rings in an angular arrangement. PHE is an isomer of anthracene in its chemical structure and appears as a colorless crystal with luster. As one of 16 PAHs listed as priority control pollutants by US EPA, PHE is one of the most widely detected PAHs in the contaminated sites and the concentration of PHE in contaminated soil ranged from 11 to 4434 mg kg⁻¹ (Bezza and Chirwa 2017; Kuppusamy et al., 2017; Petrová et al., 2017).

Table 2-1 Main characteristics of phenanthrene

IUPAC Name	Phenanthrene
Abbreviation	PHE
CAS registry No	85-01-8
Formula	C ₁₄ H ₁₀
Molecular weight (g mol ⁻¹)	178.2
Structure	
Water solubility (20 °C, mg L ⁻¹)	0.788
Density (g cm ⁻³)	1.02
Vapor pressure (Pa at 25°C)	9.07 × 10 ⁻²
Melting point (°C)	99.5
Boiling point (°C)	340.2

2.2 Surfactant aided soil washing (SW) processes

The commonly employed ex-situ soil amendment technology is the SW process, where the soil has to be excavated before the treatment and then the soil pollutants are

transferred to a liquid phase with aiding additives (Befkadu and Quanyuan 2018). SW process is one of the few treatments which can effectively separate great diversity of contaminants such as heavy metals, organics, and radionuclides from contaminated soils with a broad range of pollution concentration (Mao et al., 2015). Moreover, SW is time-efficient and versatile process and allow for the return of clean coarse fractions of soils to the site at a relative low cost after elimination of the soil pollutants (Dermont et al., 2008). To enhance the removal efficiency and reduce the restoration time, additives are indispensable in the SW processes. Organic solvents (i.e. esters, ketones, alcohols, alkylamines and aromatics for example), synthetic surfactants and vegetable oil can be used as the extraction agents (Trellu et al., 2016a). However, most organic solvents are costly, toxic, flammable or highly flammable, which increases the economic input and risks of operating during SW processes (Von Lau et al., 2014). Likewise, the cost of production of huge quantities of vegetable oil and the environmental risks of using large amounts of pesticides during planting vegetable are worth to be considered (Yap et al., 2010).

Among diversified extracting agents, synthetic surfactants are more favored due to its high extracting efficiency (Mulligan et al., 2001a). Surfactants are composed of the hydrophobic tail and the hydrophilic head and they are characterized by their chemical structure, hydrophilic-lipophilic balance and critical micellar concentration (CMC) (Mulligan et al., 2001a). Nonionic surfactants are superior to anionic and cationic surfactants due to their lower soil affinity, higher extracting capacity and cost effectiveness (Trellu et al., 2016a). As a nonionic surfactant, Tween 80 (TW80) is more frequently used for PAHs desorption from soil due to its more biodegradable and less toxic effect than other surfactants (Lamichhane et al., 2017a; Zhang and Zhu 2012). TW80 is observed to have better solubilization ability for various PAHs such as PHE,

Pyrene, Fluorene, Acenaphthene, Naphthalene than other nonionic surfactants such as Tween 20, Triton X-100, Triton X-305, Triton X-405 (Zhu and Zhou 2008). Other researchers found the extraction capacity of PHE from the soils followed the order of TW80 > Triton X-100 > Brij 35 (Ahn et al., 2008; Iglesias et al., 2014).

2.3 Advanced oxidation processes (AOPs) for SW effluent treatment

Advanced oxidation processes (AOPs) have attracted intensive interest in SW effluent treatment owing to their advantages of time-efficient and superiority for the complete degradation of soil pollutants over other treatment processes such as biological treatments and adsorption technologies (Mousset et al., 2014b; Vidales et al., 2019). Available AOPs in the literature for SW effluent treatment mainly include processes based on generation of highly oxidative species hydroxyl radical (HO^\bullet) and sulfate radical ($\text{SO}_4^{\bullet-}$).

2.3.1 Hydroxyl radical (HO^\bullet) based AOPs

HO^\bullet is highly reactive and non-selective species able to attack and destroy the most persistent and toxic organic molecules with rate constants in the range of 10^6 - $10^9 \text{ M}^{-1} \text{ s}^{-1}$ by OH-addition, H abstraction and electron transfer reactions (Cheng et al., 2016; Rubio-Clemente et al., 2014). The commonly involved hydroxyl radical based AOPs for SW effluent treatments are UV/ H_2O_2 , Fenton/Fenton like process, photo-Fenton, electrochemical oxidation and heterogeneous photocatalysis. Some examples are shown in Table 2-2.

I) UV/ H_2O_2

The UV/H₂O₂ process is triggered by photolytic cleavage of the O-O bond of H₂O₂ into two HO• under UV irradiation (reaction 2-1) (I Litter and Quici 2010; Ledakowicz et al., 1999).



UV/H₂O₂ system has been examined as an effective treatment method for pyrene (PYR) and PHE removal in perfluorinated surfactant solutions (Table 2-2). The micellar ammonium perfluorooctanoate (APFO) solutions was found retarded PHE photolysis and enhanced PYR photolysis (An and Carraway 2002).

II) Fenton/Fenton like processes

Fenton process is the combination of ferrous iron (Fe²⁺) and H₂O₂ at acidic conditions lead to the formation of reactive HO• (reaction 2-2). In the Fenton process, Fe²⁺ acts as a catalyst with optimal catalytic activity at pH around 3 since the precipitation of ferric oxyhydroxide at higher pH value retard the catalytic activity. Subsequently, the newly formed ferric ions (Fe³⁺) can react with H₂O₂ to regenerate Fe²⁺ at acidic pH < 5 via reaction (2-3), which is known as Fenton-like process (Cheng et al., 2016; Parsons 2004; Umar et al., 2010).



Fenton oxidation was tested for degradation of a variety of soil pollutants such as PAHs (Lindsey et al., 2003; Veignie et al., 2009), cresols (Rosas et al., 2013), pesticides (Di Palma et al., 2003; Villa et al., 2010) and PCBs (Lindsey et al., 2003) in different surfactants involved in SW effluents.

III) Photo-Fenton

The photo-Fenton processes include two main categories: i) The conventional reactions of reduction of Fe³⁺ to Fe²⁺ to produce HO• via photolysis as reaction (2-4)

(Kavitha and Palanivelu 2004); ii) The modified processes by polycarboxylates and aminopolycarboxylates (L) as related to the photo-decarboxylation reaction (2-5) (Clarizia et al., 2017; Kuma et al., 1995; Miralles-Cuevas et al., 2014).



The traditional photo-Fenton reactions occur at pH around 3, while the working pH condition of modified photo-Fenton process is broadened to near neutral pH (Clarizia et al., 2017). Photo-Fenton processes have been reported for the treatment of SW solution containing surfactants and soil contaminants such as 2,4,6-trinitrotoluene (Yardin and Chiron 2006), PCBs (Riaza-Frutos et al., 2007), total petroleum hydrocarbons (TPH) (Mehrasbi et al., 2012) and various pesticides (Bandala et al., 2013; Villa et al., 2010).

IV) Electrochemical oxidation

HO^{\bullet} based electrochemical AOPs are mainly anodic oxidation and electro Fenton processes. Anodic oxidation is based on the production of HO^{\bullet} from water oxidation on the surface of the anode materials (M) such as platinum, carbon-based anodes, boron-doped diamond (BDD) as shown in reaction (2-6) (Panizza and Cerisola 2009; Panizza and Martinez-Huitle 2013; Trellu et al., 2016b). Another popular electrochemical technique is electro-Fenton, in which H_2O_2 is generated at the cathode with O_2 or air feeding with the addition of iron catalysts (Fe^{2+} , Fe^{3+} , or iron oxides) (reaction 2-7) (Brillas et al., 2009). Fe^{2+} can be electro-regenerated at the cathode to continuously enhance the formation of HO^{\bullet} for pollutants mineralization (reaction 2-8) (Oturán and Aaron 2014; Oturan et al., 2010).





Electrochemical oxidation has been frequently reported to treat SW wastewater to eliminate multiple PAHs such as PHE (Mousset et al., 2014a; 2014b), PYR (Tran et al., 2010), anthracene (Alcántara et al., 2009; Hussein and Ismail 2013), naphtalene (Tran et al., 2010), fluoranthene (FLU) (Alcántara et al., 2009), benzantracene (Alcántara et al., 2009) and benzo[a]pyrene (BaP) (Mousset et al., 2016) and other hydrophobic soil pollutants (Dos Santos et al., 2015; Hanna et al., 2005; Muñoz-Morales et al., 2017).

V) Heterogeneous photocatalysis

Heterogeneous photocatalysis, in which light irradiation couple with catalytic semiconductor materials is another HO[•] based technology being applied for treatment for SW effluents (Ibhadon and Fitzpatrick 2013). Although a variety of materials have been confirmed to interact with light to produce reactive species for various hydrophilic organic decomposition, TiO₂ is the most commonly used semiconductor in SW effluent treatment processes probably due to its cost effectiveness and inert nature (Trellu et al., 2016a). The TiO₂ photocatalysis initiates with the absorption of UV light to generate conduction band electrons (e⁻) and valence band holes (h⁺) (reaction 2-9), and subsequently lead to the production of HO[•] and other species through a series of reactions (Rubio-Clemente et al., 2014; Trellu et al., 2016a).



The degradation of PAHs and other soil contaminants in various surfactants present SW solutions has been extensively investigated by TiO₂ photocatalysis (Hanna et al., 2004; Occulti et al., 2008; Petitgirard et al., 2009; Zhang et al., 2011).

Table 2-2 Examples of SW solution treatment by HO• based AOPs

Process	Pollutant	Surfactant	Operating conditions	Removal efficiency	Reference
UV/H ₂ O ₂	PHE (5.6 µM) PYR (0.49 µM)	APFO ^a (10 mM)	[H ₂ O ₂] = 10 mM, 90 min reaction	100% removal of PHE and PYR	(An and Carraway 2002)
Fenton	BaP ^b (0.01 µM)	CD ^c (5 mM)	[H ₂ O ₂] = 1 mM, [Fe ²⁺] = 0.2 mM, over light reaction	80%	(Veignie et al., 2009)
Photo Fenton	DDT ^d (19 mg L ⁻¹) DDE ^e (9 mg L ⁻¹) Diesel (230 mg L ⁻¹)	Triton X-100 (2.1 g L ⁻¹)	[H ₂ O ₂] = 1.4 M, [Fe ²⁺] = 12 mM, solar light, 6h	98.9% removal of DDT, 99% removal of DDE, 100% removal of diesel	(Villa et al., 2010)
Electro Fenton	PHE (90 µM)	HPCD ^f (8 mM)	Pt anode, carbon felt cathode, 6 h reaction [Fe ²⁺] = 0.2 mM, [Na ₂ SO ₄] = 150 mM, I = 500 mA, 150 min	94.6%	(Mousset et al., 2014a)
UV/TiO ₂	PHE (5.6 µM)	Triton X-100 (1 g L ⁻¹)	8W UV lamp, [TiO ₂] = 0.2 g L ⁻¹ , 30 min reaction	Around 85%	(Zhang et al., 2011)

^aAPFO: Ammonium perfluorooctanoate^bBaP: benzo[a]pyrene^cCD: Cyclodextrin^dDDT: Dichlorodiphenyltrichloroethane^eDDE: Dichlorodiphenyldichloroethylene^fHPCD: Hydroxypropyl-beta-cyclodextrin

2.3.2 Sulfate radical (SO₄^{•-}) based AOPs

SO₄^{•-} is a promising alternative of HO• due to its strong oxidizing capacity, longer lifetime and higher selectivity than HO• (Yang et al., 2019). SO₄^{•-} is typically formed from the oxidant peroxydisulfate (PDS), which is generally referred to persulfate (PS, S₂O₈²⁻) and peroxymonosulfate (PMS, HSO₅⁻) possessing the O-O bond (known as

peroxide or peroxy group). PS is more stable than H_2O_2 and it is easy to be stored and transported for long distance without alteration (Wacławek et al., 2017a). PS is the latest persulfate based advanced chemical oxidant and successfully gets extensive applications due to its low commercial pricing and higher stability (Zhou et al., 2018). The O-O bond dissociation energies are 140 kJ mol^{-1} and 377 kJ mol^{-1} respectively for PS and PMS with the bond lengths being determined to be 1.497 \AA for PS and 1.46 \AA for PMS (Benson 1978; Kolthoff and Miller 1951; Wacławek et al., 2017a; Yang et al., 2010). The molecular structures of PS and PMS are shown as Figure 2-2 (Wacławek et al., 2017a).

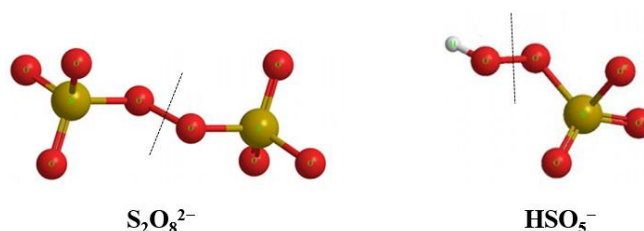


Figure 2-2 Molecular structure of persulfates

$\text{SO}_4^{\bullet-}$ can be generated by various activation methods of persulfates including heat energy, irradiation, transition metal ions, electro activation, alkaline, metal or metal free catalysts (Wacławek et al., 2017a; Zhou et al., 2018). $\text{SO}_4^{\bullet-}$ based AOPs (SR-AOPs) are less investigated as HO^{\bullet} based processes for SW effluent treatment though $\text{SO}_4^{\bullet-}$ is preferred oxidant in *in-situ* chemical oxidation (ISCO) for soil remediation (Tsitonaki et al., 2010; Zhao et al., 2013). The available SR-AOPs for SW effluent treatment in the literature include processes of persulfates activation by heat energy, UV irradiation, transition metals and electrochemical activation and some examples are listed in Table 2-3.

I) Heat activated persulfates

Two $\text{SO}_4^{\bullet-}$ radicals are formed from the fracture of the peroxide bond of persulfates after absorption of heat energy (reactions 2-10 and 2-11) (Kolthoff and Miller 1951).

The activation energies range from 100 kJ mol⁻¹ to 139 kJ mol⁻¹ under acidic, neutral, and basic conditions (House 1962).



The technique of heat activated persulfates has been investigated for selective oxidation of PHE in the presence of compatible surfactant Lauryl Betaine (LB) (Bouزيد et al., 2017).

II) UV activated persulfates

PS can be cleaved to $\text{SO}_4^{\bullet-}$ by UV irradiation (reaction 2-12) (Mark et al., 1990b). PS is superior to H_2O_2 as oxidizing agent under UVC irradiation since the quantum yield of $\text{S}_2\text{O}_8^{2-}$ is higher than H_2O_2 (1.4 for $\text{S}_2\text{O}_8^{2-}$ and 1.0 for H_2O_2) and the molar absorption coefficient at 254 nm for $\text{S}_2\text{O}_8^{2-}$ ($22 \text{ M}^{-1} \text{ cm}^{-1}$) is also larger than that of H_2O_2 ($18.6 \text{ M}^{-1} \text{ cm}^{-1}$) (Legrini et al., 1993; Miklos et al., 2018; Xiao et al., 2016). PMS is activated by UV radiation into a $\text{SO}_4^{\bullet-}$ and a HO^\bullet with a lower quantum yield than PS (reaction 2-13) (Guan et al., 2011).

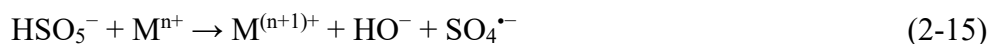
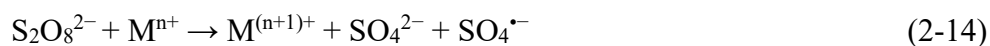


Recent study has reported the advantages of UV/PS system over UV/ H_2O_2 process for PHE oxidation for SW solution management as shown in Table 2-3 (Bai et al., 2019). It is also found UVC/PS is an efficient technology to decompose PHE (Wang et al., 2020) and toluene (Long et al., 2013) in the SW effluent with recovery of the extracting surfactant.

III) Metals activated persulfates

PS and PMS can be activated by transition metals (M) such as iron, silver, copper, cobalt and manganese through one-electron transfer to generate the main oxidizing

species $\text{SO}_4^{\bullet-}$ (reactions 2-14 and 2-15) (Anipsitakis and Dionysiou 2003; House 1962). Cobalt is determined to be the most efficient activator for PMS (Anipsitakis and Dionysiou 2003). Iron is the most frequently applied metal for PS activation, which is similar to Fenton reaction (Tan et al., 2012).

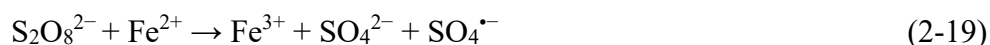
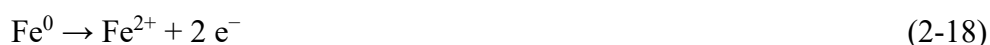


The removal efficiencies of three PAHs (PHE, fluoranthene and pyrene) from anionic surfactant coexisting SW effluents have been explored by iron activated PS (Qiu et al., 2019). Treatments of SW effluent for degradation of toluene (Long et al., 2014) and nitrobenzene (Yan et al., 2015) in SW effluent were compared by Fe^{2+} /PS and Fe^{2+} / H_2O_2 systems (Table 2-3). Another study reported the decontamination of SW wastewater by comparison of photo-Fenton reaction and the UV/cobalt/PMS process (Bandala et al., 2008).

IV) Electrochemically activated persulfates

$\text{SO}_4^{\bullet-}$ can be produced by one electron transfer reactions at the cathode (Eqs. 2-16 and 2-17) following the same mechanism as the redox reaction for metals activated persulfates (Lin et al., 2014; Zhi et al., 2020). According to the literature, numerous parameters including iron addition and regeneration, as well as involvement of materials have been introduced into the systems of electrochemical activation of persulfates (Cai et al., 2014; Lin et al., 2014; Yan et al., 2017). Solid iron such as zero valent iron (Fe^0) produces Fe^{2+} through chemical and anodic reactions (reaction 2-18), and activates the persulfate via reactions (2-19) and Eq. (2-20), which leads to Fe^{2+} regeneration at the cathode (reaction 2-8) for continuously activation of persulfates (Kim et al., 2020; Matzek and Carter 2016).





PS, generated from the electrolysis of surfactant SDS, was activated to $\text{SO}_4^{\bullet-}$ by electrolysis and the generated $\text{SO}_4^{\bullet-}$ was applied to decompose herbicide during the treatment of SW solution (Almazán-Sánchez et al., 2017).

Table 2-3 Examples of SW solution treatment by $\text{SO}_4^{\bullet-}$ based AOPs

Process	Pollutant	Surfactant	Operating conditions	Removal efficiency	Reference
UV/PS	PHE (56 μM)	TW 80 (10 g L ⁻¹)	UVC power = 6 W, [PS] = 10 mM, pH: 6.4, 30 min	97.1%	(Bai et al., 2019)
UV/PS	PHE (56 μM)	SDS ^a (10 g L ⁻¹)	UVC power = 6 W, [PS] = 2 mM, pH: 8.6, 8 min reaction	100%	(Wang et al., 2020)
Fe ²⁺ /PS	Toluene (1 mM)	SDS (5 g L ⁻¹)	[Fe ²⁺] = 8.1 mM, [PS] = 27.3 mM, pH 7.0, 15 min reaction	63.1%	(Long et al., 2014)
Fe ²⁺ /PS	NB ^b (15 μM)	SDBS ^c (9.4 mM)	[Fe ²⁺] = 80 mM, [PS] = 80 mM, pH 3.0, 15 min reaction	100%	(Yan et al., 2015)
Fe ⁰ /PS	PHE (21.3 μM) FLU (19.8 μM) PYR (23.7 μM)	SDS (16 mg L ⁻¹)	[Fe ⁰] = 2 g L ⁻¹ , [PS] = 50 mM, 30 min reaction	84% removal for PHE, 89% removal for FLU, 91% removal for PYR	(Qiu et al., 2019)

^a SDS: Sodium dodecyl sulfate

^b NB: Nitrobenzene

^c SDBS: Sodium dodecylbenzenesulfonate

References

Ahn, C., Kim, Y., Woo, S., Park, J., 2008. Soil washing using various nonionic surfactants and their recovery by selective adsorption with activated carbon. Journal of Hazardous Materials 154 (1-3), 153-160.

- Alcántara, M.T., Gómez, J., Pazos, M., Sanromán, M.A., 2009. PAHs soil decontamination in two steps: desorption and electrochemical treatment. *Journal of Hazardous Materials* 166 (1), 462-468.
- Almazán-Sánchez, P.T., Cotillas, S., Saez, C., Solache-Ríos, M.J., Martínez-Miranda, V., Cañizares, P., Linares-Hernández, I., Rodrigo, M.A., 2017. Removal of pendimethalin from soil washing effluents using electrolytic and electro-irradiated technologies based on diamond anodes. *Applied Catalysis B: Environmental* 213, 190-197.
- An, Y.-J., Carraway, E.R., 2002. PAH degradation by UV/H₂O₂ in perfluorinated surfactant solutions. *Water Research* 36 (1), 309-314.
- Anipsitakis, G.P., Dionysiou, D.D., 2003. Degradation of organic contaminants in water with sulfate radicals generated by the conjunction of peroxymonosulfate with cobalt. *Environmental Science & Technology* 37 (20), 4790-4797.
- Armstrong, B., Hutchinson, E., Unwin, J., Fletcher, T., 2004. Lung cancer risk after exposure to polycyclic aromatic hydrocarbons: a review and meta-analysis. *Environmental Health Perspectives* 112 (9), 970-978.
- Bai, X., Wang, Y., Zheng, X., Zhu, K., Long, A., Wu, X., Zhang, H., 2019. Remediation of phenanthrene contaminated soil by coupling soil washing with Tween 80, oxidation using the UV/S₂O₈²⁻ process and recycling of the surfactant. *Chemical Engineering Journal*.
- Bandala, E.R., Cossio, H., Sánchez-Lopez, A.D., Córdova, F., Peralta-Herández, J.M., Torres, L.G., 2013. Scaling-up parameters for site restoration process using surfactant-enhanced soil washing coupled with wastewater treatment by Fenton and Fenton-like processes. *Environmental technology* 34 (3), 363-371.
- Bandala, E.R., Velasco, Y., Torres, L.G., 2008. Decontamination of soil washing

- wastewater using solar driven advanced oxidation processes. *Journal of Hazardous Materials* 160 (2-3), 402-407.
- Befkadu, A.A., Quanyuan, C., 2018. Surfactant-enhanced soil washing for removal of petroleum hydrocarbons from contaminated soils: a review. *Pedosphere* 28 (3), 383-410.
- Benson, S.W., 1978. Thermochemistry and kinetics of sulfur-containing molecules and radicals. *Chemical Reviews* 78 (1), 23-35.
- Bezza, F.A., Chirwa, E.M.N., 2017. The role of lipopeptide biosurfactant on microbial remediation of aged polycyclic aromatic hydrocarbons (PAHs)-contaminated soil. *Chemical Engineering Journal* 309, 563-576.
- Bouزيد, I., Maire, J., Brunol, E., Caradec, S., Fatin-Rouge, N., 2017. Compatibility of surfactants with activated-persulfate for the selective oxidation of PAH in groundwater remediation. *Journal of Environmental Chemical Engineering* 5 (6), 6098-6106.
- Brillas, E., Sirés, I., Oturan, M.A., 2009. Electro-Fenton process and related electrochemical technologies based on Fenton's reaction chemistry. *Chemical Reviews* 109 (12), 6570-6631.
- Brombal, D., Wang, H., Pizzol, L., Critto, A., Giubilato, E., Guo, G., 2015. Soil environmental management systems for contaminated sites in China and the EU. Common challenges and perspectives for lesson drawing. *Land Use Policy* 48, 286-298.
- Burchiel, S.W., Luster, M.I., 2001. Signaling by environmental polycyclic aromatic hydrocarbons in human lymphocytes. *Clinical Immunology* 98 (1), 2-10.
- Cai, C., Zhang, H., Zhong, X., Hou, L., 2014. Electrochemical enhanced heterogeneous activation of peroxydisulfate by Fe-Co/SBA-15 catalyst for the degradation of

- Orange II in water. *Water Research* 66, 473-485.
- Cheng, M., Zeng, G., Huang, D., Lai, C., Xu, P., Zhang, C., Liu, Y., 2016. Hydroxyl radicals based advanced oxidation processes (AOPs) for remediation of soils contaminated with organic compounds: a review. *Chemical Engineering Journal* 284, 582-598.
- Clarizia, L., Russo, D., Di Somma, I., Marotta, R., Andreozzi, R., 2017. Homogeneous photo-Fenton processes at near neutral pH: a review. *Applied Catalysis B: Environmental* 209, 358-371.
- Dermont, G., Bergeron, M., Mercier, G., Richer-Laflèche, M., 2008. Soil washing for metal removal: a review of physical/chemical technologies and field applications. *Journal of Hazardous Materials* 152 (1), 1-31.
- Di Palma, L., Ferrantelli, P., Petrucci, E., 2003. Experimental study of the remediation of atrazine contaminated soils through soil extraction and subsequent peroxidation. *Journal of Hazardous Materials* 99 (3), 265-276.
- Diggs, D.L., Huderson, A.C., Harris, K.L., Myers, J.N., Banks, L.D., Rekhadevi, P.V., Niaz, M.S., Ramesh, A., 2011. Polycyclic aromatic hydrocarbons and digestive tract cancers: a perspective. *Journal of Environmental Science and Health, Part C* 29 (4), 324-357.
- Dos Santos, E.V., Sáez, C., Martínez-Huitle, C.A., Cañizares, P., Rodrigo, M.A., 2015. Combined soil washing and CDEO for the removal of atrazine from soils. *Journal of Hazardous Materials* 300, 129-134.
- Duan, L., Naidu, R., Thavamani, P., Meaklim, J., Megharaj, M., 2015. Managing long-term polycyclic aromatic hydrocarbon contaminated soils: a risk-based approach. *Environmental Science and Pollution Research* 22 (12), 8927-8941.
- Dudhagara, D.R., Rajpara, R.K., Bhatt, J.K., Gosai, H.B., Sachaniya, B.K., Dave, B.P.,

2016. Distribution, sources and ecological risk assessment of PAHs in historically contaminated surface sediments at Bhavnagar coast, Gujarat, India. *Environmental Pollution* 213, 338-346.
- Edwards, S.C., Jedrychowski, W., Butscher, M., Camann, D., Kieltyka, A., Mroz, E., Flak, E., Li, Z., Wang, S., Rauh, V., 2010. Prenatal exposure to airborne polycyclic aromatic hydrocarbons and children's intelligence at 5 years of age in a prospective cohort study in Poland. *Environmental Health Perspectives* 118 (9), 1326-1331.
- Gamboa, R.T., Gamboa, A.R., Bravo, A.H., Ostrosky, W.P., 2008. Genotoxicity in child populations exposed to polycyclic aromatic hydrocarbons (PAHs) in the air from Tabasco, Mexico. *International journal of environmental research and public health* 5 (5), 349-355.
- Gan, S., Lau, E.V., Ng, H.K., 2009. Remediation of soils contaminated with polycyclic aromatic hydrocarbons (PAHs). *Journal of Hazardous Materials* 172 (2), 532-549.
- Guan, Y.-H., Ma, J., Li, X.-C., Fang, J.-Y., Chen, L.-W., 2011. Influence of pH on the formation of sulfate and hydroxyl radicals in the UV/peroxymonosulfate system. *Environmental Science & Technology* 45 (21), 9308-9314.
- Hanna, K., Chiron, S., Oturan, M.A., 2005. Coupling enhanced water solubilization with cyclodextrin to indirect electrochemical treatment for pentachlorophenol contaminated soil remediation. *Water Research* 39 (12), 2763-2773.
- Hanna, K., De Brauer, C., Germain, P., Chovelon, J., Ferronato, C., 2004. Degradation of pentachlorophenol in cyclodextrin extraction effluent using a photocatalytic process. *Science of The Total Environment* 332 (1-3), 51-60.
- Haritash, A., Kaushik, C., 2009. Biodegradation aspects of polycyclic aromatic hydrocarbons (PAHs): a review. *Journal of Hazardous Materials* 169 (1-3), 1-15.

- House, D.A., 1962. Kinetics and mechanism of oxidations by peroxydisulfate. *Chemical Reviews* 62 (3), 185-203.
- Hussein, I., Mona, S., 2016. A review on polycyclic aromatic hydrocarbons: Source, environmental impact, effect on human health and remediation. *Egyptian Journal of Petroleum* 25 (1), 107-123.
- Hussein, T.A., Ismail, Z.Z., 2013. Validation of recycling electrochemically treated surfactant solutions for washing the PAHs-contaminated soil. *Polycyclic Aromatic Compounds* 33 (3), 208-220.
- I Litter, M., Quici, N., 2010. Photochemical advanced oxidation processes for water and wastewater treatment. *Recent Patents on Engineering* 4 (3), 217-241.
- Ibhadon, A.O., Fitzpatrick, P., 2013. Heterogeneous photocatalysis: recent advances and applications. *Catalysts* 3 (1), 189-218.
- Iglesias, O., Sanromán, M.A., Pazos, M., 2014. Surfactant-enhanced solubilization and simultaneous degradation of phenanthrene in marine sediment by electro-Fenton treatment. *Industrial & Engineering Chemistry Research* 53 (8), 2917-2923.
- Kadri, T., Rouissi, T., Brar, S.K., Cledon, M., Sarma, S., Verma, M., 2017. Biodegradation of polycyclic aromatic hydrocarbons (PAHs) by fungal enzymes: A review. *Journal of Environmental Sciences* 51, 52-74.
- Kaushik, C., Haritash, A., 2006. Polycyclic aromatic hydrocarbons (PAHs) and environmental health. *Our earth* 3 (3), 1-7.
- Kavitha, V., Palanivelu, K., 2004. The role of ferrous ion in Fenton and photo-Fenton processes for the degradation of phenol. *Chemosphere* 55 (9), 1235-1243.
- Kim, C., Ahn, J.-Y., Kim, T.Y., Hwang, I., 2020. Mechanisms of electro-assisted persulfate/nano-Fe⁰ oxidation process: Roles of redox mediation by dissolved Fe. *Journal of Hazardous Materials* 388, 121739.

- Kolthoff, I., Miller, I., 1951. The chemistry of persulfate. I. The kinetics and mechanism of the decomposition of the persulfate ion in aqueous medium. *Journal of The American Chemical Society* 73 (7), 3055-3059.
- Kuma, K., Nakabayashi, S., Matsunaga, K., 1995. Photoreduction of Fe (III) by hydroxycarboxylic acids in seawater. *Water Research* 29 (6), 1559-1569.
- Kuppusamy, S., Thavamani, P., Venkateswarlu, K., Lee, Y.B., Naidu, R., Megharaj, M., 2017. Remediation approaches for polycyclic aromatic hydrocarbons (PAHs) contaminated soils: Technological constraints, emerging trends and future directions. *Chemosphere* 168, 944-968.
- Lamichhane, S., Bal Krishna, K.C., Sarukkalige, R., 2017. Surfactant-enhanced remediation of polycyclic aromatic hydrocarbons: A review. *Journal of Environmental Management* 199, 46-61.
- Ledakowicz, S., Miller, J.S., Olejnik, D., 1999. Oxidation of PAHs in water solutions by ultraviolet radiation combined with hydrogen peroxide. *International Journal of Photoenergy* 1.
- Legrini, O., Oliveros, E., Braun, A., 1993. Photochemical processes for water treatment. *Chemical Reviews* 93 (2), 671-698.
- Lin, H., Wu, J., Zhang, H., 2014. Degradation of clofibric acid in aqueous solution by an EC/Fe³⁺/PMS process. *Chemical Engineering Journal* 244, 514-521.
- Lindsey, M.E., Xu, G., Lu, J., Tarr, M.A., 2003. Enhanced Fenton degradation of hydrophobic organics by simultaneous iron and pollutant complexation with cyclodextrins. *Science of The Total Environment* 307 (1-3), 215-229.
- Long, A., Lei, Y., Zhang, H., 2014. Degradation of toluene by a selective ferrous ion activated persulfate oxidation process. *Industrial & Engineering Chemistry Research* 53 (3), 1033-1039.

- Long, A., Zhang, H., Lei, Y., 2013. Surfactant flushing remediation of toluene contaminated soil: Optimization with response surface methodology and surfactant recovery by selective oxidation with sulfate radicals. *Separation and Purification Technology* 118, 612-619.
- Makkar, R.S., Rockne, K.J., 2003. Comparison of synthetic surfactants and biosurfactants in enhancing biodegradation of polycyclic aromatic hydrocarbons. *Environmental Toxicology and Chemistry: An International Journal* 22 (10), 2280-2292.
- Man, Y.B., Kang, Y., Wang, H.S., Lau, W., Li, H., Sun, X.L., Giesy, J.P., Chow, K.L., Wong, M.H., 2013. Cancer risk assessments of Hong Kong soils contaminated by polycyclic aromatic hydrocarbons. *Journal of Hazardous Materials* 261, 770-776.
- Mao, X., Jiang, R., Xiao, W., Yu, J., 2015. Use of surfactants for the remediation of contaminated soils: A review. *Journal of Hazardous Materials* 285, 419-435.
- Mark, G., Schuchmann, M.N., Schuchmann, H.-P., von Sonntag, C., 1990. The photolysis of potassium peroxodisulphate in aqueous solution in the presence of tert-butanol: a simple actinometer for 254 nm radiation. *Journal of Photochemistry and Photobiology A: Chemistry* 55 (2), 157-168.
- Matzek, L.W., Carter, K.E., 2016. Activated persulfate for organic chemical degradation: a review. *Chemosphere* 151, 178-188.
- McKay, D., Shiu, W.Y., Ma, K.-C., 1992. *Illustrated Handbook of Physical-chemical Properties and Environmental Fate for Organic Chemicals: Polynuclear aromatic hydrocarbons, polychlorinated dioxins and dibenzofurans*, Lewis Publishers.
- Mehrasbi, M.R., Safa, S., Mahvi, A.H., Assadi, A., Mohammadi, H., 2012. Application of photo-Fenton process for COD removal from wastewater produced from surfactant-washed oil-contaminated (TPH) soils. *Iranian Journal of Health and*

- Environment 5 (3), 295-306.
- Miklos, D.B., Remy, C., Jekel, M., Linden, K.G., Drewes, J.E., Hübner, U., 2018. Evaluation of advanced oxidation processes for water and wastewater treatment—A critical review. *Water Research* 139, 118-131.
- Miralles-Cuevas, S., Oller, I., Pérez, J.S., Malato, S., 2014. Removal of pharmaceuticals from MWTP effluent by nanofiltration and solar photo-Fenton using two different iron complexes at neutral pH. *Water Research* 64, 23-31.
- Mousset, E., Huguenot, D., van Hullebusch, E.D., Oturan, N., Guibaud, G., Esposito, G., Oturan, M.A., 2016. Impact of electrochemical treatment of soil washing solution on PAH degradation efficiency and soil respirometry. *Environmental Pollution* 211 (6), 354-362.
- Mousset, E., Oturan, N., Hullebusch, E.D.V., Guibaud, G., Esposito, G., Oturan, M.A., 2014a. Influence of solubilizing agents (cyclodextrin or surfactant) on phenanthrene degradation by electro-Fenton process – study of soil washing recycling possibilities and environmental impact. *Water Research* 48 (1), 306-316.
- Mousset, E., Oturan, N., Van Hullebusch, E.D., Guibaud, G., Esposito, G., Oturan, M.A., 2014b. Treatment of synthetic soil washing solutions containing phenanthrene and cyclodextrin by electro-oxidation. Influence of anode materials on toxicity removal and biodegradability enhancement. *Applied Catalysis B: Environmental* 160, 666-675.
- Mulligan, C.N., Yong, R., Gibbs, B., 2001. Surfactant-enhanced remediation of contaminated soil: a review. *Engineering Geology* 60 (1-4), 371-380.
- Muñoz-Morales, M., Braojos, M., Sáez, C., Cañizares, P., Rodrigo, M., 2017. Remediation of soils polluted with lindane using surfactant-aided soil washing and electrochemical oxidation. *Journal of Hazardous Materials* 339, 232-238.

- Occulti, F., Roda, G.C., Berselli, S., Fava, F., 2008. Sustainable decontamination of an actual-site aged PCB-polluted soil through a biosurfactant-based washing followed by a photocatalytic treatment. *Biotechnology and bioengineering* 99 (6), 1525-1534.
- Oturan, M.A., Aaron, J.-J., 2014. Advanced oxidation processes in water/wastewater treatment: principles and applications. A review. *Critical Reviews in Environmental Science and Technology* 44 (23), 2577-2641.
- Oturan, N., Zhou, M., Oturan, M.A., 2010. Metomyl degradation by electro-Fenton and electro-Fenton-like processes: a kinetics study of the effect of the nature and concentration of some transition metal ions as catalyst. *The Journal of Physical Chemistry A* 114 (39), 10605-10611.
- Panagos, P., Van Liedekerke, M., Yigini, Y., Montanarella, L., 2013. Contaminated sites in Europe: review of the current situation based on data collected through a European network. *Journal of Environmental and Public Health* 2013.
- Panizza, M., Cerisola, G., 2009. Direct and mediated anodic oxidation of organic pollutants. *Chemical Reviews* 109 (12), 6541-6569.
- Panizza, M., Martinez-Huitle, C.A., 2013. Role of electrode materials for the anodic oxidation of a real landfill leachate—Comparison between Ti–Ru–Sn ternary oxide, PbO₂ and boron-doped diamond anode. *Chemosphere* 90 (4), 1455-1460.
- Parsons, S., 2004. *Advanced oxidation processes for water and wastewater treatment*, IWA publishing.
- Patnaik, P., 2007. *A comprehensive guide to the hazardous properties of chemical substances*, John Wiley & Sons.
- Petitgirard, A., Djehiche, M., Persello, J., Fievet, P., Fatin-Rouge, N., 2009. PAH contaminated soil remediation by reusing an aqueous solution of cyclodextrins.

Chemosphere 75 (6), 714-718.

Petrová, Š., Rezek, J., Soudek, P., Vaněk, T., 2017. Preliminary study of phytoremediation of brownfield soil contaminated by PAHs. *Science of The Total Environment* 599, 572-580.

Qiu, Y., Xu, M., Sun, Z., Li, H., 2019. Remediation of PAH-Contaminated Soil by Combining Surfactant Enhanced Soil Washing and Iron-Activated Persulfate Oxidation Process. *International journal of environmental research and public health* 16 (3), 441.

Rahmanpoor, S., Ghafourian, H., Hashtroudi, S.M., Bastami, K.D., 2014. Distribution and sources of polycyclic aromatic hydrocarbons in surface sediments of the Hormuz strait, Persian Gulf. *Marine pollution bulletin* 78 (1-2), 224-229.

Riaza-Frutos, A., Quiroga, J., Manzano, M., 2007. Remediation of contaminated soils with PCBs using an integrated treatment: desorption and oxidation. *Journal of Environmental Engineering* 133 (5), 541-547.

Rosas, J., Vicente, F., Santos, A., Romero, A., 2013. Soil remediation using soil washing followed by Fenton oxidation. *Chemical Engineering Journal* 220, 125-132.

Rubio-Clemente, A., Torres-Palma, R.A., Peñuela, G.A., 2014. Removal of polycyclic aromatic hydrocarbons in aqueous environment by chemical treatments: a review. *Science of The Total Environment* 478, 201-225.

Tan, C., Gao, N., Chu, W., Li, C., Templeton, M.R., 2012. Degradation of diuron by persulfate activated with ferrous ion. *Separation and Purification Technology* 95, 44-48.

Tran, L.-H., Drogui, P., Mercier, G., Blais, J.-F., 2010. Comparison between Fenton oxidation process and electrochemical oxidation for PAH removal from an amphoteric surfactant solution. *Journal of Applied Electrochemistry* 40 (8), 1493-

1510.

- Trellu, C., Mousset, E., Pechaud, Y., Huguenot, D., van Hullebusch, E.D., Esposito, G., Oturan, M.A., 2016a. Removal of hydrophobic organic pollutants from soil washing/flushing solutions: A critical review. *Journal of Hazardous Materials* 306, 149-174.
- Trellu, C., Pechaud, Y., Oturan, N., Mousset, E., Huguenot, D., Van Hullebusch, E.D., Esposito, G., Oturan, M.A., 2016b. Comparative study on the removal of humic acids from drinking water by anodic oxidation and electro-Fenton processes: mineralization efficiency and modelling. *Applied Catalysis B: Environmental* 194, 32-41.
- Tsitonaki, A., Petri, B., Crimi, M., Mosbæk, H., Siegrist, R.L., Bjerg, P.L., 2010. In situ chemical oxidation of contaminated soil and groundwater using persulfate: a review. *Critical Reviews in Environmental Science and Technology* 40 (1), 55-91.
- Umar, M., Aziz, H.A., Yusoff, M.S., 2010. Trends in the use of Fenton, electro-Fenton and photo-Fenton for the treatment of landfill leachate. *Waste management* 30 (11), 2113-2121.
- Veignie, E., Rafin, C., Landy, D., Fourmentin, S., Surpateanu, G., 2009. Fenton degradation assisted by cyclodextrins of a high molecular weight polycyclic aromatic hydrocarbon benzo [a] pyrene. *Journal of Hazardous Materials* 168 (2-3), 1296-1301.
- Vidales, M.J.M., Castro, M.P., Saez, C., Canizares, P., Rodrigo, M.A., 2019. Radiation-assisted electrochemical processes in semi-pilot scale for the removal of clopyralid from soil washing wastes. *Separation and Purification Technology* 208, 100-109.
- Villa, R.D., Trovó, A.G., Nogueira, R.F.P., 2010. Soil remediation using a coupled process: soil washing with surfactant followed by photo-Fenton oxidation. *Journal*

- of Hazardous Materials 174 (1-3), 770-775.
- Von Lau, E., Gan, S., Ng, H.K., Poh, P.E., 2014. Extraction agents for the removal of polycyclic aromatic hydrocarbons (PAHs) from soil in soil washing technologies. *Environmental Pollution* 184, 640-649.
- Wacławek, S., Lutze, H.V., Grübel, K., Padil, V.V., Černík, M., Dionysiou, D.D., 2017. Chemistry of persulfates in water and wastewater treatment: a review. *Chemical Engineering Journal* 330, 44-62.
- Wang, G., Kleinedam, S., Grathwohl, P., 2007. Sorption/desorption reversibility of phenanthrene in soils and carbonaceous materials. *Environmental Science & Technology* 41 (4), 1186-1193.
- Wang, Z., Sun, T., Luo, T., Shi, X., Lin, H., Zhang, H., 2020. Selective removal of phenanthrene for the recovery of sodium dodecyl sulfate by UV-C and UV-C/PDS processes: performance, mechanism and soil washing recycling. *Journal of Hazardous Materials*, 123141.
- Warshawsky, D., 2001. Polycyclic and heterocyclic aromatic hydrocarbons. *Patty's Toxicology*.
- Wassenberg, D., Di Giulio, R., 2004. Synergistic embryotoxicity of polycyclic hydrocarbon receptor agonists with cytochrome P4501A inhibitors in *Fundulus heteroclitus*. *Environ Health Perspect* 112 (17), 1658-1664.
- Wild, S.R., Waterhouse, K.S., McGrath, S.P., Jones, K.C., 1990. Organic contaminants in an agricultural soil with a known history of sewage sludge amendments: polynuclear aromatic hydrocarbons. *Environmental Science & Technology* 24 (11), 1706-1711.
- Wilson, S.C., Jones, K.C., 1993. Bioremediation of soil contaminated with polynuclear aromatic hydrocarbons (PAHs): a review. *Environmental Pollution* 81 (3), 229-

- Wolska, L., Mechlińska, A., Rogowska, J., Namieśnik, J., 2012. Sources and fate of PAHs and PCBs in the marine environment. *Critical Reviews in Environmental Science and Technology* 42 (11), 1172-1189.
- Wu, B., Zhang, Y., Zhang, X.-X., Cheng, S.-P., 2011. Health risk assessment of polycyclic aromatic hydrocarbons in the source water and drinking water of China: quantitative analysis based on published monitoring data. *Science of The Total Environment* 410, 112-118.
- Xiao, Y., Zhang, L., Zhang, W., Lim, K.-Y., Webster, R.D., Lim, T.-T., 2016. Comparative evaluation of iodoacids removal by UV/persulfate and UV/H₂O₂ processes. *Water Research* 102, 629-639.
- Yan, J., Gao, W., Qian, L., Han, L., Chen, Y., Chen, M., 2015. Remediation of nitrobenzene contaminated soil by combining surfactant enhanced soil washing and effluent oxidation with persulfate. *PloS one* 10 (8), e0132878.
- Yan, J., Wang, L., Fu, P.P., Yu, H., 2004. Photomutagenicity of 16 polycyclic aromatic hydrocarbons from the US EPA priority pollutant list. *Mutation Research/Genetic Toxicology and Environmental Mutagenesis* 557 (1), 99-108.
- Yan, S., Geng, J., Guo, R., Du, Y., Zhang, H., 2017. Hydronium jarosite activation of peroxymonosulfate for the oxidation of organic contaminant in an electrochemical reactor driven by microbial fuel cell. *Journal of Hazardous Materials* 333, 358-368.
- Yang, L., Xue, J., He, L., Wu, L., Ma, Y., Chen, H., Li, H., Peng, P., Zhang, Z., 2019. Review on ultrasound assisted persulfate degradation of organic contaminants in wastewater: Influences, mechanisms and prospective. *Chemical Engineering Journal* 378, 122146.

- Yang, S., Wang, P., Yang, X., Shan, L., Zhang, W., Shao, X., Niu, R., 2010. Degradation efficiencies of azo dye Acid Orange 7 by the interaction of heat, UV and anions with common oxidants: persulfate, peroxymonosulfate and hydrogen peroxide. *Journal of Hazardous Materials* 179 (1-3), 552-558.
- Yap, C., Gan, S., Ng, H., 2010. Application of vegetable oils in the treatment of polycyclic aromatic hydrocarbons-contaminated soils. *Journal of Hazardous Materials* 177 (1-3), 28-41.
- Yardin, G., Chiron, S., 2006. Photo-Fenton treatment of TNT contaminated soil extract solutions obtained by soil flushing with cyclodextrin. *Chemosphere* 62 (9), 1395-1402.
- Zhang, D., Zhu, L., 2012. Effects of Tween 80 on the removal, sorption and biodegradation of pyrene by *Klebsiella oxytoca* PYR-1. *Environmental Pollution* 164, 169-174.
- Zhang, P., Chen, Y., 2017. Polycyclic aromatic hydrocarbons contamination in surface soil of China: A review. *Science of The Total Environment* 605, 1011-1020.
- Zhang, Y., Wong, J., Liu, P., Yuan, M., 2011. Heterogeneous photocatalytic degradation of phenanthrene in surfactant solution containing TiO₂ particles. *Journal of Hazardous Materials* 191 (1-3), 136-143.
- Zhao, D., Liao, X., Yan, X., Huling, S.G., Chai, T., Tao, H., 2013. Effect and mechanism of persulfate activated by different methods for PAHs removal in soil. *Journal of Hazardous Materials* 254, 228-235.
- Zhi, D., Lin, Y., Jiang, L., Zhou, Y., Huang, A., Yang, J., Luo, L., 2020. Remediation of persistent organic pollutants in aqueous systems by electrochemical activation of persulfates: a review. *Journal of Environmental Management* 260, 110125.
- Zhou, Y., Xiang, Y., He, Y., Yang, Y., Zhang, J., Luo, L., Peng, H., Dai, C., Zhu, F., Tang,

- L., 2018. Applications and factors influencing of the persulfate-based advanced oxidation processes for the remediation of groundwater and soil contaminated with organic compounds. *Journal of Hazardous Materials* 359, 396-407.
- Zhu, L., Zhou, W., 2008. Partitioning of polycyclic aromatic hydrocarbons to solid-sorbed nonionic surfactants. *Environmental Pollution* 152 (1), 130-137.

**Chapter 3 Phenanthrene decomposition in soil
washing effluents using UVB/H₂O₂ and UVB/PS**

3.1 Introduction

In the past few decades, advanced oxidation processes (AOPs) have been developed and widely applied as alternative technologies for the degradation of recalcitrant pollutants in waters and soils (Liu et al., 2016a; Mousset et al., 2014a; Wan et al., 2018; Wu et al., 2015). This is mainly attributed to the formation of reactive species with high standard redox potential such as hydroxyl radical (HO^\bullet , $E^0 = 1.8\text{-}2.7\text{ V}$) or sulfate radical ($\text{SO}_4^{\bullet-}$, $E^0 = 2.5\text{-}3.1\text{ V}$) (Buxton et al., 1988a; Neta et al., 1988). As efficient and environmental friendly techniques, HO^\bullet or $\text{SO}_4^{\bullet-}$ based AOPs have been extensively investigated for the treatment of contaminants in water under UV irradiation (UVA, UVB and UVC) (Huang et al., 2018a; Minella et al., 2019; Mosteo et al., 2020; Xiao et al., 2016; Xu et al., 2016; Yang et al., 2016; Zhang et al., 2015; Zhou et al., 2017b). Compared with UVA and UVC, UVB based oxidation has great potential due to: *i*) possible use of LED *ii*) considerably less energy requirement than UVC (Beck et al., 2017) and *iii*) higher efficiency for contaminant degradation than UVA (Joseph et al., 2016). After reviewing the literature, it is found that the investigation on HOCs decomposition by UVB-based oxidation is pretty limited and no studies for systematic comparison of SW effluent treatment by UVB activation of PS and H_2O_2 are reported before.

The presence of inorganic anions has been reported to exert strong impacts on the oxidative degradation of contaminants (Bennedsen et al., 2012; Liu et al., 2016a; Yang et al., 2014b). However, the effect of these anions on the photo-degradation of PHE in the SW effluent has not been investigated before. In this study, for the first time, UVB irradiation was used to activate H_2O_2 and PS for PHE decomposition in a surfactant co-existing SW effluent. In this study PHE decomposition efficiency in the presence of TW80 by direct UVB radiation, UVB/ H_2O_2 , and UVB/PS processes was investigated.

The impact of operating factors including the oxidant dosage, the initial pH and the coexisting anions on PHE treatment efficiency was evaluated. The performance of UVB, UVB/H₂O₂ and UVB/PS systems on PHE oxidation in the real SW solutions was assessed.

3.2 Materials and methods

3.2.1 Chemicals

TW80, phenanthrene (PHE), sodium persulfate (Na₂S₂O₈, ≥ 99.0%), sodium chloride (NaCl, ≥ 99.5%), sodium bicarbonate (NaHCO₃, ≥ 99.7%) and sodium nitrate (NaNO₃, ≥ 99.0%) were purchased from Sigma-Aldrich. Hydrogen peroxide (H₂O₂, 30%) was obtained from Fluka, France. Perchloric acid (HClO₄) and sodium hydroxide (NaOH) were applied for adjusting the initial pH of the solutions. Millipore Ultra-Pure System purified water (18.2 MΩ cm) was used to prepare solutions. All the chemical reagents were of analytical grade and employed without further purification.

3.2.2 Preparation of the mimic and real SW solutions

One liter of mimic SW solution was prepared using the similar method as previously reported (Mousset et al., 2014a). Briefly, 10 mg of PHE was added to 1 L aqueous solution containing 0.5 g L⁻¹ TW80. The mixed solution was vigorously stirred for one week to obtain complete PHE dissolution before irradiation experiments.

Natural soil samples were obtained from Wuhan of Hubei Province (soil 1), Chuzhou of Anhui Province (soil 2) and Huaian of Jiangsu Province (soil 3), respectively. The collected soils were air dried and ground to obtain particles less than 2 mm before use. The PHE contaminated soil samples were prepared according to the literature (Yang et al., 2006). Briefly, the three PHE free soils were spiked with PHE dissolved in acetone solutions and vigorously stirred for 30 minutes to obtain homogeneous distribution of

PHE in the soil. The spiked soil samples were placed in three hoods for 5 days at room temperature to evaporate the solvent. The final PHE concentrations of each spiked soil were 4000 mg kg⁻¹.

To obtain the real SW solutions, 3 grams of each contaminated soil were separately weighed into 150 mL conical flasks with stoppers and 60 mL TW80 solutions (10 g L⁻¹) were added. The flasks were then placed into a constant temperature shaker for 24h with a speed of 200 rpm at 25 °C. Then, the mixtures were centrifuged at 8000 rpm for 15 min and the supernatants were filtered with 0.22 µm PTFE filters before analysis and the sequent irradiation experiments.

3.2.3 Irradiation experiments

Irradiations experiments were carried out in a cylindrical Pyrex reactor (100 mL) which was placed into a rectangular glass jacket vessel with cooling water flowing between interlayers ensuring a constant temperature of 20 ± 2 °C through a thermostat-controlled cooling system. Four UVB tubes (G15T8E, Japan) were fixed on the top of the photo-reactor as the light source, and the distance between photoreactor and the lamps was around 24 cm. The schematic diagram of experimental set-up is shown in Figure 3-1.

To perform the irradiation experiment, 100 mL SW solutions were added to the photo reactor, after addition of appreciate amount of oxidant, pH was adjusted to the pre-determined value and the experiments started with the irradiation lamps on. During the irradiation, the SW solution was continuously magnetically stirred at a fixed speed with a magnetic stirrer. At fixed interval times, 1 mL of sample was withdrawn and analyzed.

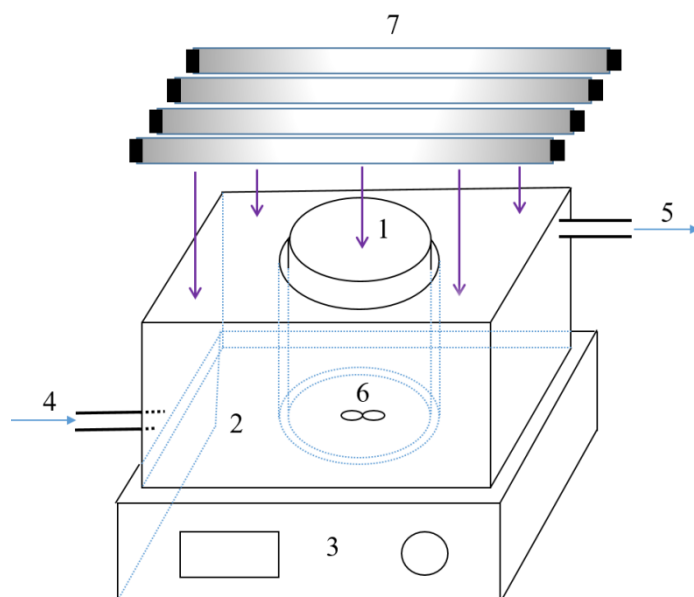


Figure 3-1 Schematic representation of the experimental setup. 1. Cylindrical Pyrex reactor; 2. Rectangular glass vessel for cooling water; 3. Magnetic stirrer; 4. Inlet of cooling water; 5. Outlet of cooling water; 6. Magnet; 7. The UVB lamps.

3.2.4 Analytic methods

The polychromatic UVB irradiation energy was recorded by an optical fiber with a charge coupled device spectrophotometer (Ocean Optics USD 2000 + UV-vis). The total irradiance reaching the solution was then estimated to be $1393 \mu\text{W cm}^{-2}$ in the UVB range (between 270 and 400 nm). The absorption spectra of PS, H_2O_2 and PHE solution in TW80 were recorded with a UV-visible spectrophotometer Cary 300. Emission spectrum of adopted UVB lamps reaching the solution was recorded using a calibrated CCD camera (Huang et al., 2018a) as presented in Figure 3-2.

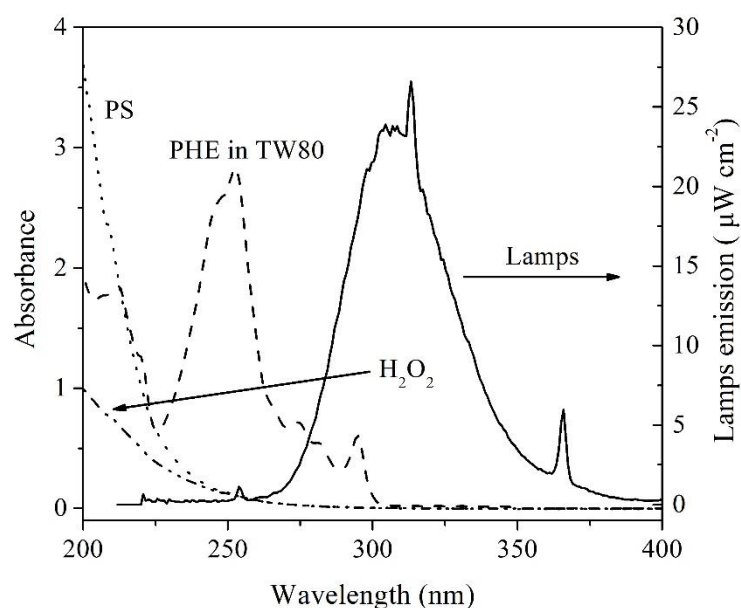


Figure 3-2 Absorption spectra of H_2O_2 (5 mM), PS (5 mM), PHE (10 mg L^{-1} in 0.5 g L^{-1} of TW80) and emission spectrum of the adopted UVB lamps.

PHE concentration was detected by a high performance liquid chromatography (HPLC, Alliance) equipped with a Waters 2998 photodiode array detector. The flow rate was 1 mL min^{-1} and an isocratic elution with water and acetonitrile (15/85, v/v) was used. The column was a Nucleodur 100-5 C18 of $150 \text{ mm} \times 4.6 \text{ mm}$, with particle size of $5 \mu\text{m}$.

The pseudo-first order rate constant of PHE decomposition (k_1) was determined from Eq. (3-1):

$$[\text{PHE}]/[\text{PHE}]_0 = \exp(-k_1 t) \quad (3-1)$$

where $[\text{PHE}]_0$ and $[\text{PHE}]$ were the PHE initial concentration and PHE concentration at time t , respectively.

Inorganic components of three real SW effluents were determined by ion chromatography. For anions, a Dionex DX320 system equipped with an IonPac AS11 column and a KOH elution in gradient mode were used. For cations, a Dionex ICS-1500 system equipped with an Ion-Pac CS16 column and a metasulfonic acid (MSA) eluent were employed (Marion et al., 2018).

TW80 concentration after soil washing process was quantified by a spectrophotometric method using cobalt ammonium thiocyanate as the chromogenic agent (Crabb and Persinger 1964).

3.3 Results and discussion

3.3.1 Comparison of UVB activation of H₂O₂ and PS

In Figure 3-3, the decomposition of PHE (10 mg L⁻¹ corresponding to ~56 µM in 0.5 g L⁻¹ TW80 solution) is reported. Under direct photolysis (UVB alone), about 23.0% of PHE decay was observed after 3 h irradiation with a first order rate constant (k_1) of $1.5 \times 10^{-3} \text{ min}^{-1}$, which is equivalent to a half-life of 7.8 h (Table 3-1). When the oxidant (H₂O₂ or PS) was applied to the irradiation system, HO[•] and SO₄^{•-} were generated through photo-dissociation of H₂O₂ and PS under UVB irradiation (reactions 3-2 and 3-3) (Mark et al., 1990a; Yu and Barker 2003b).



During UVB/H₂O₂ and UVB/PS processes PHE removal reached up to 34.0% and 72.0%, respectively. The pseudo-first order rate constants were $2.3 \times 10^{-3} \text{ min}^{-1}$ with H₂O₂ and $7.1 \times 10^{-3} \text{ min}^{-1}$ with PS. The correspondent half-lives of PHE were calculated to be 5.0 h and 1.6 h in the UVB/H₂O₂ and UVB/PS systems, respectively (Table 3-1).

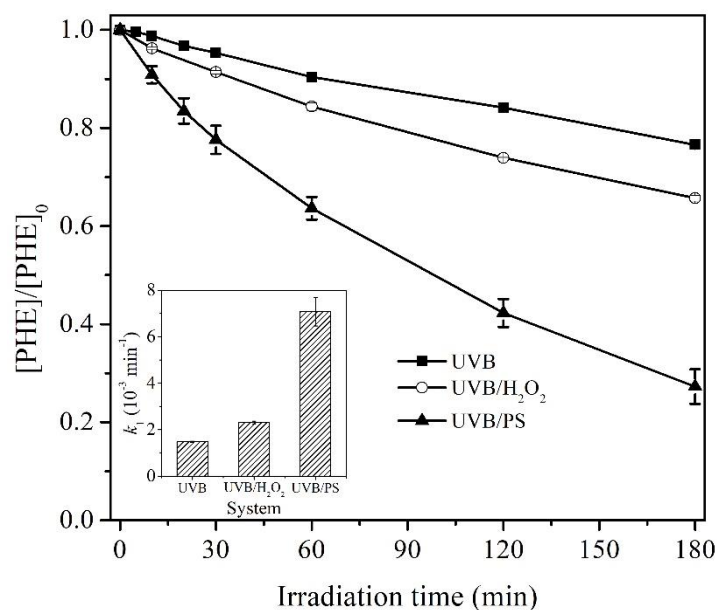


Figure 3-3 Degradation of PHE in the presence of TW80 in different systems. Inserts are the corresponding pseudo-first order rate constants. Initial conditions: [PHE] = 10 mg L⁻¹, [TW80] = 0.5 g L⁻¹, [PS] = [H₂O₂] = 5 mM, pH 3.3 ± 0.1.

Table 3-1 Pseudo-first-order rate constants and half-lives for PHE oxidation in the UVB, UVB/H₂O₂ and UVB/PS systems.

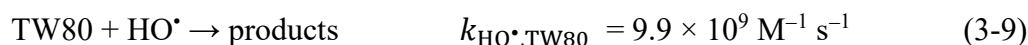
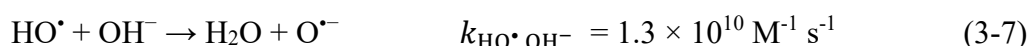
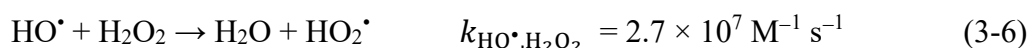
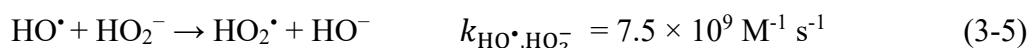
System	The pseudo-first order rate constant	Half-live	R^2
	(k_1, min^{-1})	$(t_{1/2}, \text{h})$	
UVB	$(1.5 \pm 0.05) \times 10^{-3}$	7.8 ± 0.1	0.996
UVB/H ₂ O ₂	$(2.3 \pm 0.09) \times 10^{-3}$	5.0 ± 0.1	0.993
UVB/PS	$(7.1 \pm 0.60) \times 10^{-3}$	1.6 ± 0.1	0.997

The different performance between UVB/H₂O₂ and UVB/PS systems could be ascribed to the following aspects. Firstly, the photo-dissociation quantum yield of PS is higher than that for H₂O₂. In fact, near the maximum emission wavelength of UVB (313 nm in Figure 3-2), the reported SO₄^{•-} formation quantum yield from PS photolysis ($\Phi_{\text{SO}_4^{\bullet-}}$) is 1.1 ± 0.2 (Herrmann 2007), which is higher than the quantum yield for HO[•]

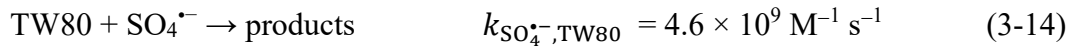
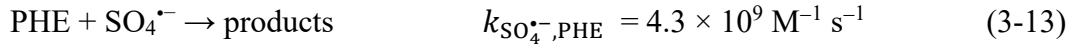
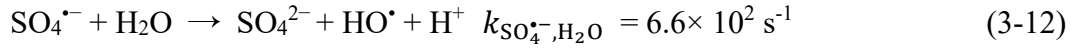
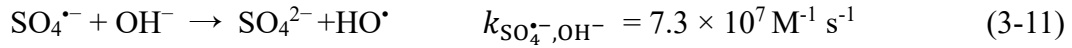
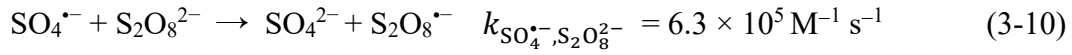
generation from H_2O_2 , i.e., 0.98 ± 0.2 (Zellner et al., 1990) or 0.8 ± 0.2 (Yu and Barker 2003b) at the wavelength of 308 nm. Secondly, the selectivity of $\text{SO}_4^{\bullet-}$ towards PHE is superior to that of HO^\bullet (Tao et al., 2019). To verify this point, the selectivity coefficient ζ_{PHE} is defined as Eq. (3-4) based on the reactions of radicals with PHE, TW80 and other species in the system.

$$\zeta_{\text{PHE}} = \frac{k_{\text{X}^\bullet, \text{PHE}}[\text{PHE}]_0}{k_{\text{X}^\bullet, \text{PHE}}[\text{PHE}]_0 + k_{\text{X}^\bullet, \text{S}}[\text{S}]_0} \quad (3-4)$$

where $k_{\text{X}^\bullet, \text{PHE}}$ and $k_{\text{X}^\bullet, \text{S}}$ are the second order rate constants of radicals with PHE and other components S (PHE, TW80, oxidant, etc.) in the system, respectively. $[\text{PHE}]_0$ and $[\text{S}]_0$ are their initial concentrations.



In the UVB/ H_2O_2 system, HO^\bullet is the main generated radical, and ζ_{PHE} was calculated to be around 8.1% according to the reactions 3-5 to 3-9, while the selectivity coefficient was about 12.1 % calculated through reactions 3-10 to 3-14 in the UVB/PS system with $\text{SO}_4^{\bullet-}$ as the major radical. This means the selectivity coefficient ζ_{PHE} for $\text{SO}_4^{\bullet-}$ towards PHE (12.1%) is about 1.5 times higher than that of HO^\bullet (8.1%). The result confirms $\text{SO}_4^{\bullet-}$ was more selective than HO^\bullet to the oxidation of PHE in the presence of TW80 (Tao et al., 2019). Lastly, the rate constant of H_2O_2 and HO^\bullet is around 43 times higher than that of PS and $\text{SO}_4^{\bullet-}$ ($k_{\text{HO}^\bullet, \text{H}_2\text{O}_2} = 2.7 \times 10^7 \text{ M}^{-1} \text{ s}^{-1}$, $k_{\text{SO}_4^{\bullet-}, \text{S}_2\text{O}_8^{2-}} = 6.3 \times 10^5 \text{ M}^{-1} \text{ s}^{-1}$), indicating HO^\bullet would be more prone to be quenched by H_2O_2 than $\text{SO}_4^{\bullet-}$ scavenged by PS (reactions 3-6 and 3-10).



3.3.2 Effect of oxidant concentration

Effects of initial concentration of H_2O_2 or PS on PHE degradation were evaluated as reported in Figure 3-4. In the UVB/ H_2O_2 process, it can be seen from Figure 3-4a that PHE decomposition after 3 hours reached around 28.0% with 2 mM H_2O_2 and 51.0% with 30 mM H_2O_2 , and the corresponding PHE oxidation rate constant increased around 1.95 folds from 2.0×10^{-3} to $3.9 \times 10^{-3} \text{ min}^{-1}$. In the UVB/PS process as illustrated in Figure 3-4b, with 2 mM of PS, the PHE decomposition efficiency reached around 61.0% and rate constant was $5.1 \times 10^{-3} \text{ min}^{-1}$. With further addition of PS to 30 mM, the PHE elimination efficiency was around 83.0% and k_1 increased around 1.90 folds to $9.7 \times 10^{-3} \text{ min}^{-1}$. In comparison with the effect of oxidant type, the results indicated that the decomposition efficiency of PHE followed the order of $\text{PS} > \text{H}_2\text{O}_2$ at the same oxidant dosage.

Some researchers reported that the decomposition rate of contaminant increased linearly with the oxidant dosage (Deng et al., 2013; Tan et al., 2013; Xu et al., 2016), while others found that the removal rate would drop when the oxidant concentration exceeds its threshold level (Olmez-Hanci and Arslan-Alaton 2013; Yang et al., 2010; Zhou et al., 2017a). In our case, PHE removal increased almost linearly with increasing H_2O_2 concentration from 2 to 30 mM, probably because more HO^{\bullet} radicals were formed for PHE decomposition with higher H_2O_2 concentration and the maximum dosage (30

mM) was still below its threshold level. In the UVB/PS system, PHE removal efficiency also increased with the increasement of PS. However, insignificant improvement of PHE decomposition was observed at PS concentration higher than 10 mM, which possibly because the PS concentration was beyond the threshold and quenching effect of $\text{SO}_4^{\bullet-}$ radicals via Eq. (3-10) (Herrmann et al., 1995) became pronounced.

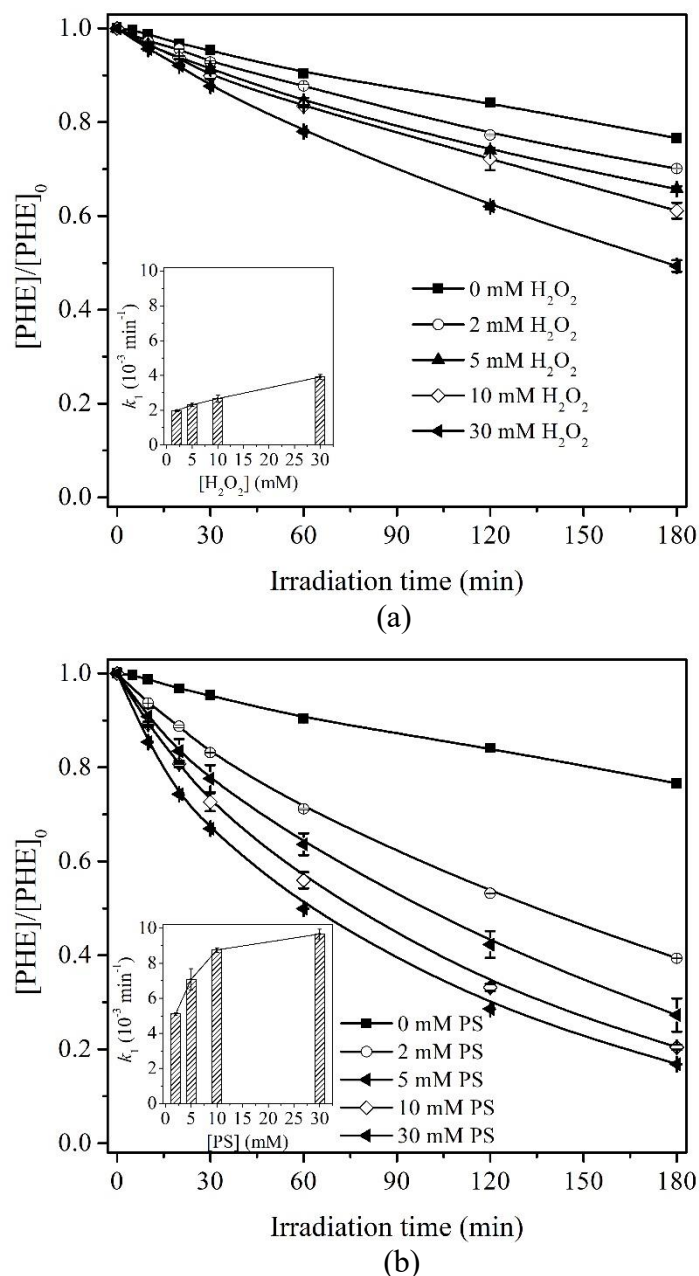


Figure 3-4 Influence of oxidant concentration on the photo-degradation of PHE. Inserts are the corresponding pseudo first order rate constants. (a) UVB/ H_2O_2 ; (b) UVB/PS.

Initial conditions: $[\text{PHE}] = 10 \text{ mg L}^{-1}$, $[\text{TW80}] = 0.5 \text{ g L}^{-1}$, $\text{pH} = 3.3 \pm 0.1$.

3.3.3 Effect of initial pH

The influence of initial pH on the photo-degradation of PHE by the UVB/H₂O₂ and UVB/PS processes is given in Figure 3-5. In the UVB/H₂O₂ system, a slight difference (less than 10.0%) was obtained from pH 3.3 to pH 10.1, though the maximum PHE decomposition extent of 40.0% and a first order rate constant of $2.8 \times 10^{-3} \text{ min}^{-1}$ were observed at pH 4.5 (Figure 3-5a). In the UVB/PS system, pH had insignificant effect on PHE decay, and the difference of PHE photo-degradation efficiency was less than 5.0% with pH value ranging from acidic to basic (Figure 3-5b). The little difference of PHE degradation with pH is probably due to the chemical stability of PHE with pH ranging from 3.3 to 10.1 and also the photolysis of H₂O₂ or PS is not pH dependent. Moreover, although the PHE degradation was performed in a quite wide initial pH range (from 3.3 to 10.1), the pH varied from 3.4 to 6.6 after UVB/H₂O₂ process, or from 3.3 to 3.8 after UVB/PS process as indicated in Table 3-2. The difference of final pH (3.3~3.8) in the UVB/PS system is less than that (3.4~6.6) in the UVB/H₂O₂ system. It is probably due to the higher degradation efficiency of PHE and more production of acidic intermediates in the UVB/PS system than in the UVB/H₂O₂ system.

Table 3-2 Initial and final pH in UVB/H₂O₂ and UVB/PS systems

Initial pH	Final pH (UVB/H ₂ O ₂)	Final pH (UVB/PS)
3.3	3.4	3.3
4.5	4.3	3.4
5.6	5.2	3.5
7.1	5.8	3.5
8.6	6.3	3.6
10.1	6.6	3.8

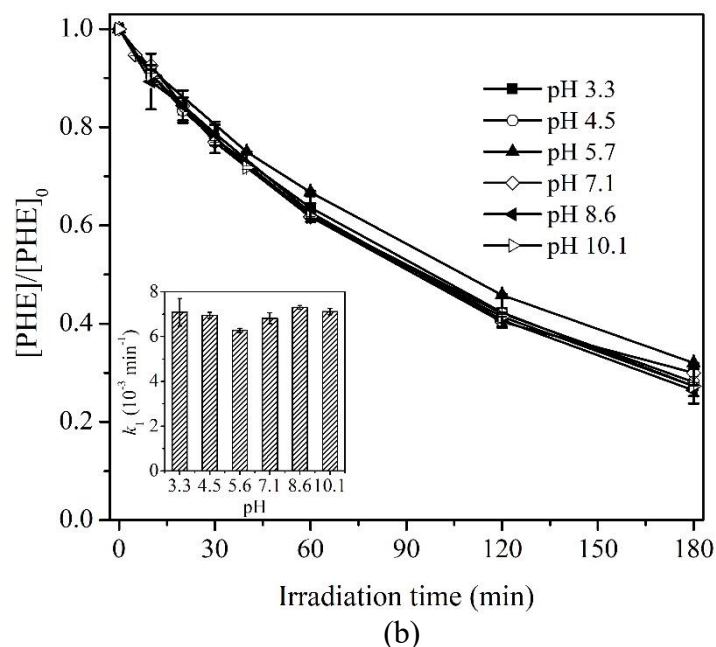
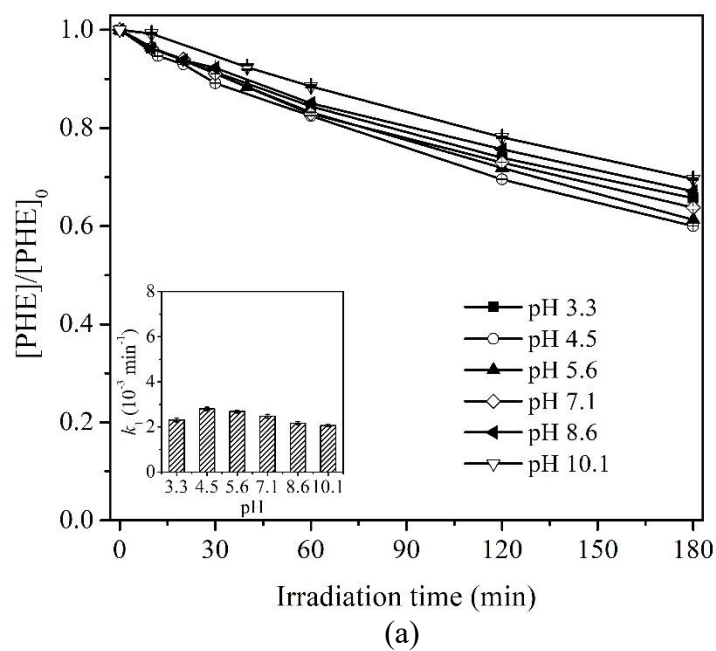


Figure 3-5 Influence of initial solution pH on the photo-degradation of PHE. Inserts are the corresponding pseudo first order rate constants. (a) UVB/H₂O₂; (b) UVB/PS. Initial conditions: $[PHE] = 10 \text{ mg L}^{-1}$, $[TW80] = 0.5 \text{ g L}^{-1}$, $[PS] = [H_2O_2] = 5 \text{ mM}$.

3.3.4 Effect of inorganic anions- chloride

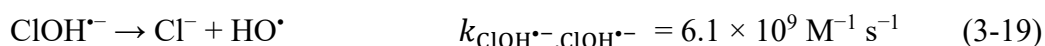
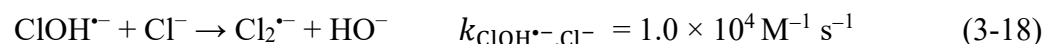
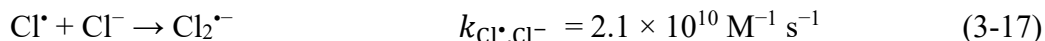
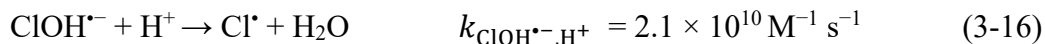
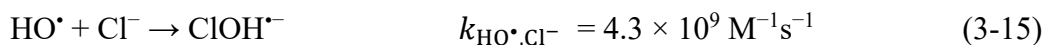
Inorganic species (such as carbonate, chloride and nitrate) are widely found in the soil due to many factors: (i) the parent soil substrate, (ii) depositions through fertilization, and (iii) other human activities such as irrigation (Du et al., 2013; Wang

et al., 2019a). These anions are generally considered to be freely mobile in soils and can be released into groundwater *via* rainfall (Bastviken et al., 2006; Lu et al., 2019b). Therefore, inorganic species (Cl^- , HCO_3^- and NO_3^-) are inevitably dissolved in the SW effluent and they may exert impact on the PHE decomposition by UVB/ H_2O_2 and UVB/PS processes.

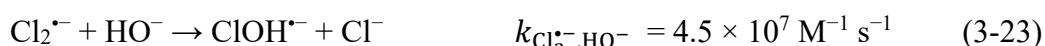
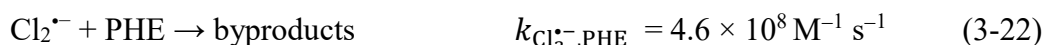
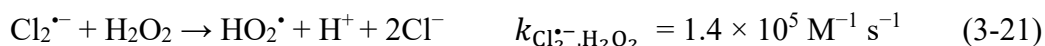
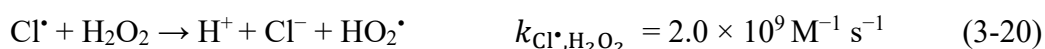
The PHE elimination as a function of Cl^- dosage at pH 3.3 of the two AOP systems is presented in Figure 3-6. The results clearly revealed that the presence of Cl^- had adverse effect on the two AOPs. In the UVB/ H_2O_2 process as shown in Figure 3-6a, the effect of 2 and 10 mM Cl^- on PHE oxidation was insignificant, while PHE decay was inhibited by around 10% with addition of 50 mM Cl^- . In the UVB/PS process as depicted in Figure 3-6b, PHE oxidation gradually increased by 9% when Cl^- concentration ranging from 0 to 10 mM and no further improvement of PHE removal can be achieved with 50 mM Cl^- . At pH 7.1, the influence of Cl^- from 2 to 50 mM on PHE removal is negligible in the UVB/ H_2O_2 system (Figure 3-6c), while PHE removal increased by 15% with Cl^- dose varying from 0 to 50 mM in the UVB/PS process (Figure 3-6d). At alkaline pH 8.6, Cl^- exerted negative effect on PHE oxidation and larger inhibition was observed with higher Cl^- concentration in the UVB/ H_2O_2 system and PHE decomposition decreased by 17% in the presence of 50 mM Cl^- (Figure 3-6e). Under the same pH condition, the effect of 2 mM Cl^- on PHE removal was insignificant and PHE removal was slightly promoted by around 6% with 10 and 50 mM Cl^- in the UVB/PS system (Figure 3-6f).

Various conflicting results were reported in the different UV based AOPs with the presence of Cl^- for organic degradation (Huang et al., 2018a; Luo et al., 2015; Yang et al., 2016). Usually, Cl^- can react with HO^\bullet and $\text{SO}_4^{\bullet-}$ to yield secondary active chlorine radical species such as ClOH^\bullet , Cl^\bullet , and $\text{Cl}_2^{\bullet-}$ through a series of intricate chain

reactions (Eqs. 3-15 to 3-18) (Grigor'ev et al., 1987; Jayson et al., 1973; Neta et al., 1988).

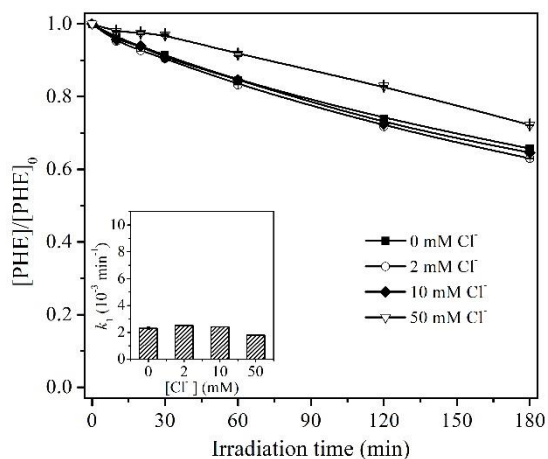
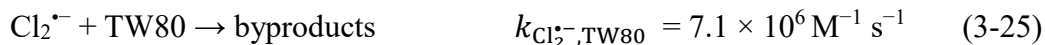
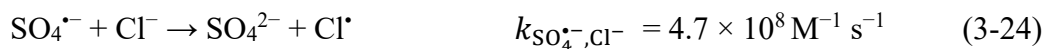


The negligible effect of low Cl^- concentration (2-10 mM) on PHE removal in the UVB/ H_2O_2 system was mainly due to the reaction (3-19). The negative effect of 50 mM Cl^- on PHE oxidation observed can be ascribed to the consumption of H_2O_2 by Cl^\bullet and $\text{Cl}_2^{\bullet-}$ (reactions 3-20 and 3-21) (Hasegawa and Neta 1978; Kläning and Wolff 1985). These reactions reduced the amount of available HO^\bullet and $\text{Cl}_2^{\bullet-}$ radicals reacting with PHE (reactions 3-8 and 3-22) (Tao et al., 2019), leading to the lower PHE elimination. Moreover, the finding of inhibition of PHE at pH 8.6 could be explained by the reduction of $\text{Cl}_2^{\bullet-}$ triggered by reaction (3-23) and also the higher consumption of H_2O_2 via reactions (3-20) and (3-21) at alkaline pH, which restrained active species reacting with PHE and consequently retarded PHE oxidation.

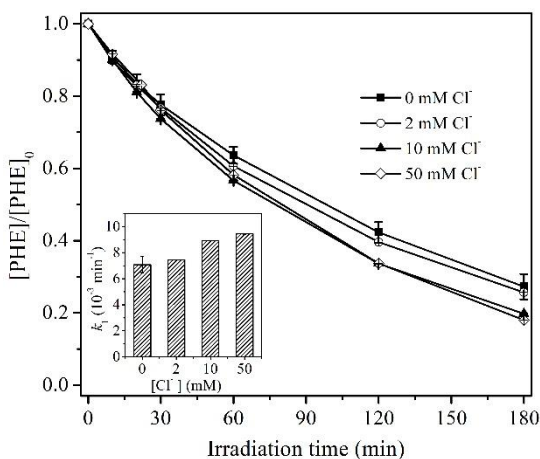


In the UVB/PS system, the weak enhancement of PHE decay was attributed to the production of $\text{Cl}_2^{\bullet-}$ radicals through a series of chain reactions (3-17 and 3-24). According to our previous study (Tao et al., 2019), $\text{Cl}_2^{\bullet-}$ was more selective towards

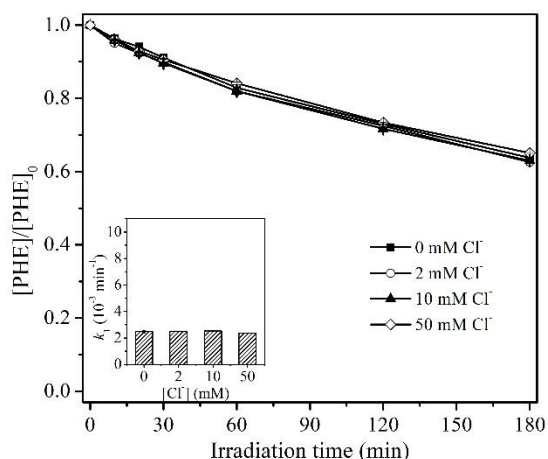
PHE than $\text{SO}_4^{\bullet-}$ in the presence of TW80 (reactions 3-22 and 3-25), therefore PHE elimination could be promoted.



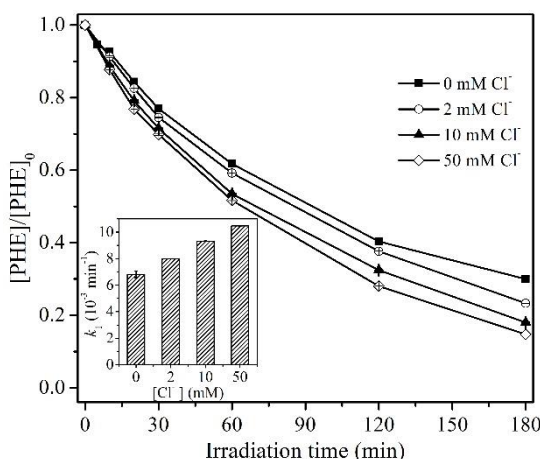
(a)



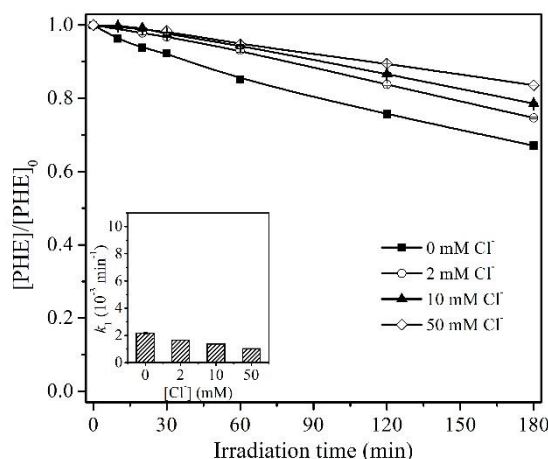
(b)



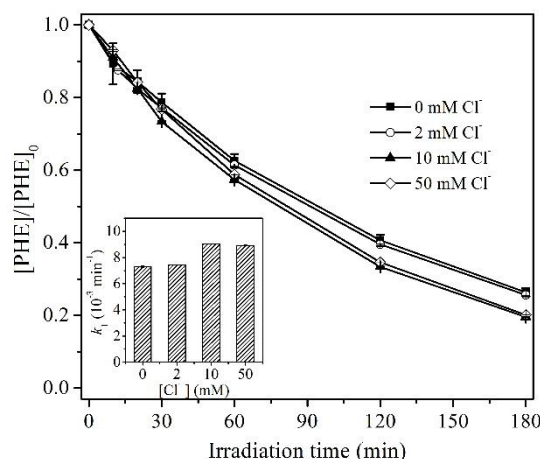
(c)



(d)



(e)

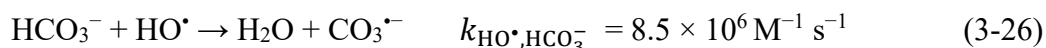


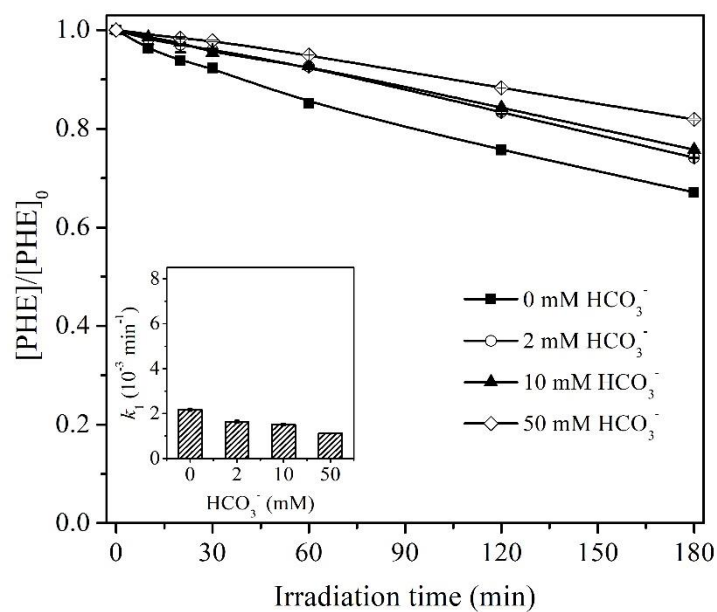
(f)

Figure 3-6 Influence of Cl^- concentration on the photo-degradation of PHE. (a) UVB/ H_2O_2 at $\text{pH} = 3.3 \pm 0.1$; (b) UVB/PS at $\text{pH} = 3.3 \pm 0.1$; (c) UVB/ H_2O_2 at $\text{pH} = 7.1 \pm 0.1$; (d) UVB/PS at $\text{pH} = 7.1$; (e) UVB/ H_2O_2 at $\text{pH} = 8.6$; (f) UVB/PS at $\text{pH} = 8.6$. Insets are the corresponding first-order rate constants. Initial conditions: $[\text{PS}] = [\text{H}_2\text{O}_2] = 5 \text{ mM}$.

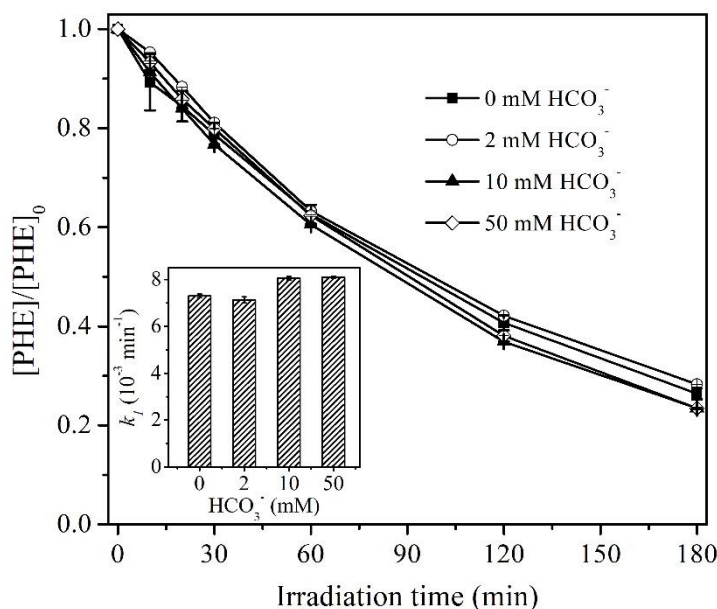
3.3.5 Effect of inorganic anions- bicarbonate

Figure 3-7 depicts the elimination efficiency of PHE in the presence of various concentrations of bicarbonate (HCO_3^-) in the UVB/ H_2O_2 and UVB/PS processes at initial pH of around 8.6. As presented in Figure 3-7a, the oxidation of PHE was obviously inhibited with the addition of HCO_3^- , which is in accordance with most reports investigated in aqueous phase in the absence of surfactant (Lee et al., 2018; Xiao et al., 2016; Yang et al., 2014b). With the addition of 50 mM bicarbonate, the PHE removal efficiency decreased by almost one-half in comparison with 33.0% removal in the absence of bicarbonate. HCO_3^- could react with HO^\bullet to generate carbonate radicals ($\text{CO}_3^{\bullet-}$) via reaction (3-26). However, the generated $\text{CO}_3^{\bullet-}$ are considered to be a weaker oxidant and the reactions with most organic pollutants are insignificant (Crittenden et al., 1999; Zuo et al., 1999). As a consequence, available HO^\bullet was reduced and PHE decomposition was depressed.





(a)

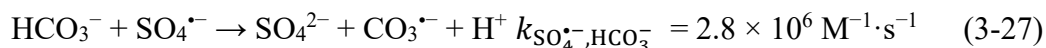


(b)

Figure 3-7 Influence of HCO_3^- concentration on the photo-degradation of PHE. (a) UVB/ H_2O_2 ; (b) UVB/PS. Insets are the corresponding first-order rate constants. Initial conditions: $[\text{PHE}] = 10 \text{ mg L}^{-1}$, $[\text{TW80}] = 0.5 \text{ g L}^{-1}$, $[\text{PS}] = [\text{H}_2\text{O}_2] = 5 \text{ mM}$, $\text{pH} = 8.6 \pm 0.1$.

The effect of bicarbonate in the UVB/PS system is illustrated in Figure 3-7b. Insignificant effect of HCO_3^- was observed, which may be ascribed to the negligible scavenging effect of $\text{SO}_4^{\cdot-}$ by HCO_3^- (reaction 3-27) since the rate constant between

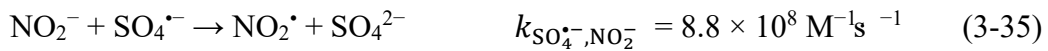
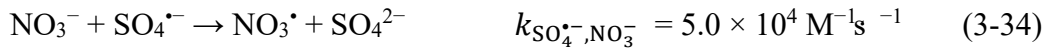
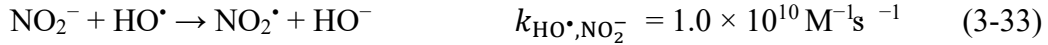
$\text{SO}_4^{\bullet-}$ and HCO_3^- is around 3 orders of magnitudes smaller than that between PHE and $\text{SO}_4^{\bullet-}$. In the meanwhile, the little influence of HCO_3^- on the performance of UVB/PS system was ascribed to the unpronounced variation of selectivity coefficient (12.1% ~ 11.3%) with the HCO_3^- concentration ranging from 0 ~ 50 mM.



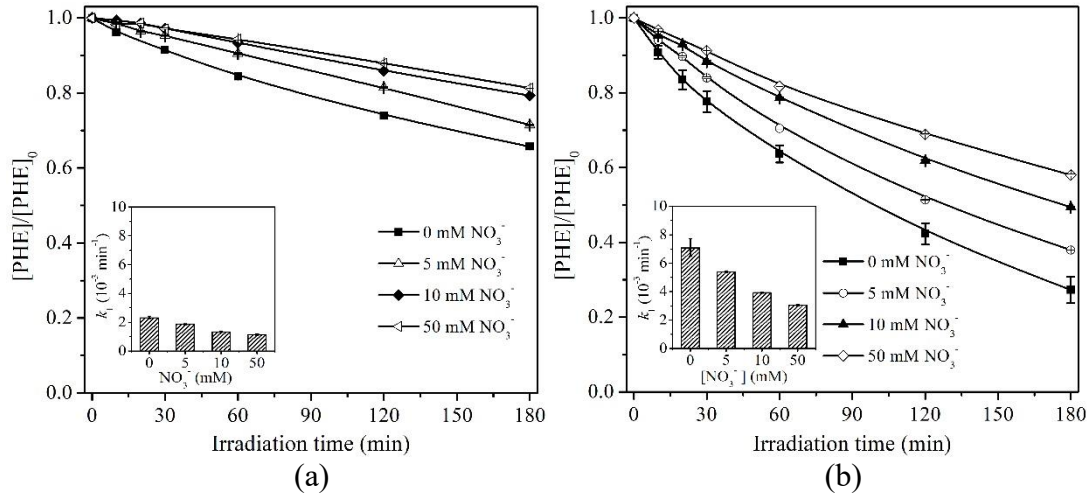
3.3.6 Effect of inorganic anions- nitrate

The influence of NO_3^- with different doses and pH conditions on the decomposition of PHE in the UVB/PS and UVB/ H_2O_2 systems were studied. NO_3^- led to a strong inhibitory effect on the two AOPs, which is in agreement with other reports for removal of hydrophilic compounds (Gao et al., 2018; Tan et al., 2013; Yang et al., 2016). At pH 3.3, with the concentration of NO_3^- ranging from 0 to 50 mM, the PHE decomposition efficacy decreased from 34.5% to 19.0% in the UVB/ H_2O_2 system (Figure 3-8a), while it dropped from 73.0% to 42.0% in the UVB/PDS system (Figure 3-8b).

The stronger inhibition of NO_3^- on PHE decomposition can be explained by the screen effect of light due to the photoreactivity of NO_3^- (reactions 3-28 and 3-29) (Keen et al., 2012) and its secondary substance (i.e. NO_2^-), leading to competition with H_2O_2 and PDS for UVB radiation. It is reported that both NO_3^- and NO_2^- have absorption in the range of UVB light (around 260 – 330 nm) (Mack and Bolton 1999). This is supported by the strong decrease of the direct photolysis of PHE under UVB irradiation in presence of 5 mM NO_3^- . In the UVB alone, PHE removal was 23.0% while it dropped to only 7.0% with the addition of 5 mM NO_3^- . The production of HO^\bullet from the NO_3^- and NO_2^- photolysis (reactions 3-30 to 3-32) (Keen et al., 2012; Lyon et al., 2012; Sørensen and Frimmel 1997) probably did not compensate the negative screen effect. On the other hand, NO_3^- and NO_2^- had quenching effect for both $\text{SO}_4^{\bullet-}$ and HO^\bullet via reactions (3-33)-(3-35), which could also restrain PHE degradation.



The influence of 5 mM NO_3^- on PHE degradation at different initial pH was also investigated in the two AOPs. In comparison with the absence of NO_3^- , the decrease of PHE removal at pH 3.3, 7.1 and 8.6 was respectively 5.0%, 14.5%, 13.6% in the UVB/ H_2O_2 system in Figure 3-8c, while it was respectively 10.7%, 10.3% and 14.3% in the UVB/PS system in Figure 3-8d.



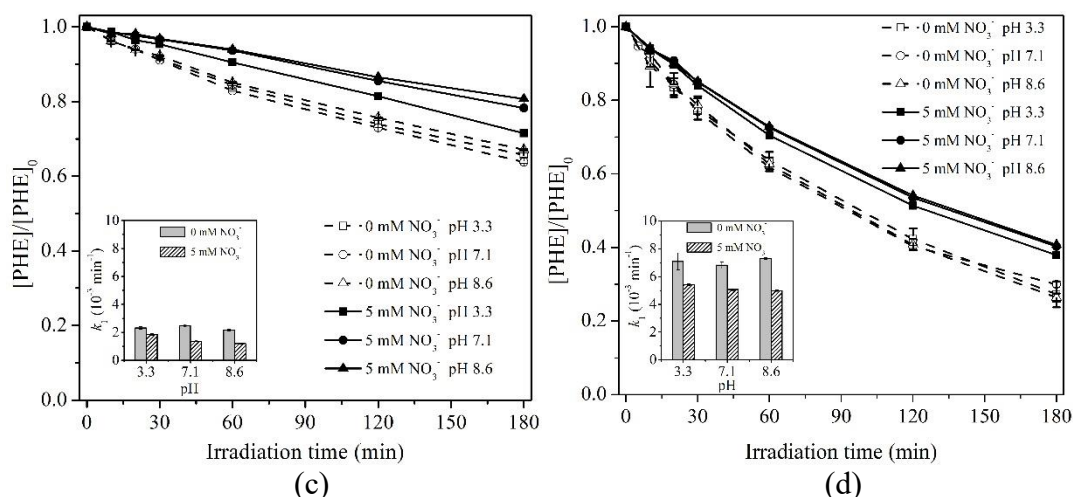


Figure 3-8 Influence of NO_3^- concentration on the photo-degradation of PHE. (a) UVB/ H_2O_2 at pH 3.3 ± 0.1 ; (b) UVB/PS at pH 3.3 ± 0.1 ; (c) UVB/ H_2O_2 at different pH; (d) UVB/PS at different pH. Insets are the corresponding first-order rate constants. Initial conditions: $[PHE] = 10 \text{ mg L}^{-1}$, $[TW80] = 0.5 \text{ g L}^{-1}$, $[PS] = [H_2O_2] = 5 \text{ mM}$.

3.3.7 Treatment of real SW effluent

The treatment of real effluents after washing three types of soils spiked with PHE was further carried out to evaluate the feasibility of UVB/ H_2O_2 and UVB/PS systems. The various ions and constituents in the soils are listed in Table 3-3, and the results of SW effluent treatment are displayed in Figure 3-9. As can be seen, UVB/PS system was more effective for PHE decomposition than UVB/ H_2O_2 and UVB alone for the three SW samples, corroborating our former results with mimic SW samples. Direct PHE photolysis in the UVB system was less than 10.0% for all the three SW effluents. The lower efficiency compared with synthetic SW samples (around 23.0%) could be ascribed to the screening effect of light due to the diverse mixture of substances in the solution. For UVB/ H_2O_2 or UVB/PS process the efficiencies of PHE degradation in the SW effluents from soil 1 and 2 were comparable with those in the synthetic SW effluents, while for soil 3, the PHE removal efficiency was lower in both UVB/ H_2O_2 and UVB/PS systems. In fact, with H_2O_2 , PHE degradation efficiencies after 6 h

irradiation were 47.5%, 51.6% and 33.5% in soil 1, 2 and 3 respectively. With PS the removal of PHE achieved around 85.0% for soil 1 and 2 and 78.0% for soil 3.

The results of PHE degradation with the three real SW effluents using the two AOPs validated our previous observations on the mimic SW solutions and the effects of the main co-existing inorganic species. Moreover, although the intricate mixed effects of the various soil components in real SW effluent, the PHE oxidation efficiency with UVB/PS is similar to the removal in the synthetic solutions, implying UVB/PS remains to be the most efficient process for PHE elimination.

Table 3-3 Composition of SW effluent samples (in $\mu\text{g L}^{-1}$)

Parameter	From soil 1 (pH 6.4)	From soil 2 (pH 7.1)	From soil 3 (pH 7.1)
TW80	488000	473000	492000
PHE	6627	6340	6959
NO_3^-	20.8	17.1	45.5
Cl^-	88.1	150.2	267.0
SO_4^{2-}	102.2	< LOD	106.7
Na^+	50.9	315.0	289.9
NH_4^+	< LOD	< LOD	< LOD
K^+	43.9	424.1	257.5
Mg^{2+}	12.6	94.6	119.0
Ca^{2+}	61.2	573.4	816.0
Inorganic Carbon	1420	1720	1740

Notes: LOD = limit of detection.

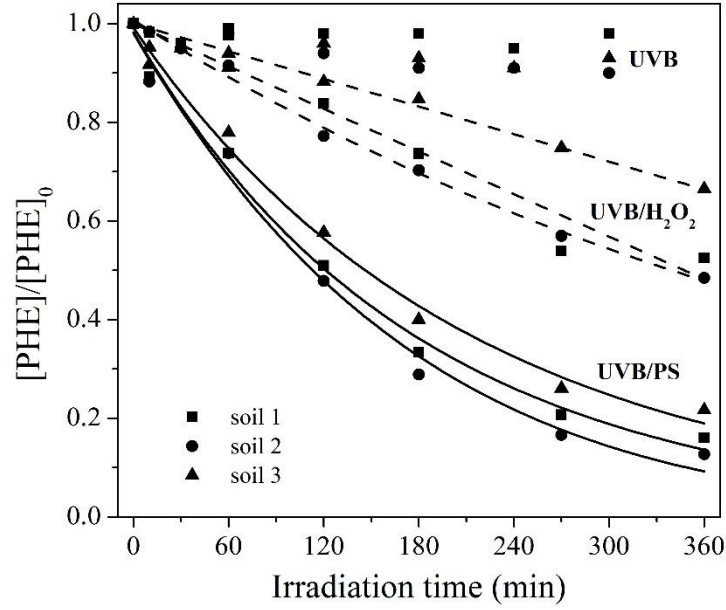


Figure 3-9 Degradation of PHE with three real SW effluents in different systems. Initial conditions: $[PS] = [H_2O_2] = 5 \text{ mM}$.

3.3.8 Economic comparison

The electrical energy per order (EE/O) was used as an index of the cost-effectiveness of the three AOPs. EE/O is defined as the electric energy in kWh required to decompose the target pollutant by one order of magnitude in 1 m^3 of water (Xiao et al., 2016) and can be determined according to the Eq. (3-36).

$$EE/O = \frac{1000 P t}{V \log \frac{C_i}{C_f}} = \frac{38.4 P}{V k} \text{ (kWh m}^{-3} \text{ order}^{-1}) \quad (3-36)$$

where P is the UVB lamp power emission (kWh); t is the irradiation time (h); V is the volume of the testing SW effluent (L); k is the first-order rate constant (min^{-1}); C_i and C_f are the initial and the final concentrations of PHE (mg L^{-1}), respectively.

Generally, the EE/O was significantly lower for UVB/PS and UVB/ H_2O_2 compared with direct photolysis process for all the testing SW effluents (Figure 3-10). For example, the EE/O for UVB/PS ($3380.8 \text{ kWh m}^{-3} \text{ order}^{-1}$) and UVB/ H_2O_2 ($9309.1 \text{ kWh m}^{-3} \text{ order}^{-1}$) with simulated soil washing effluent were significantly lower than that by direct UVB photolysis ($15567.6 \text{ kWh m}^{-3} \text{ order}^{-1}$). In addition, the EE/O for UVB/PS

were commonly 62.0% to 77.0% lower than for UVB/H₂O₂ process. Overall, the energy consumption for UVB/PS process was much lower than the corresponding value for UVB/H₂O₂ under different conditions, implying UVB/PS oxidation process was more economically competitive and relevant for PHE elimination and SW effluent treatment.

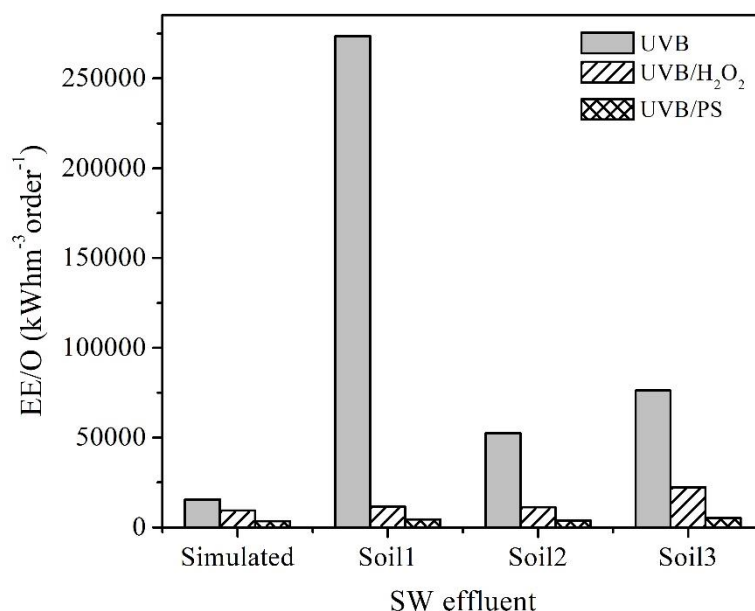


Figure 3-10 The electrical energy consumption for UVB, UVB/H₂O₂ and UVB/PS for PHE degradation with both simulated and real SW effluents.

3.4 Conclusion

The results obtained from this study indicate that the UVB based AOPs, e.g., UVB/PS and UVB/H₂O₂, can eliminate PHE in both simulated and real SW effluents. The photo-degradation efficiency of PHE is influenced by various parameters including the concentration of oxidants, initial pH and widespread soil inorganic anions (Cl⁻, HCO₃⁻ and NO₃⁻). Opposite results are obtained for the effect of Cl⁻ for UVB assisted H₂O₂ and PS activation. The presence of Cl⁻ at alkaline pH inhibits PHE degradation in UVB/H₂O₂, while slightly enhances PHE elimination in the UVB/PS process at different pH. The experimental results reveal the negligible effect of HCO₃⁻ in the UVB/PS system but negative effect in the UVB/H₂O₂ process. Nitrate has negative

effect on the PHE degradation in both AOPs. Overall, the UVB/PS process is much more efficient than UVB/H₂O₂ due to the formation of sulfate radical which is less sensitive to the main inorganic ions present in soil, and could be a promising process to be applied for real SW effluents treatment.

References

- Bastviken, D., Sandén, P., Svensson, T., Ståhlberg, C., Magounakis, M., Öberg, G., 2006. Chloride retention and release in a boreal forest soil: effects of soil water residence time and nitrogen and chloride loads. *Environmental Science & Technology* 40 (9), 2977-2982.
- Beck, S.E., Ryu, H., Boczek, L.A., Cashdollar, J.L., Jeanis, K.M., Rosenblum, J.S., Lawal, O.R., Linden, K.G., 2017. Evaluating UV-C LED disinfection performance and investigating potential dual-wavelength synergy. *Water Research* 109, 207-216.
- Bennedsen, L.R., Muff, J., Sogaard, E.G., 2012. Influence of chloride and carbonates on the reactivity of activated persulfate. *Chemosphere* 86 (11), 1092-1097.
- Buxton, G.V., Greenstock, C.L., Helman, W.P., Ross, A.B., 1988. Critical review of rate constants for reactions of hydrated electrons, hydrogen atoms and hydroxyl radicals ($\cdot\text{OH}/\cdot\text{O}^-$) in aqueous solution. *Journal of Physical and Chemical Reference Data* 17 (2), 513-886.
- Crabb, N.T., Persinger, H.E., 1964. The determination of polyoxyethylene nonionic surfactants in water at the parts per million level. *Journal of the American Oil Chemists' Society* 41 (11), 752-755.
- Crittenden, J.C., Hu, S., Hand, D.W., Green, S.A., 1999. A kinetic model for H₂O₂/UV process in a completely mixed batch reactor. *Water Research* 33 (10), 2315-2328.
- Deng, J., Shao, Y., Gao, N., Xia, S., Tan, C., Zhou, S., Hu, X., 2013. Degradation of the

- antiepileptic drug carbamazepine upon different UV-based advanced oxidation processes in water. *Chemical Engineering Journal* 222, 150-158.
- Du, C., Ma, Z., Zhou, J., Goyne, K.W., 2013. Application of mid-infrared photoacoustic spectroscopy in monitoring carbonate content in soils. *Sensors and Actuators, B: Chemical* 188, 1167-1175.
- Gao, Y.-q., Gao, N.-y., Yin, D.-q., Tian, F.-x., Zheng, Q.-f., 2018. Oxidation of the β -blocker propranolol by UV/persulfate: effect, mechanism and toxicity investigation. *Chemosphere* 201, 50-58.
- Grigor'ev, A., Makarov, I., Pikaev, A., 1987. Formation of Cl_2^- in the bulk of solution during radiolysis of concentrated aqueous solutions of chlorides. *Khimiya Vysokikh Ehnergij* 21 (2), 123-126.
- Hasegawa, K., Neta, P., 1978. Rate constants and mechanisms of reaction of chloride (Cl_2^-) radicals. *The Journal of Physical Chemistry* 82 (8), 854-857.
- Herrmann, H., 2007. On the photolysis of simple anions and neutral molecules as sources of O^-/OH , SO_x^- and Cl in aqueous solution. *Physical Chemistry Chemical Physics* 9 (30), 3935-3964.
- Herrmann, H., Reese, A., Zellner, R., 1995. Time-resolved UV/Vis diode array absorption spectroscopy of SO_x^- ($x = 3, 4, 5$) radical anions in aqueous solution. *Journal of Molecular Structure* 348, 183-186.
- Huang, W., Bianco, A., Brigante, M., Mailhot, G., 2018. UVA-UVB activation of hydrogen peroxide and persulfate for advanced oxidation processes: efficiency, mechanism and effect of various water constituents. *Journal of Hazardous Materials* 347, 279-287.
- Jayson, G., Parsons, B., Swallow, A.J., 1973. Some simple, highly reactive, inorganic chlorine derivatives in aqueous solution. their formation using pulses of radiation

- and their role in the mechanism of the fricke dosimeter. *Journal of The Chemical Society, Faraday Transactions 1: Physical Chemistry in Condensed Phases* 69, 1597-1607.
- Joseph, C.G., Taufiq-Yap, Y.H., Li Puma, G., Sanmugam, K., Quek, K.S., 2016. Photocatalytic degradation of cationic dye simulated wastewater using four radiation sources, UVA, UVB, UVC and solar lamp of identical power output. *Desalination and Water Treatment* 57 (17), 7976-7987.
- Keen, O.S., Love, N.G., Linden, K.G., 2012. The role of effluent nitrate in trace organic chemical oxidation during UV disinfection. *Water Research* 46 (16), 5224-5234.
- Kläning, U.K., Wolff, T., 1985. Laser flash photolysis of HClO , ClO^- , HBrO , and BrO^- in aqueous solution. reactions of Cl^- and Br^- atoms. *Berichte der Bunsengesellschaft für Physikalische Chemie* 89 (3), 243-245.
- Lee, M.-Y., Wang, W.-L., Wu, Q.-Y., Huang, N., Xu, Z.-B., Hu, H.-Y., 2018. Degradation of dodecyl dimethyl benzyl ammonium chloride (DDBAC) as a non-oxidizing biocide in reverse osmosis system using UV/persulfate: kinetics, degradation pathways, and toxicity evaluation. *Chemical Engineering Journal* 352, 283-292.
- Liu, Y., He, X., Duan, X., Fu, Y., Fatta-Kassinos, D., Dionysiou, D.D., 2016. Significant role of UV and carbonate radical on the degradation of oxytetracycline in UV-AOPs: kinetics and mechanism. *Water Research* 95, 195-204.
- Lu, J., Bai, Z., Velthof, G.L., Wu, Z., Chadwick, D., Ma, L., 2019. Accumulation and leaching of nitrate in soils in wheat-maize production in China. *Agricultural Water Management* 212, 407-415.
- Luo, C., Ma, J., Jiang, J., Liu, Y., Song, Y., Yang, Y., Guan, Y., Wu, D., 2015. Simulation and comparative study on the oxidation kinetics of atrazine by $\text{UV}/\text{H}_2\text{O}_2$,

- UV/HSO₅⁻ and UV/S₂O₈²⁻. *Water Research* 80, 99-108.
- Lyon, B.A., Dotson, A.D., Linden, K.G., Weinberg, H.S., 2012. The effect of inorganic precursors on disinfection byproduct formation during UV-chlorine/chloramine drinking water treatment. *Water Research* 46 (15), 4653-4664.
- Mack, J., Bolton, J.R., 1999. Photochemistry of nitrite and nitrate in aqueous solution: a review. *Journal of Photochemistry and Photobiology A* 128 (1), 1-13.
- Marion, A., Brigante, M., Mailhot, G., 2018. A new source of ammonia and carboxylic acids in cloud water: The first evidence of photochemical process involving an iron-amino acid complex. *Atmospheric Environment* 195, 179-186.
- Mark, G., Schuchmann, M.N., Schuchmann, H.-P., von Sonntag, C., 1990. The photolysis of potassium peroxodisulphate in aqueous solution in the presence of tert-butanol: a simple actinometer for 254 nm radiation. *Journal of Photochemistry and Photobiology A* 55 (2), 157-168.
- Minella, M., Bertinetti, S., Hanna, K., Minero, C., Vione, D., 2019. Degradation of ibuprofen and phenol with a Fenton-like process triggered by zero-valent iron (ZVI-Fenton). *Environmental Research* 179, 108750.
- Mosteo, R., Varon-Lopez, A., Muzard, D., Benitez, N., Giannakis, S., Pulgarin, C., 2020. Visible light plays a significant role during bacterial inactivation by the photo-Fenton process, even at sub-critical light intensities. *Water Research*, 115636.
- Mousset, E., Oturan, N., Hullebusch, E.D.V., Guibaud, G., Esposito, G., Oturan, M.A., 2014. Influence of solubilizing agents (cyclodextrin or surfactant) on phenanthrene degradation by electro-Fenton process – study of soil washing recycling possibilities and environmental impact. *Water Research* 48 (1), 306-316.
- Neta, P., Huie, R.E., Ross, A.B., 1988. Rate constants for reactions of inorganic radicals in aqueous solution. *Journal of Physical and Chemical Reference Data* 17 (3),

1027-1284.

- Olmez-Hanci, T., Arslan-Alaton, I., 2013. Comparison of sulfate and hydroxyl radical based advanced oxidation of phenol. *Chemical Engineering Journal* 224, 10-16.
- Sörensen, M., Frimmel, F.H., 1997. Photochemical degradation of hydrophilic xenobiotics in the UVH₂O₂ process: Influence of nitrate on the degradation rate of EDTA, 2-amino-1-naphthalenesulfonate, diphenyl-4-sulfonate and 4, 4'-diaminostilbene-2, 2'-disulfonate. *Water Research* 31 (11), 2885-2891.
- Tan, C., Gao, N., Deng, Y., Zhang, Y., Sui, M., Deng, J., Zhou, S., 2013. Degradation of antipyrine by UV, UV/H₂O₂ and UV/PS. *Journal of Hazardous Materials* 260, 1008-1016.
- Tao, Y., Brigante, M., Zhang, H., Mailhot, G., 2019. Phenanthrene degradation using Fe (III)-EDDS photoactivation under simulated solar light: A model for soil washing effluent treatment. *Chemosphere* 236, 124366.
- Wan, D., Zuo, J., Chen, Y., Chen, Q., Zuo, Y., 2018. Photodegradation of amitriptyline in Fe(III)-citrate-oxalate binary system: Synergistic effect and mechanism. *Chemosphere* 210, 224-231.
- Wang, C., Shu, L., Zhou, S., Yu, H., Zhu, P., 2019. Effects of alternate partial root-zone irrigation on the utilization and movement of nitrates in soil by tomato plants. *Scientia Horticulturae* 243, 41-47.
- Wu, Y., Bianco, A., Brigante, M., Dong, W., de Sainte-Claire, P., Hanna, K., Mailhot, G., 2015. Sulfate radical photogeneration using Fe-EDDS: influence of critical parameters and naturally occurring scavengers. *Environmental Science & Technology* 49 (24), 14343-14349.
- Xiao, Y., Zhang, L., Zhang, W., Lim, K.-Y., Webster, R.D., Lim, T.-T., 2016. Comparative evaluation of iodoacids removal by UV/persulfate and UV/H₂O₂

- processes. *Water Research* 102, 629-639.
- Xu, Y., Lin, Z., Zhang, H., 2016. Mineralization of sucralose by UV-based advanced oxidation processes: UV/PDS versus UV/H₂O₂. *Chemical Engineering Journal* 285, 392-401.
- Yang, K., Zhu, L., Xing, B., 2006. Enhanced soil washing of phenanthrene by mixed solutions of TX100 and SDBS. *Environmental Science & Technology* 40 (13), 4274-4280.
- Yang, S., Wang, P., Yang, X., Shan, L., Zhang, W., Shao, X., Niu, R., 2010. Degradation efficiencies of azo dye acid orange 7 by the interaction of heat, UV and anions with common oxidants: persulfate, peroxymonosulfate and hydrogen peroxide. *Journal of Hazardous Materials* 179 (1-3), 552-558.
- Yang, Y., Pignatello, J.J., Ma, J., Mitch, W.A., 2014. Comparison of halide impacts on the efficiency of contaminant degradation by sulfate and hydroxyl radical-based advanced oxidation processes (AOPs). *Environmental Science & Technology* 48 (4), 2344-2351.
- Yang, Y., Pignatello, J.J., Ma, J., Mitch, W.A., 2016. Effect of matrix components on UV/H₂O₂ and UV/S₂O₈²⁻ advanced oxidation processes for trace organic degradation in reverse osmosis brines from municipal wastewater reuse facilities. *Water Research* 89, 192-200.
- Yu, X.-Y., Barker, J.R., 2003. Hydrogen peroxide photolysis in acidic aqueous solutions containing chloride ions. II. Quantum yield of HO•(Aq) radicals. *Journal of Physical Chemistry A* 107 (9), 1325-1332.
- Zellner, R., Exner, M., Herrmann, H., 1990. Absolute OH quantum yields in the laser photolysis of nitrate, nitrite and dissolved H₂O₂ at 308 and 351 nm in the temperature range 278–353 K. *Journal of Atmospheric Chemistry* 10 (4), 411-425.

- Zhang, R., Sun, P., Boyer, T.H., Zhao, L., Huang, C.-H., 2015. Degradation of pharmaceuticals and metabolite in synthetic human urine by UV, UV/H₂O₂, and UV/PDS. *Environmental Science & Technology* 49 (5), 3056-3066.
- Zhou, L., Ferronato, C., Chovelon, J.-M., Sleiman, M., Richard, C., 2017a. Investigations of diatrizoate degradation by photo-activated persulfate. *Chemical Engineering Journal* 311, 28-36.
- Zhou, L., Sleiman, M., Ferronato, C., Chovelon, J.-m., Sainte-claire, P.D., Richard, C., 2017b. Sulfate radical induced degradation of β_2 -adrenoceptor agonists salbutamol and terbutaline: Phenoxyl radical dependent mechanisms.
- Zuo, Z., Cai, Z., Katsumura, Y., Chitose, N., Muroya, Y., 1999. Reinvestigation of the acid–base equilibrium of the (bi) carbonate radical and pH dependence of its reactivity with inorganic reactants. *Radiation Physics and Chemistry* 55 (1), 15-23.

**Chapter 4 Oxidation of phenanthrene in soil washing
effluent by photo-Fenton process using Fe(III)-citric
acid complex**

4.1 Introduction

Advanced oxidation processes (AOPs) have been widely employed in SW effluent treatment for quickly and non-selectively oxidizing refractory and poisonous soil pollutants (Trellu et al., 2016a). Among different AOPs, the homogeneous photo-Fenton process is commonly one of the most effective and promising method to decompose contaminants by HO^\bullet generated through the reactions of iron with H_2O_2 and/or light energy (Liu et al., 2018). Photo-Fenton processes have been applied to various kinds of SW solutions treatment with high efficiency (Bandala et al., 2013; Villa et al., 2010). For example, it has been reported 98.9% removal of DDT, 99% removal of DDE, 100% removal of diesel after 6 h reaction in a solution with 2.1 g L^{-1} of surfactant Triton X-100 by using 12 mM of Fe^{2+} and 1.4 M H_2O_2 in the photo-Fenton process (Villa et al., 2010). However, traditional photo-Fenton treatments are probably involve high cost and are limited in large-scale operations since the working pH has to be adjusted to around 2.8 for achievement of best efficiency (Pignatello et al., 2006).

The drawbacks encountered with the insufficient efficiency of contaminants degradation at pH greater than 2.8 can be alleviated by addition of organic complexes. The application of iron complexes in photo-Fenton processes has exhibited huge advantages over traditional processes due to the higher absorption of light radiation, the stabilization of Fe(II) or Fe(III) in the soluble forms over a wider pH range as well as the better performance of pollutants oxidation by using the iron organic complexes (Clarizia et al., 2017; Pignatello et al., 2006). The commonly used organic chelating agents are ethylenediaminetetraacetic acid (EDTA), ethylenediaminedisuccinate (EDDS), citric acid (CA), nitrilotriacetic acid (NTA) and oxalate (Clarizia et al., 2017). Among those polycarboxylates and aminopolycarboxylates, CA is more attractive than other iron ligand for application due to its inexpensive availability (it present with high

concentration in lemon juice), easy biodegradability, and therefore environmental friendly (citrate is a safe food additive) (Hoehl et al., 2014; Silva et al., 2010). It is reported that Fe(III)-CA complex can be efficiently photo-transferred to Fe(II) with relatively high quantum yields between 0.2 and 0.5 (Abrahamson et al., 1994).

Fe(III)-CA involved photo-Fenton processes have been employed to eliminate various contaminants in wastewater (Baba et al., 2015; Miralles-Cuevas et al., 2014; Silva et al., 2010). However, photo-Fenton process using Fe(III)-CA has not been evaluated for destruction of hydrophobic soil pollutant in the SW effluent. In this study the oxidation performance of phenanthrene (PHE), one representative of PAHs, was investigated by Fe(III)-CA enhanced photo-Fenton process under UV irradiation. The effect of operating parameters such as solution pH, Fe(III) to CA ration, H₂O₂ and Fe(III)-CA concentration on PHE degradation was assessed. The degradation mechanism of PHE oxidation was identified through H₂O₂ decomposition, Fe(II) generation and radical scavenging experiments.

4.2 Materials and methods

4.2.1 Chemicals

Tween 80 (TW80), phenanthrene (PHE, C₁₄H₁₀), ethylenediaminetetraacetic acid (EDTA, 99%), citric acid (CA, 99%), nitrilotriacetic acid (NTA, 99%), ethylenediamine-N,N'-disuccinic acid trisodium salt solution (EDDS, 35% in water), Ferrous sulfate (FeSO₄·7H₂O), L-ascorbic acid (AA, reagent grade), 3-(2pyridyl)-5,6-diphenyl-1,2,4-triazine-4',4''-disulfonic acid sodium salt (ferrozine, 97%), 4-hydroxyphenylacetic acid (HPAA, 98%), peroxidase from horseradish (POD), sodium dihydrogen phosphate (NaH₂PO₄), sodium hydrogen phosphate (Na₂HPO₄) were purchased from Sigma-Aldrich. Ferric perchlorate (Fe(ClO₄)₃·9H₂O) and hydrogen

peroxide (H_2O_2 , 30%) were obtained from Fluka, France. Chloroform (CF , CHCl_3) was from Carlo Erba. Tert-butanol (TBA, $\text{C}_4\text{H}_{10}\text{O}$) was supplied by Fisher Chemical. Perchloric acid (HClO_4) and sodium hydroxide (NaOH) were used for adjustment of the initial pH. Ultra-pure water (Millipore Ultra-Pure System, $18.2 \text{ M}\Omega \text{ cm}$) was employed to prepare solutions. The chemical reagents were of analytical grade and applied without further purification.

4.2.2 Experimental procedures and irradiation setup

The synthetic SW solution was prepared by addition of 10 mg PHE and 0.5 g TW80 to 1 L purified water. The mixture was intensely stirred until PHE was completely dissolved. The prepared solution was then used for the degradation experiments.

To prepare the iron complexes, predefined dosages of $\text{Fe}(\text{ClO}_4)_3 \cdot 9\text{H}_2\text{O}$ and organic ligands were added to pure water and placed in dark for 20 minutes to ensure the complete complexation and the homogeneity of the mixture. Since Fe(II) was easily oxidized in water, high concentration of Fe(II) solution was prepared by dissolving $\text{FeSO}_4 \cdot 7\text{H}_2\text{O}$ into acidic water (pH was around 2.5). At this pH, Fe(II) ions are stable in water. Ferrous complexes were then synthesized by mixing appropriate amount of the Fe(II) and ligand solutions.

Irradiation experiments were carried out in the same irradiation system as displayed in section 3.2.3. Predetermined amounts of iron complexes were mixed with the prepared SW solution, and the solution pH was adjusted to a predefined value. After addition of H_2O_2 to the solution, the pH value was rechecked and it was found that the pH was almost unchanged. The reactions began with turning on the light radiation and samples were withdrawn from the reactor at fixed time intervals to be analyzed.

4.2.3 Analytical methods

The UV-vis spectrum of Fe(III)-CA complex and other chemicals in water solution as displayed in Figure 4-1 was recorded with a Cary 300 UV-visible spectrophotometer to show the spectral overlap with the emission spectral irradiance of the four UVB tubes.

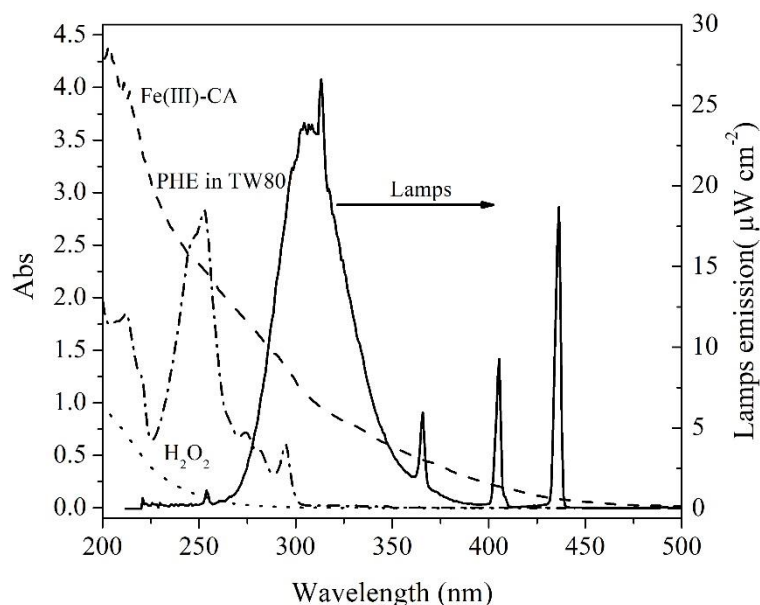


Figure 4-1 Absorption spectra of Fe(III)-CA (0.5 mM), H₂O₂ (5 mM), PHE (10 mg L⁻¹ in 0.5 g L⁻¹ of TW80) and emission spectrum of the adopted UVB tubes.

PHE concentration was analyzed by a high performance liquid chromatography (HPLC, Alliance) equipped with a photodiode array detector (Waters 2998, U.S.A) at the wavelength of 250 nm. The eluent was composed with water and acetonitrile (15/85, v/v) and a flow rate of 1 mL min⁻¹ was applied.

The removal and the pseudo-first order rate constant of PHE decomposition (k) were determined through Eqs. (4-1) and (4-2):

$$\text{Removal of PHE (\%)} = (1 - C_t/C_0) \times 100 \quad (4-1)$$

$$k = -\ln(C_t/C_0)/t \quad (4-2)$$

where C_0 and C_t were the initial PHE concentration and PHE concentration at time t , respectively.

Fe(II) generation in solution was quantified by spectrophotometric method of ferrozine complex (Stookey 1970). Briefly, 0.5 mL sample was mixed with 0.05 mL of

20 mM ferrozine solution and 0.1 mL of phosphate buffer solution (pH = 7.2). Then, the absorbance of Fe(II)-ferrozine complex was recorded with a UV-visible spectrophotometer Cary 300 at 562 nm and the Fe(II) concentration was calculated using the Beer–Lambert law with an extinction coefficient of $27900 \text{ M}^{-1} \text{ cm}^{-1}$. To determine the total dissolved iron in the solution, 0.5 mL sample was withdrawn and mixed with 0.1 mL of 0.5 M fresh prepared L-ascorbic acid solution for 10 min. In this way, all the soluble iron species were reduced to Fe(II) and can be determined using the ferrozine complexing method.

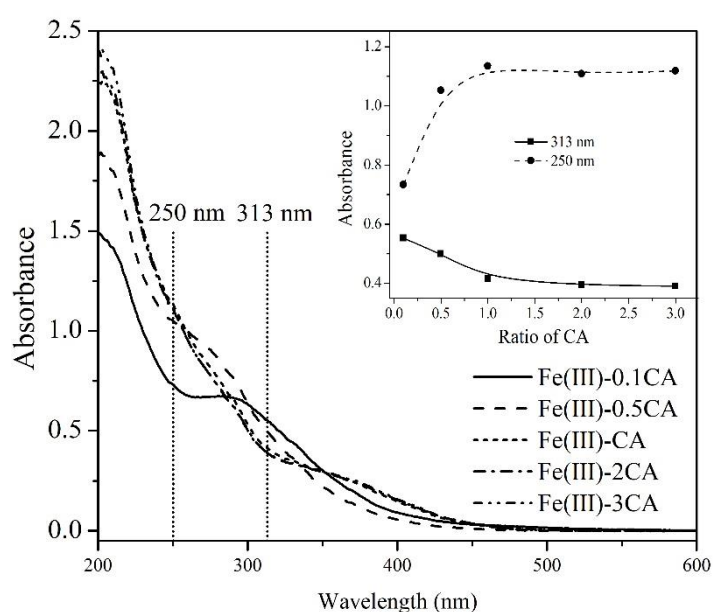
H₂O₂ concentration was determined using fluorescence method based on the reaction of 4-hydroxyphenylacetic acid (HPAA) and H₂O₂ being catalyzed to form a stable fluorescent dimer at neutral pH. Briefly, 0.1 mL sample was added to a mixture of 2 mL of 1 mM HPAA and 1 mL of a phosphate buffer solution (pH = 7.2) containing 10 mM EDTA and few amount of peroxidase from horseradish (POD). The sample was measured using Varian Cary Eclipse fluorescence spectrophotometer at 408 nm for an excitation wavelength set at 320 nm.

4.3 Results and discussion

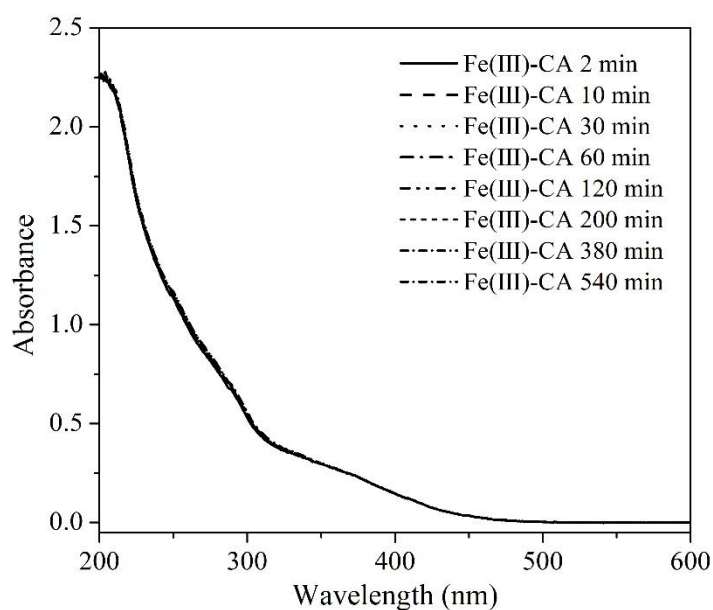
4.3.1 Physicochemical and photochemical properties of Fe(III)-CA

The iron/ligand molar ratio is an important parameter to yield adequate chelation efficiency and to achieve better operating conditions of work. If the quantity of ligand is inadequate, the metal will not be completely chelated (De Luca et al., 2014). The photochemical absorption of complexes with different CA molar ratios was checked to determine the optimal ligand ratio of satisfactory chelation. The test was performed using Fe(III) and CA solutions with fixed Fe(III) dosage and different amount of CA. As illustrated in Figure 4-2a, the spectrum of complexes shifted with Fe(III)/CA ratio

less than 1:1, while the absorbance become stable and the spectra were well overlapped with the Fe(III)/CA ratio ranging from 1:1 to 1:3, demonstrating complete complexation of Fe(III) by CA with CA molar ratio equal to or higher than 1:1. Therefore, the Fe(III)/CA ratio was fixed at 1:1 and the Fe(III)-CA complex was used for the following experiments. The evolution spectra of Fe(III)-CA in dark with time was also recorded in Figure 4-2b and it was found that the spectra maintained unchanged, suggesting the stabilization of Fe(III)-CA in dark.



(a)



(b)

Figure 4-2 UV-vis absorption spectra of: (a) complexes with different Fe(III)/CA ratios, inset is the absorbance at 250 and 313 nm; (b) spectra of Fe(III)-CA in dark with time. Initial conditions: $[\text{Fe(III)}] = 0.3 \text{ mM}$, pH at 3.0.

It is known that iron organic complexes can be easily photo-decomposed. The evolution of 0.5 mM Fe(III)-CA complex with time in the present of the adopted UVB radiation was recorded in Figure 4-3. It could be seen that the Fe(III)-CA complex undergo quick photo dissociation and it was almost thoroughly decomposed after 60 min of irradiation.

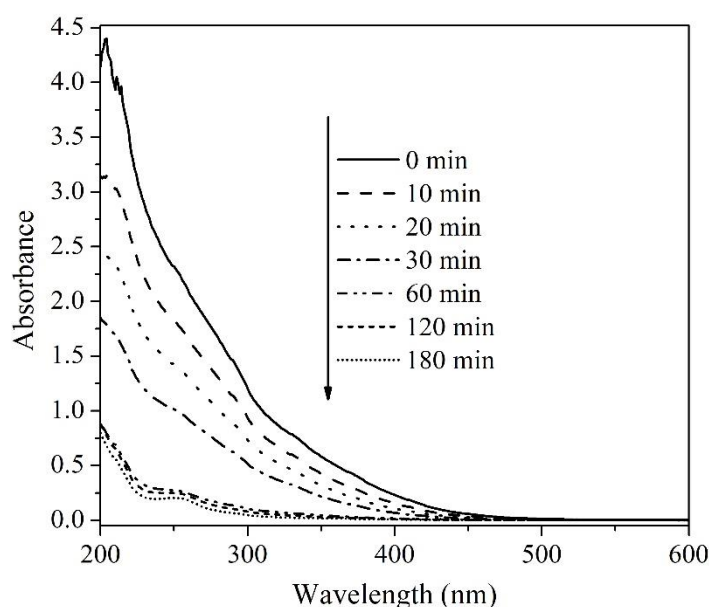


Figure 4-3 UV-vis absorption spectra evolution of 0.5 mM Fe(III)-CA under the adopted UVB irradiation. Initial conditions: $[\text{Fe(III)-CA}] = 0.5 \text{ mM}$, initial pH = 3.0.

4.3.2 Comparison of PHE oxidation under various systems

PHE degradation performance was evaluated using five different systems, including UVB/ H_2O_2 , $\text{H}_2\text{O}_2/\text{Fe(III)-CA}$ and $\text{H}_2\text{O}_2/\text{Fe(III)}$ systems with or without irradiation. As displayed in Figure 4-4a, in the dark Fenton-like or $\text{H}_2\text{O}_2/\text{Fe(III)-CA}$ process, PHE oxidation efficiencies were very low. With Fe(III)-CA complex only few percent of PHE degradation and less than 14% with the Fenton-like process were achieved after 3

h of reaction, indicating the generation of active species in dark systems were slow. The photolysis of PHE in UVB/H₂O₂ process reached 34.8% after 3 h irradiation. It was interesting to find that PHE oxidation was scarcely enhanced in the UVB/H₂O₂/Fe(III) photo-Fenton process comparing with the photolysis of PHE in UVB/H₂O₂ process. Although Fe(III) can adsorb UV light in the form of Fe(OH)²⁺ to yield Fe(II) and additional HO[•] radical through reaction (4-3), the quantum yield of HO[•] was very low (Benkelberg and Warneck 1995). In the meanwhile, the produced Fe(II) through series of reactions such as reactions (4-3)-(4-6) (Hayyan et al., 2016; Yap et al., 2011; Yu et al., 2018a) was inadequate (less than 0.06 mM in 3 h as shown in Figure 4-4b) reacting with H₂O₂ to generate sufficient HO[•] for intensification of PHE degradation. Similar results, i. e. that photo-Fenton process was no more efficient than UVB/H₂O₂ process, were also reported in previous researches (Giannakis et al., 2017; Karci et al., 2014).



In UVB/H₂O₂/Fe(III)-CA process, PHE oxidation was strongly intensified and reached a final removal of 46.4% (Figure 4-4a). It was also observed that PHE degradation exhibited two-stages in the Fe(III)-CA involved photo-Fenton process. In the initial 30 min, PHE was decomposed rapidly (removal of 42.6%), then nearly ceased within the left irradiation time. Pollutant degradation with the two-stages decay was also observed in organic iron complexes involved photo-degradation processes (Huang et al., 2012; Wu et al., 2014a).

To better understand PHE decay mechanism in the Fe(III)-CA employed photo-Fenton process, H₂O₂ consumption and Fe(II) generation were measured as presented

in Figure 4-4b. It is obviously observed that the consumption of H₂O₂ and production of Fe(II) in the UVB/H₂O₂/Fe(III)-CA system also exhibited a two-step pattern. In initial 30 min, around 84% of H₂O₂ was fast decomposed, contrarily, the generated Fe(II) was within very low concentration. As a contrary, in the absence of H₂O₂ (UVB/Fe(III)-CA system), Fe(II) was accumulated quickly within 30 min. It is known that Fe(III)-CA undergoes rapid photodecomposition under irradiation (Figure 4-3) through reaction (4-4) (Nansheng et al., 1998; Zhou et al., 2014). Concurrently, in the presence of H₂O₂, the generated Fe(II) was oxidized immediately to Fe(III) and an abundant amounts of HO[•] radicals were produced via Fenton reaction (4-8). Again, the amount of Fe(III) were reduced to Fe(II) by intermediate radicals R[•] through reactions (4-7) and (4-9) (Dulova et al., 2017; Han et al., 2015) to maintain the cycle of Fe(III)/Fe(II) and decomposition of H₂O₂, which lead to the production of abundant amounts of HO[•] useful for PHE oxidation. Therefore, the photodissociation of Fe(III)-CA was the rate limiting step for subsequent Fenton reaction to generate active species for decomposition of PHE. In the second stage, although Fe(II) was continuously accumulated, H₂O₂ was rarely remained. Consequently, insufficient production of reactive species (i.e. HO[•]) was responsible for negligible PHE degradation.



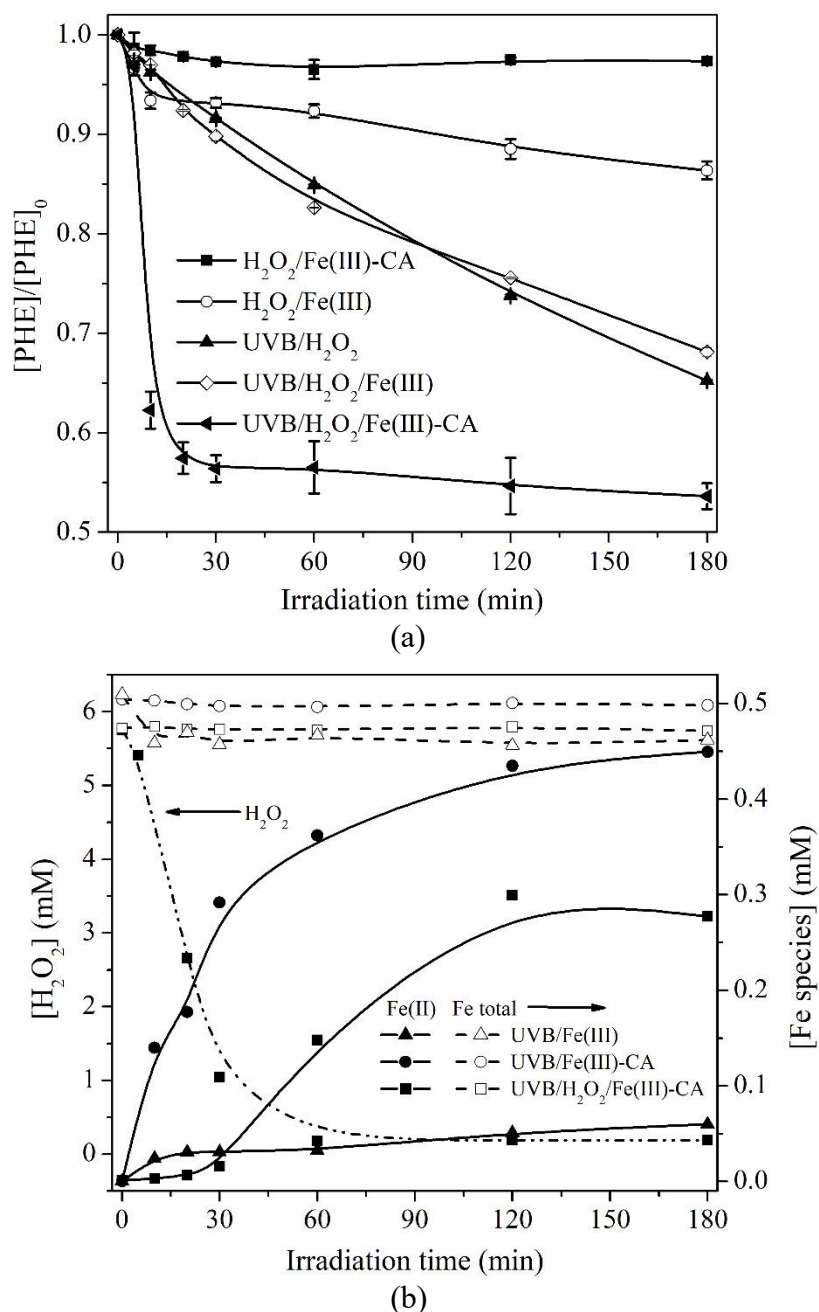


Figure 4-4 (a) Degradation of PHE in different systems; (b) H_2O_2 consumption in UVB/ $H_2O_2/Fe(III)$ -CA system and Fe species variation in different systems. Initial conditions: $[PHE] = 10\text{ mg L}^{-1}$, $[TW80] = 0.5\text{ g L}^{-1}$, $[H_2O_2] = 5\text{ mM}$, $[Fe(III)\text{-CA}] = [Fe(III)] = 0.5\text{ mM}$, $pH = 3.0 \pm 0.2$.

The performance of PHE degradation in the photo-Fenton process was also compared using $Fe(III)$ -CA and $Fe(II)$ -CA. As can be seen in Figure 4-5a, PHE degradation curve in the UVB/ $H_2O_2/Fe(II)$ was similar to that in the UVB/ $H_2O_2/Fe(III)$ system and PHE

oxidation efficiency was around 31% in both Fe(II) and Fe(III) used photo-Fenton processes. In comparison with the UVB/H₂O₂/Fe(III)-CA process, PHE decay also present a two-step pattern using Fe(II)-CA, and with the introduction of CA, PHE degradation was significantly enhanced in the first step. In the first 30 min, PHE removal was 30.5% in the UVB/H₂O₂/Fe(II)-CA process, which was less than 42.6% removal obtained in the UVB/H₂O₂/Fe(III)-CA system.

Actually, as long as H₂O₂ was added to the solution of Fe(II) or Fe(II)-CA, Fe(II) was detected with low concentration (Figure 4-5b) since Fe(II) was immediately oxidized to Fe(III). The same finding was reported by other researchers that the chelated Fe(II) was instantaneously oxidized to chelated Fe(III) in the present of oxidants (Yu et al., 2018a). Therefore, the photo-Fenton processes by using Fe(II) and Fe(II)-CA were similar to the systems using Fe(III) and Fe(III)-CA, respectively. The accumulation of Fe(II) in the first step by using Fe(III)-CA was as low as in the system of using Fe(II)-CA, suggesting the efficient transformation of Fe(II) to Fe(III) by the Fenton reaction in the two systems. The lower PHE oxidation efficiency in Fe(II)-CA involved photo-Fenton processes probably can be attribute to the lower initial H₂O₂ dosage (Figure 4-5b) since part of H₂O₂ was consumed immediately to oxidize Fe(II)-CA before the irradiation tests.

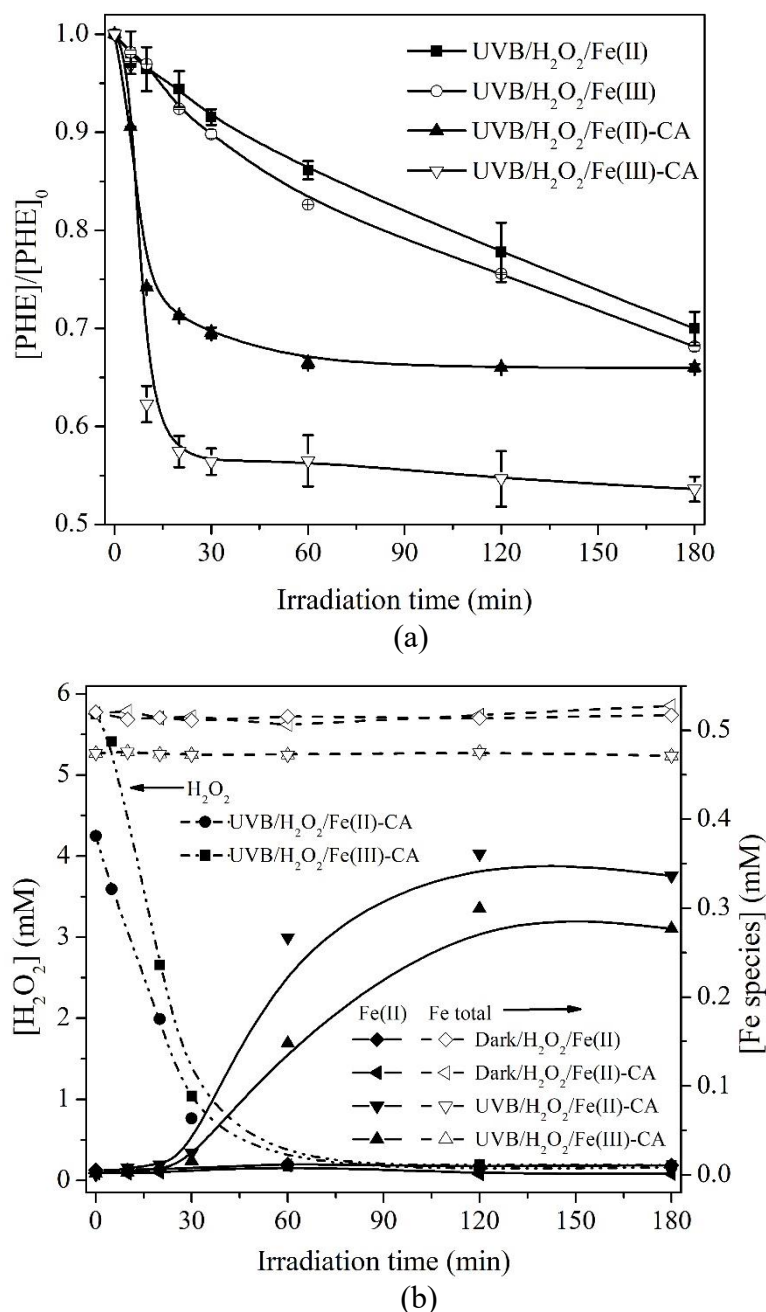


Figure 4-5 (a) Degradation of PHE; (b) H_2O_2 consumption and Fe species variation in different systems; Initial conditions: $[PHE] = 10\text{ mg L}^{-1}$, $[TW80] = 0.5\text{ g L}^{-1}$, $[H_2O_2] = 5\text{ mM}$, $[Fe(III)\text{-CA}] = [Fe(II)\text{-CA}] = 0.5\text{ mM}$, $pH = 3.0 \pm 0.2$.

4.3.3 PHE oxidation using different ligands chelated Fe(III) complexes

EDTA, EDDS and NTA were also commonly used organic ligands in the photo-Fenton process for pollutants oxidation (De Luca et al., 2014; Klamerth et al., 2012; Zhang et al., 2016). Experiments of oxidizing PHE using different ligands chelated

Fe(III) complexes were performed and the results are depicted in Figure 4-6. PHE oxidation efficiencies were also enhanced with EDTA, NTA and EDDS chelated Fe(III) complexes, and PHE oxidation efficiency with application of the four different complexes followed the order of Fe(III)-CA > Fe(III)-EDDS > Fe(III)-NTA > Fe(III)-EDTA. With Fe(III)-EDTA and Fe(III)-NTA being employed, PHE decay presented the same one-stage pattern with that in the UVB/H₂O₂ system. The removal of PHE appeared similar to two-stages model with involvement of Fe(III)-EDDS when compared with the photo-Fenton system of Fe(III)-CA, however the duration of the first stage prolonged to 60 min.

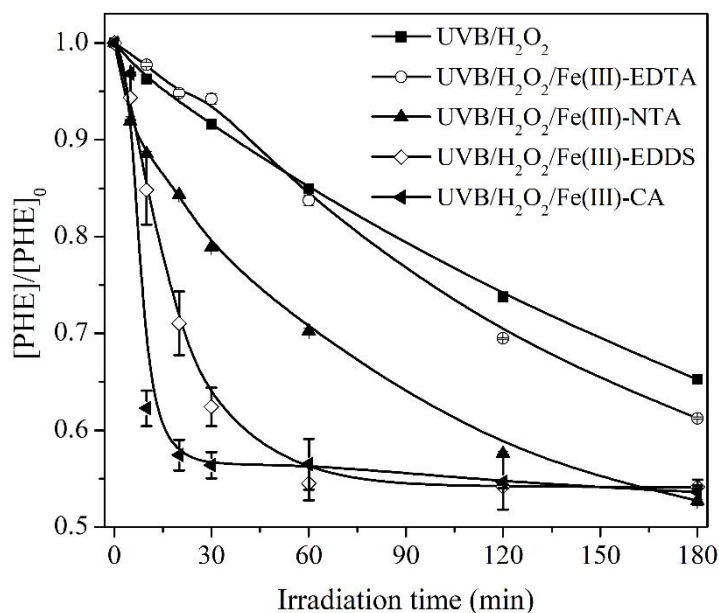


Figure 4-6 Degradation of PHE using different organic ligand chelated Fe(III) complexes. Initial conditions: [PHE] = 10 mg L⁻¹, [TW80] = 0.5 g L⁻¹, [H₂O₂] = 5 mM, [Iron complexes] = 0.5 mM, pH = 3.0 ± 0.2.

The decomposition of H₂O₂ and formation of Fe(II) were also monitored in those systems of different organic ligands to help to clarify the mechanism. It is presented in Figure 4-7a, the detected Fe(II) concentrations remained low within 3 h with the use of EDTA, NTA and EDDS as chelating agent. H₂O₂ was not completely depleted in 3 h in the presence of EDTA and NTA, while in the photo-Fenton system with EDDS, H₂O₂

was almost completely consumed at the end of irradiation. Therefore, as explained before, with the presence of unconsumed H_2O_2 , Fe(II) could not be accumulated but transferred to Fe(III) in EDTA, NTA and EDDS employed processes. As a consequence, it can be deduced that CA chelated Fe(III) complex was more efficient than the other three ligands chelated complexes to enhance the catalytic cycle Fe(III)/Fe(II) and so the decomposition of H_2O_2 , which was crucial for active species generation (HO^\bullet).

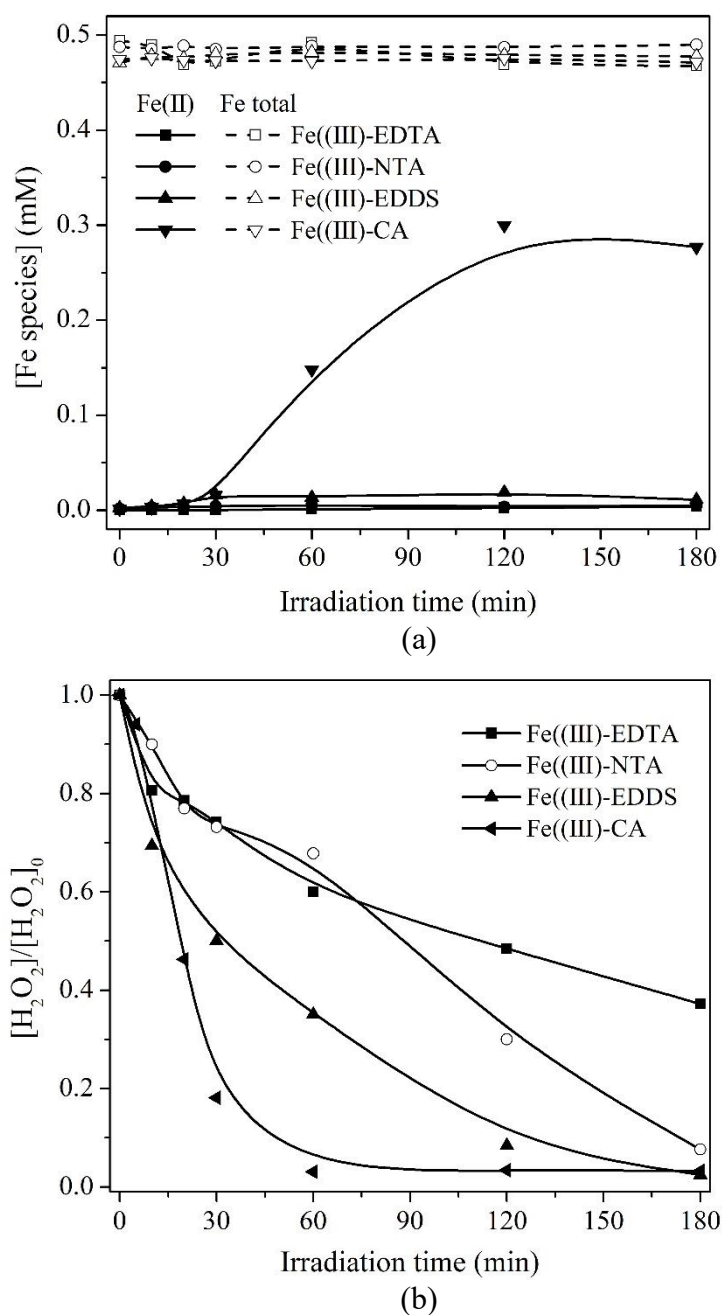


Figure 4-7 (a) Fe species variation and (b) H_2O_2 consumption in systems using different

organic ligands; Initial conditions: [PHE] = 10 mg L⁻¹, [TW80] = 0.5 g L⁻¹, [H₂O₂] = 5 mM, [iron complexes] = 0.5 mM, pH = 3.0 ± 0.2.

4.3.4 Effect of Fe(III)/CA molar ratio

The iron/ligand molar ratio is an essential parameter to control the complexation efficiency which probably affect the performance when applying the complexes into photo-Fenton process. Tests were conducted to ascertain the effect of the Fe(III)/CA molar ratio on PHE removal by fixing Fe(III) concentration. As illustrated in Figure 4-8, with low molar ratio of CA (1:0.1), PHE decay followed the one-stage pattern. It can be ascribed to the incomplete complexation of Fe(III) leading to the presence of high percentage of Fe(III) aqua-complexes. Hence, the processes with low CA ratio were actually similar to the photo-Fenton systems without CA and insufficient Fe(III)-CA dosage restrained the generation of active species for PHE degradation. With Fe(III)/CA ratio increasing to 1:0.5 and 1:1, the two-stages pattern of PHE oxidation appeared due to the increased amount of Fe(III)-CA because the chelated complexes were predominantly responsible for the radical formation. Larger PHE removal was obtained with CA ratio of 1:1 than with 1:0.5, since the chelated Fe(III) complexes with CA molar ratio of 1:1 was higher than that with CA ratio of 1:0.5. When a Fe(III)/CA molar ratio of 1:2 being applied, the two-stages model of PHE maintained and the final removal of PHE (46.2%) was the same than with Fe(III)/CA molar ratio of 1:1, though the rate of PHE decay slowed down and the duration of the first step prolonged. With further increase of Fe(III)/CA molar ratio to 1:3, PHE disappearance reappeared the one-stage model. The variation of PHE decay rate and efficiency were possibly attributed to the presence of CA in excess and the photo-dissociation of Fe(III)-CA was restrained. This series of reactions indicated that the formation and the concentration of the complex Fe(III)-CA and its photo-decomposition were decisive parameters for PHE

degradation.

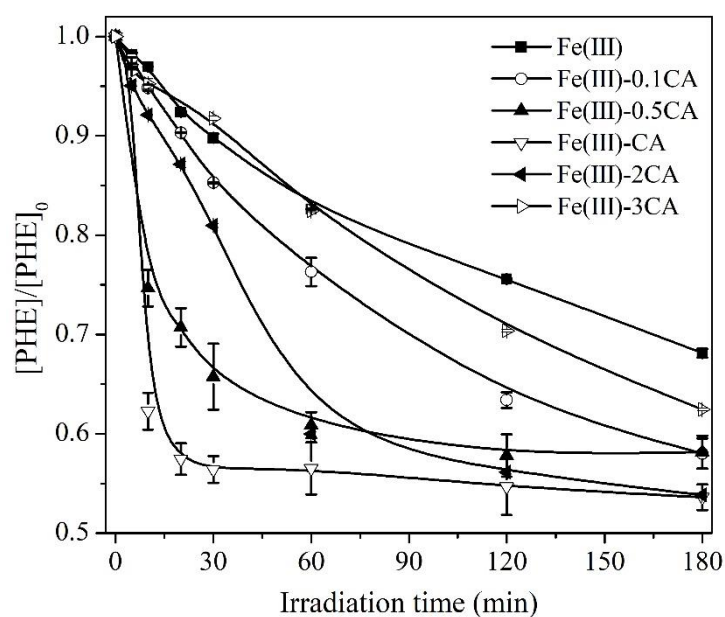


Figure 4-8 Effect of Fe(III)/CA molar ratio on PHE degradation; Initial conditions: $[PHE] = 10 \text{ mg L}^{-1}$, $[TW80] = 0.5 \text{ g L}^{-1}$, $[H_2O_2] = 5 \text{ mM}$, $[Fe(III)] = 0.5 \text{ mM}$, $[CA] = 0 \text{ to } 1.5 \text{ mM}$, $pH = 3.0 \pm 0.2$.

4.3.5 Effect of Fe(III)-CA concentration

According to the results of comparison with various systems and the effect of Fe(III)/CA ratio, the dosage of Fe(III)-CA is very important for PHE oxidation efficacy. Thus, the degradation of PHE with different concentrations of Fe(III)-CA was investigated and the results are displayed in Figure 4-9. It was evidently observed that, with addition of different dosages of Fe(III)-CA, the two-stages pattern of PHE oxidation was maintained (Figure 4-9a), and PHE decay rate increased then decreased in the first step and the maximum first order rate constant of $3.05 \times 10^{-2} \text{ min}^{-1}$ was achieved with 0.5 mM Fe(III)-CA (Figure 4-9b). With addition of Fe(III)-CA higher than 0.5 mM, more Fe(II) were generated from the photo-dissociation of Fe(III)-CA which would quench active HO^\bullet radicals via reaction (4-10), which resulted in the suppression of PHE decay rate and efficiency in the first step. The results of Fe(III)-CA

concentration effect confirmed our previous conclusion that Fe(III)-CA is crucial and rate limiting step for PHE oxidation.

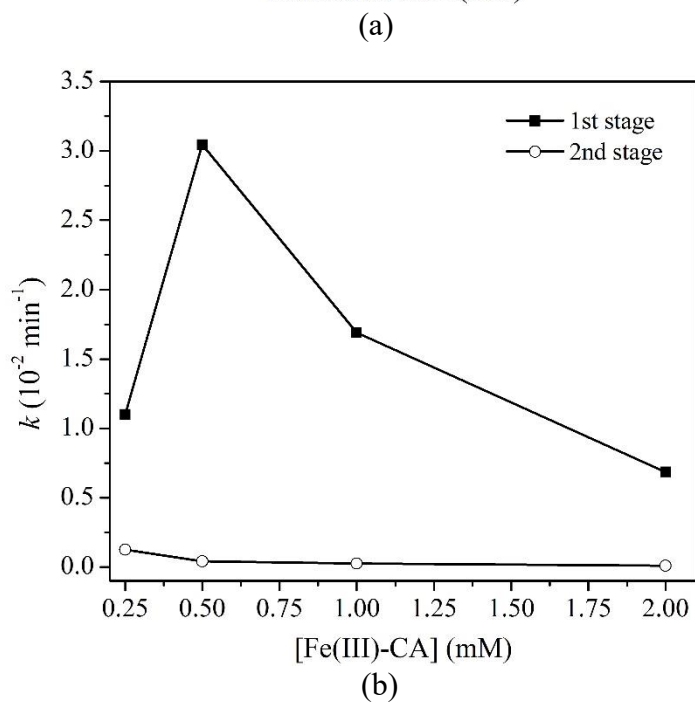
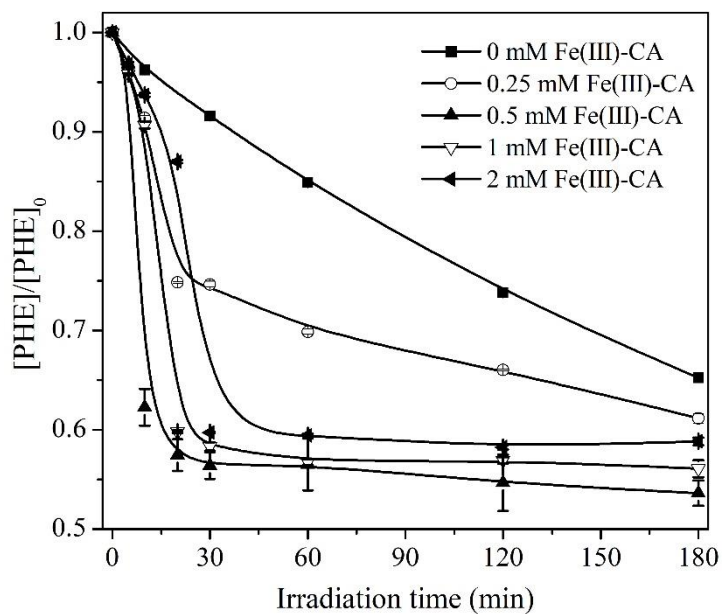
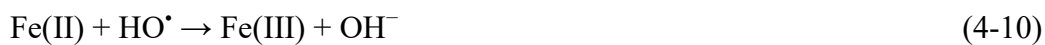


Figure 4-9 Effect of Fe(III)-CA concentration on (a)PHE oxidation and (b) the variation of pseudo first order rate constants of PHE decay. Initial conditions: [PHE] = 10 mg L⁻¹, [TW80] = 0.5 g L⁻¹, [H₂O₂] = 5 mM, pH = 3.0 ± 0.2.

4.3.6 Effect of H₂O₂ concentration

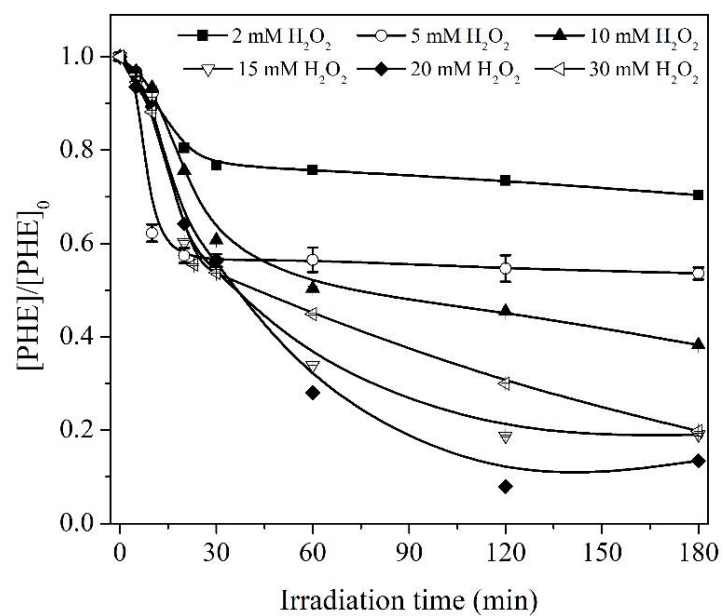
In photo-Fenton processes, the concentration of H_2O_2 is also an essential factor to be considered since H_2O_2 is the source of radical species. It is interesting to find that H_2O_2 concentration exerted different impact on PHE oxidation in the initial 30 min and the following reaction time as described in Figure 4-10a. In the initial 30 min, PHE oxidizing rate increased rapidly when H_2O_2 addition was less than 5 mM, with the first order rate constants increased from $1.07 \times 10^{-2} \text{ min}^{-1}$ with 2 mM H_2O_2 to $3.05 \times 10^{-2} \text{ min}^{-1}$ with 5 mM H_2O_2 (Table 4-1). When H_2O_2 loading was above 10 mM, the decay rate of PHE scarcely ranged with the rate constants were around $2.0 \times 10^{-2} \text{ min}^{-1}$ (Table 4-1). In the second reaction stage, PHE oxidation efficiency increased when H_2O_2 concentration was lower than 20 mM with the rate constants varying from 0.057×10^{-2} with 2 mM H_2O_2 to $0.86 \times 10^{-2} \text{ min}^{-1}$ with 20 mM H_2O_2 . Further addition of H_2O_2 up to 30 mM, PHE degradation rate decreased with the rate constant dropped to $0.66 \times 10^{-2} \text{ min}^{-1}$. Therefore, it can be concluded that the optimal H_2O_2 dosage were 5 mM and 20 mM respectively for the first and second stage of PHE oxidation. In the first step, active HO^\bullet radicals were mainly from Fe(III)-CA dominated photo-Fenton reaction. 2 mM addition of H_2O_2 was probably inadequate to yield enough active species for PHE oxidation, while the generation of available HO^\bullet radicals were limited by the concentration of Fe(III)-CA with H_2O_2 concentration higher than 5 mM. In the second step, HO^\bullet radicals were predominantly produced from Fe(II) through the Fenton reaction or from the photolysis of H_2O_2 when H_2O_2 was abundantly present. Therefore, with the increase of H_2O_2 concentration, the yielded HO^\bullet radicals increased for improvement of PHE oxidation. It is possible that the concentration of 30 mM H_2O_2 was beyond the threshold and quenching effect of HO^\bullet radicals through reaction (4-11) became prominent. Finally, at the end of the irradiation, the best PHE removal efficiency of 86.5% was achieved with 20 mM H_2O_2 .



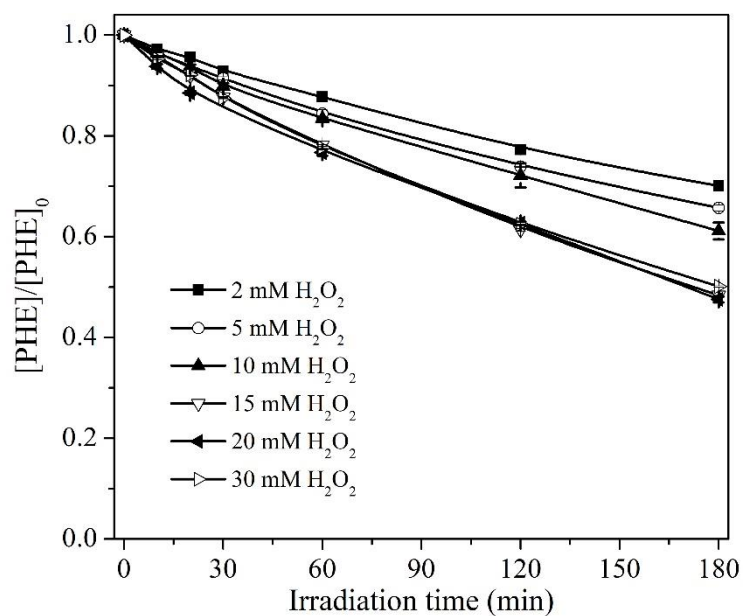
The effect of H_2O_2 concentration on total PHE removal in the photo-Fenton process was also compared with that in the UVB/ H_2O_2 process (Figure 4-10b) as shown in Figure 4-10c. The Fe(III)-CA invoveled photo-Fenton processes were more efficient for PHE oxidation than the UVB/ H_2O_2 processes with different H_2O_2 concentrations. The difference of total PHE removal enlarged with H_2O_2 being increased up to 20 mM and then the defference declined with 30 mM loading of H_2O_2 . The maxmium of total PHE removal difference, with or without Fe(III)-CA complexe, of 34% was observed at H_2O_2 concentration of 20 mM.

Table 4-1 First order rate constants of PHE decay with different H_2O_2 concentrations

[H_2O_2] (mM)	Initial 30 min		30-180 min	
	k (10^{-2} min^{-1})	R^2	k (10^{-2} min^{-1})	R^2
2	1.07	0.98	0.057	0.98
5	3.05	0.88	0.045	0.98
10	1.72	0.95	0.28	0.93
15	2.08	0.95	0.64	0.85
20	1.94	0.98	0.86	0.81
30	1.96	0.97	0.66	0.99



(a)



(b)

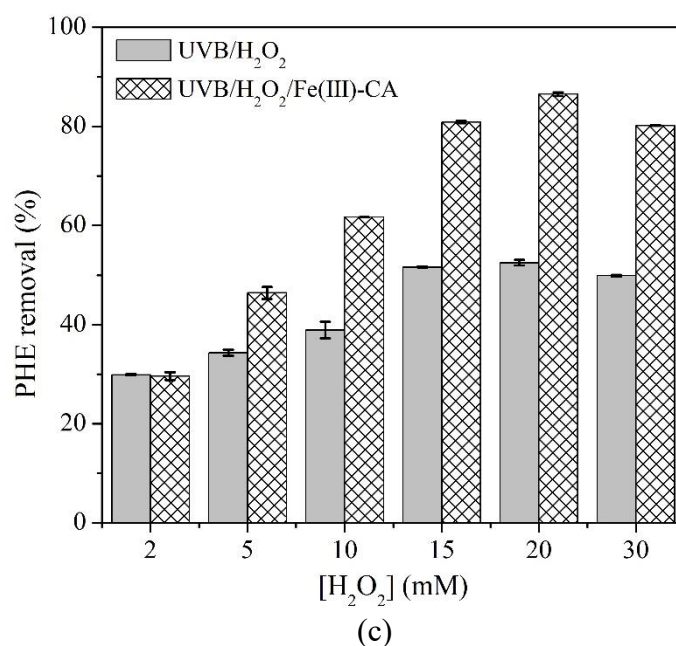
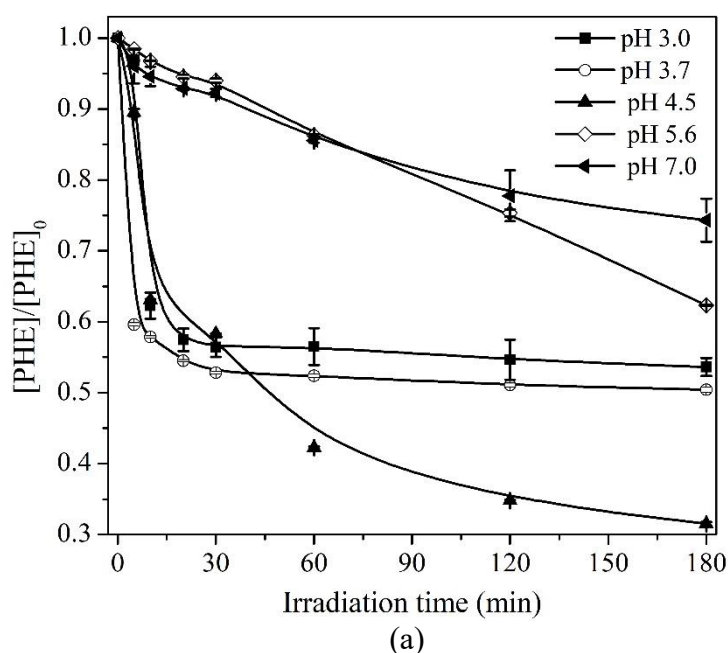


Figure 4-10 Effect of H₂O₂ concentration on PHE oxidation in (a) the UVB/H₂O₂/Fe(III)-CA system; (b) UVB/H₂O₂ system; (c) PHE removal in UVB/H₂O₂ and UVB/H₂O₂/Fe(III)-CA systems. Initial conditions: [PHE] = 10 mg L⁻¹, [TW80] = 0.5 g L⁻¹, [Fe(III)-CA] = 0.5 mM, pH = 3.0 ± 0.2.

4.3.7 Effect of initial solution pH

The pH is also an important parameter in pilot scale application to avoid unfavorable cost for adjusting the pH condition to meet the best operating efficiency. Therefore the effect of initial pH on PHE oxidation was ascertained over the pH range of 3.0-7.0 and the results are shown in Figure 4-11a. The oxidation efficiencies of PHE were relatively high over the pH range of 3.0-4.5. PHE decomposition was strongly facilitated at pH 4.5 and the final removal reached 70.0%. At the pH above 5.6, PHE decomposition presented a descending trend. Actually, at pH higher than 5.6, the acceleration of PHE oxidation became indistinctive with the introduction of Fe(III)-CA when comparing with UVB/H₂O₂ process (Figure 4-11b). It has been reported that Fe(III)-CA exists mainly in the forms of Fecit, FeOHcit⁻, and Fe₂(OH)₂cit₂²⁻ in aqueous solution within the pH range of 3.0-7.0 (Field et al., 1974; Morgan and Stumm 1996). Among those

species, Fecit^- and FeOHcit^- are the main photo reactive species to undergo ligand-to-metal charge transfer (LMCT) process upon irradiation (reactions 4-7 and 4-12). The photo reactive species shift from Fecit^- at lower pH to FeOHcit^- and $\text{Fe}_2(\text{OH})_2\text{cit}_2^{2-}$ at higher pH (Feng et al., 2012; Zhou et al., 2014). In addition, the precipitation of Fe(III) become pronounced at higher pH, which could hinder the photo-Fenton reactions (Clarizia et al., 2017). Therefore, the performance of PHE oxidation was strongly depend on the composition of Fe(III) species. The optimum pH condition near 4.5 for organics oxidation with Fe(III)-CA involved photo-Fenton process was also found in previous studies (Katsumata et al., 2006; Trovó and Nogueira 2011; Zhou et al., 2014).



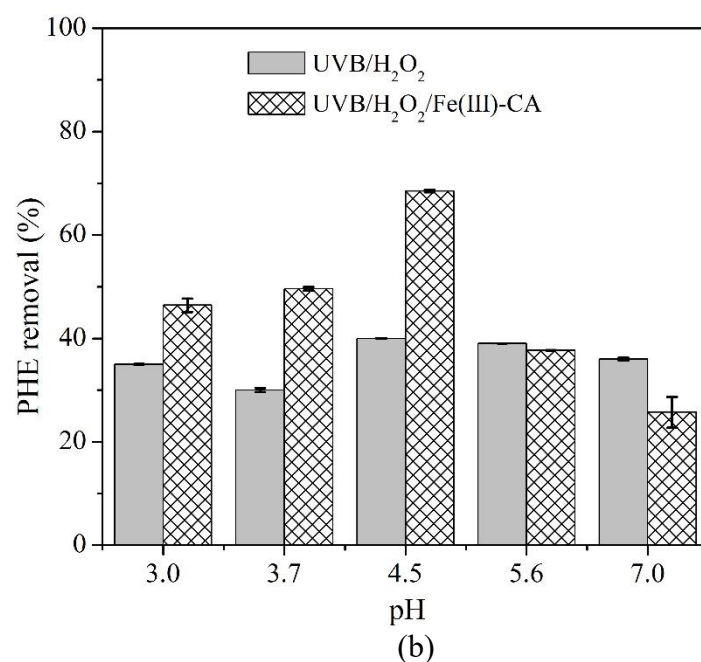


Figure 4-11 Effect of initial solution pH on (a) PHE oxidation in the UVB/H₂O₂/Fe(III)-CA system; (b) PHE removal in UVB/H₂O₂ and UVB/H₂O₂/Fe(III)-CA systems. Initial conditions: [PHE] = 10 mg L⁻¹, [TW80] = 0.5 g L⁻¹, [H₂O₂] = 5 mM, [Fe(III)-CA] = 0.5 mM.

Experiments of PHE oxidation in different systems were performed at the optimum pH condition as depicted in Figure 4-12. PHE oxidation was strongly promoted with addition of Fe(III)-CA, while it was evidently repressed with loading of Fe(III) comparing with the UVB/H₂O₂ process. The results indicated the possibility to extend the available pH range of the photo-Fenton processes replacing traditional Fe(II) or Fe(III) by Fe(III)-CA.

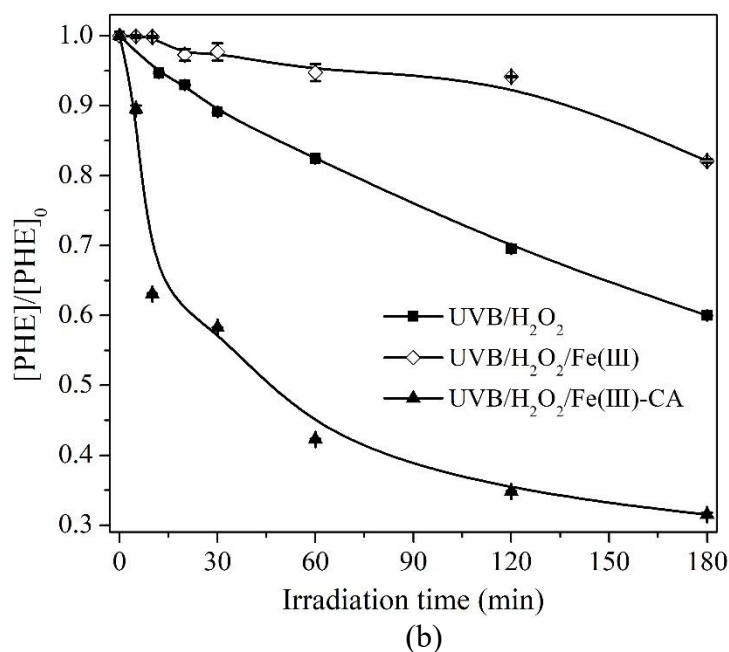


Figure 4-12 PHE degradation in different systems at $\text{pH} = 4.5 \pm 0.1$. Initial conditions: $[\text{PHE}] = 10 \text{ mg L}^{-1}$, $[\text{TW80}] = 0.5 \text{ g L}^{-1}$, $[\text{H}_2\text{O}_2] = 5 \text{ mM}$, $[\text{Fe(III)-CA}] = [\text{Fe(III)}] = 0.5 \text{ mM}$.

4.3.8 Radicals scavenging tests

According to the equations involved in the photo-Fenton reactions as discussed above, $\text{O}_2^{\bullet-}$ and HO^\bullet probably exerted important role on PHE oxidation. Hence, scavenging tests were performed to ascertain the role of the two types of radicals. Chloroform (CF) was employed as a quencher of $\text{O}_2^{\bullet-}$ due to its high reactivity with reductants ($3.0 \times 10^{10} \text{ M}^{-1} \text{ s}^{-1}$) and poor reactivity with HO^\bullet ($7.0 \times 10^6 \text{ M}^{-1} \text{ s}^{-1}$) (Teel and Watts 2002). Owing to the strong reactivity with HO^\bullet ($5.2 \times 10^8 \text{ M}^{-1} \text{ s}^{-1}$), tert-butanol (TBA) is used as a scavenger of HO^\bullet (Buxton et al., 1988a). As illustrated in Figure 4-13, with absence of radical quenchers, 46.4% of PHE removal could be achieved in 180 min. PHE removal was negligibly inhibited by the addition of CF, demonstrating that $\text{O}_2^{\bullet-}$ barely contributed to PHE oxidation. With the addition of TBA,

PHE degradation was intensely suppressed and PHE removal dramatically lessened to 12.8%, which suggested HO^\bullet was predominantly responsible for PHE oxidation in Fe(III)-CA employed photo-Fenton process.

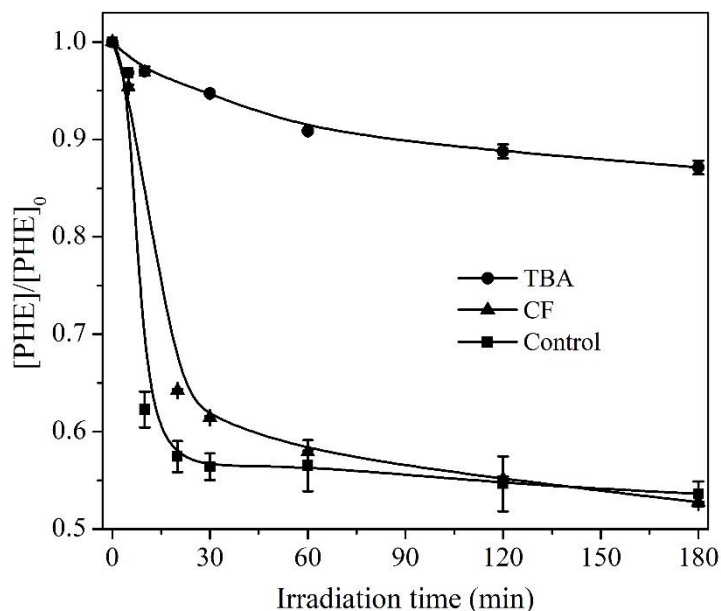


Figure 4-13 Free radicals scavenging tests for PHE oxidation. Initial conditions: $[\text{PHE}] = 10 \text{ mg L}^{-1}$, $[\text{TW80}] = 0.5 \text{ g L}^{-1}$, $[\text{H}_2\text{O}_2] = 5 \text{ mM}$, $[\text{Fe(III)-CA}] = 0.5 \text{ mM}$, $[\text{CF}] = [\text{TBA}] = 50 \text{ mM}$, $\text{pH} = 3.0 \pm 0.2$.

4.4 Conclusion

In this work, Fe(III)-CA was employed to replace traditional iron ions in the photo-Fenton systems for oxidizing PHE from mimic SW solution. Compared with Fe(III) involved photo-Fenton process, the employment of Fe(III)-CA strongly facilitated PHE oxidation in the initial stage of 30 min. However PHE degradation almost ceased in the following irradiation time. Fe(III)-CA is more efficient for PHE oxidation than other organic ligand chelated complexes. The impact of Fe(III)/CA ratio, Fe(III)-CA and H_2O_2 concentrations, and initial pH on PHE oxidation was investigated. The most suitable Fe(III)/CA ratio was 1:1, and the optimal Fe(III)-CA concentration was 0.5 mM. H_2O_2 dosage was one of the crucial factors for total PHE removal and PHE

oxidation efficiency could be achieved as high as 86.5% in 180 min with 20 mM H₂O₂. The most appropriate pH for PHE removal was 4.5. The dominant active species was HO[•] though O₂^{•-} were also involved in the photo-Fenton reactions.

References

- Abrahamson, H.B., Rezvani, A.B., Brushmiller, J.G., 1994. Photochemical and spectroscopic studies of complexes, of iron (III) with citric acid and other carboxylic acids. *Inorganica Chimica Acta* 226 (1-2), 117-127.
- Baba, Y., Yatagai, T., Harada, T., Kawase, Y., 2015. Hydroxyl radical generation in the photo-Fenton process: Effects of carboxylic acids on iron redox cycling. *Chemical Engineering Journal* 277, 229-241.
- Bandala, E.R., Cossio, H., Sánchez-Lopez, A.D., Córdova, F., Peralta-Herández, J.M., Torres, L.G., 2013. Scaling-up parameters for site restoration process using surfactant-enhanced soil washing coupled with wastewater treatment by Fenton and Fenton-like processes. *Environmental technology* 34 (3), 363-371.
- Benkelberg, H.-J., Warneck, P., 1995. Photodecomposition of iron (III) hydroxo and sulfato complexes in aqueous solution: wavelength dependence of OH and SO₄-quantum yields. *The Journal of Physical Chemistry* 99 (14), 5214-5221.
- Buxton, G.V., Greenstock, C.L., Helman, W.P., Ross, A.B., 1988. Critical review of rate constants for reactions of hydrated electrons, hydrogen atoms and hydroxyl radicals ($\cdot\text{OH}/\cdot\text{O}^-$) in aqueous solution. *Journal of Physical and Chemical Reference Data* 17 (2), 513-886.
- Clarizia, L., Russo, D., Di Somma, I., Marotta, R., Andreozzi, R., 2017. Homogeneous photo-Fenton processes at near neutral pH: a review. *Applied Catalysis B: Environmental* 209, 358-371.
- De Luca, A., Dantas, R.F., Esplugas, S., 2014. Assessment of iron chelates efficiency

- for photo-Fenton at neutral pH. *Water Research* 61, 232-242.
- Dulova, N., Kattel, E., Trapido, M., 2017. Degradation of naproxen by ferrous ion-activated hydrogen peroxide, persulfate and combined hydrogen peroxide/persulfate processes: the effect of citric acid addition. *Chemical Engineering Journal* 318, 254-263.
- Feng, X., Wang, Z., Chen, Y., Tao, T., Wu, F., Zuo, Y., 2012. Effect of Fe (III)/citrate concentrations and ratio on the photoproduction of hydroxyl radicals: application on the degradation of diphenhydramine. *Industrial & Engineering Chemistry Research* 51 (20), 7007-7012.
- Field, T.B., McCourt, J.L., McBryde, W., 1974. Composition and stability of iron and copper citrate complexes in aqueous solution. *Canadian Journal of Chemistry* 52 (17), 3119-3124.
- Giannakis, S., Hendaoui, I., Jovic, M., Grandjean, D., De Alencastro, L.F., Girault, H., Pulgarin, C., 2017. Solar photo-Fenton and UV/H₂O₂ processes against the antidepressant Venlafaxine in urban wastewaters and human urine. Intermediates formation and biodegradability assessment. *Chemical Engineering Journal* 308, 492-504.
- Han, D., Wan, J., Ma, Y., Wang, Y., Li, Y., Li, D., Guan, Z., 2015. New insights into the role of organic chelating agents in Fe (II) activated persulfate processes. *Chemical Engineering Journal* 269, 425-433.
- Hayyan, M., Hashim, M.A., AlNashef, I.M., 2016. Superoxide ion: generation and chemical implications. *Chemical Reviews* 116 (5), 3029-3085.
- Hoehl, K., Schoenberger, G., Busch-Stockfisch, M., 2014. Stimulus and recognition thresholds for the basic tastes in deionized water. Are the recommendations for citric acid too high. *Ernahrungs Umschau* 61 (8), 130-136.

- Huang, W., Brigante, M., Wu, F., Hanna, K., Mailhot, G., 2012. Development of a new homogenous photo-Fenton process using Fe (III)-EDDS complexes. *Journal of Photochemistry and Photobiology A: Chemistry* 239, 17-23.
- Karci, A., Arslan-Alaton, I., Bekbolet, M., Ozhan, G., Alpertunga, B., 2014. H₂O₂/UV-C and Photo-Fenton treatment of a nonylphenol polyethoxylate in synthetic freshwater: follow-up of degradation products, acute toxicity and genotoxicity. *Chemical Engineering Journal* 241, 43-51.
- Katsumata, H., Kaneco, S., Suzuki, T., Ohta, K., Yobiko, Y., 2006. Photo-Fenton degradation of alachlor in the presence of citrate solution. *Journal of Photochemistry and Photobiology A: Chemistry* 180 (1-2), 38-45.
- Klamerth, N., Malato, S., Agüera, A., Fernandez-Alba, A., Mailhot, G., 2012. Treatment of municipal wastewater treatment plant effluents with modified photo-Fenton as a tertiary treatment for the degradation of micro pollutants and disinfection. *Environmental Science & Technology* 46 (5), 2885-2892.
- Liu, X., Zhou, Y., Zhang, J., Luo, L., Yang, Y., Huang, H., Peng, H., Tang, L., Mu, Y., 2018. Insight into electro-Fenton and photo-Fenton for the degradation of antibiotics: mechanism study and research gaps. *Chemical Engineering Journal* 347, 379-397.
- Miralles-Cuevas, S., Oller, I., Pérez, J.S., Malato, S., 2014. Removal of pharmaceuticals from MWTP effluent by nanofiltration and solar photo-Fenton using two different iron complexes at neutral pH. *Water Research* 64, 23-31.
- Morgan, J.J., Stumm, W., 1996. *Aquatic chemistry: chemical equilibria and rates in natural waters*, Wiley.
- Nansheng, D., Feng, W., Fan, L., Mei, X., 1998. Ferric citrate-induced photodegradation of dyes in aqueous solutions. *Chemosphere* 36 (15), 3101-3112.

- Pignatello, J.J., Oliveros, E., MacKay, A., 2006. Advanced oxidation processes for organic contaminant destruction based on the Fenton reaction and related chemistry. *Critical Reviews in Environmental Science and Technology* 36 (1), 1-84.
- Silva, M.R., Vilegas, W., Zandoni, M.V.B., Nogueira, R.F.P., 2010. Photo-Fenton degradation of the herbicide tebuthiuron under solar irradiation: iron complexation and initial intermediates. *Water Research* 44 (12), 3745-3753.
- Stookey, L.L., 1970. Ferrozine---a new spectrophotometric reagent for iron. *Analytical chemistry* 42 (7), 779-781.
- Teel, A.L., Watts, R.J., 2002. Degradation of carbon tetrachloride by modified Fenton's reagent. *Journal of Hazardous Materials* 94 (2), 179-189.
- Trellu, C., Mousset, E., Pechaud, Y., Huguenot, D., van Hullebusch, E.D., Esposito, G., Oturan, M.A., 2016. Removal of hydrophobic organic pollutants from soil washing/flushing solutions: A critical review. *Journal of Hazardous Materials* 306, 149-174.
- Trovó, A.G., Nogueira, R.F., 2011. Diclofenac abatement using modified solar photo-Fenton process with ammonium iron (III) citrate. *Journal of the Brazilian Chemical Society* 22 (6), 1033-1039.
- Villa, R.D., Trovó, A.G., Nogueira, R.F.P., 2010. Soil remediation using a coupled process: soil washing with surfactant followed by photo-Fenton oxidation. *Journal of Hazardous Materials* 174 (1-3), 770-775.
- Wu, X., Gu, X., Lu, S., Xu, M., Zang, X., Miao, Z., Qiu, Z., Sui, Q., 2014. Degradation of trichloroethylene in aqueous solution by persulfate activated with citric acid chelated ferrous ion. *Chemical Engineering Journal* 255, 585-592.
- Yap, C.L., Gan, S., Ng, H.K., 2011. Fenton based remediation of polycyclic aromatic

- hydrocarbons-contaminated soils. *Chemosphere* 83 (11), 1414-1430.
- Yu, S., Gu, X., Lu, S., Xue, Y., Zhang, X., Xu, M., Qiu, Z., Sui, Q., 2018. Degradation of phenanthrene in aqueous solution by a persulfate/percarbonate system activated with CA chelated-Fe (II). *Chemical Engineering Journal* 333, 122-131.
- Zhang, Y., Klammerth, N., Chelme-Ayala, P., Gamal El-Din, M., 2016. Comparison of Nitrilotriacetic Acid and [S, S]-Ethylenediamine-N, N'-disuccinic Acid in UV-Fenton for the Treatment of Oil Sands Process-Affected Water at Natural pH. *Environmental Science & Technology* 50 (19), 10535-10544.
- Zhou, D., Wu, Y., Feng, X., Chen, Y., Wang, Z., Tao, T., Wei, D., 2014. Photodegradation of hexabromocyclododecane (HBCD) by Fe (III) complexes/H₂O₂ under simulated sunlight. *Environmental Science and Pollution Research* 21 (9), 6228-6233.

Chapter 5 Phenanthrene degradation in soil washing effluent by Fe(III)-EDDS photoactivation of persulfate

5.1 Introduction

AOPs, based on radical oxidation mechanism have been developed to the most popular and common applied technology for PAHs and various surfactant involved in soil washing effluent treatments due to its advantages of effective and complete decomposition of PAHs from the effluents. Among multiple AOPs, sulfate radicals ($\text{SO}_4^{\bullet-}$) based advanced oxidation processes (SR-AOPs) have been widely applied as effective and practice techniques for remediation of contaminated waters and soils (Wacławek et al., 2017b; Yen et al., 2011). $\text{SO}_4^{\bullet-}$ is a promising alternative of hydroxyl radical (HO^{\bullet}) due to its better stability and selectivity, longer half-life time as well as a wider pH range for the application (Anipsitakis and Dionysiou 2004). Persulfate ($\text{S}_2\text{O}_8^{2-}$, PS) is an ideal alternative oxidant ($E_0 = 2.01 \text{ V}$), which can be activated by various chemical or physical methods to generate stronger $\text{SO}_4^{\bullet-}$ ($E_0 = 2.6 \text{ V}$) (Usman et al., 2012a). In addition to its strong oxidation capacity, sulfate radical has revealed several advantages over other over other oxidants.

Iron, one of the chemical activators of PS, is the most abundant transition metal present in the earth's crust and exists in a variety of forms in water such as soluble, colloidal and particulate forms. In natural water, insoluble iron-containing oxides account for a large proportion (Faust and Zepp 1993), while dissolved iron is only found in a small percentage and most of them exists in the form of complex with organic ligands (Zhou et al., 2004). Polycarboxylates and (amino-)polycarboxylates like citrate, malonate, oxalate, EDTA, etc. can react with ferric ions (Fe^{3+}) to form stable and strong complexes and improve its solubility and stability in natural water (Chen et al., 2007). Moreover, such (amino-)polycarboxylate complexes are reported to have strong and fast photochemical reactivity under sunlight irradiation giving rise to oxidative species (Zhang et al., 2009). Those iron complexes such as Fe(III)-EDTA, Fe(III)-EDDS,

Fe(III)-oxalate or Fe(III)-citrate have exhibited high efficiency as photo-catalysts and as persulfate and hydrogen peroxide activators for the elimination of a variety of contaminants (Manenti et al., 2015; Miralles-Cuevas et al., 2018; Soriano-Molina et al., 2019). Ethylenediamine-N,N'-disuccinic acid (EDDS) is a structural isomer of EDTA, and [S,S]-EDDS, [R,R]-EDDS and [R,S/S,R]-EDDS are three stereo isomers of EDDS. Among those isomers, [S,S]-EDDS is recognized and employed as a environmentally safe and friendly substitution for EDTA for environmental restoration since it is easier biodegraded than EDTA (Nagaraju et al., 2007).

In this work, Fe(III)-EDDS complex was used to improve the PS photo-activation for the phenanthrene (PHE) degradation in TW80 present SW solution under simulated solar light irradiation. Main physicochemical parameters such as concentration of chemical species and pH were investigated through the PHE degradation efficiency. The second-order rate constants of the reactions for generated radicals ($\text{SO}_4^{\cdot-}$, HO^{\cdot} , $\text{Cl}_2^{\cdot-}$) with PHE and Tween 80 in solution were identified to help elucidating the performance of PHE degradation in different systems. This work provides a novel proposal of application of Fe(III)-EDDS for SW effluent treatments.

5.2 Experimental details

5.2.1 Chemicals

Tween 80 (TW80), phenanthrene (PHE), ferric perchlorate ($\text{Fe}(\text{ClO}_4)_3 \cdot 9\text{H}_2\text{O}$), sodium chloride (NaCl , $\geq 99.5\%$) were obtained from Sigma-Aldrich. Ethylenediamine-N,N'-disuccinic acid trisodium salt solution (EDDS, 35% in water) was purchased from Fluka. Tert-butanol (TBA, $\text{C}_4\text{H}_{10}\text{O}$) and methanol (MeOH , CH_3OH) were supplied by Fisher Chemical. All the other used reagents and chemicals were of analytical grade and all the solutions employed in this work were prepared with purified water from

Millipore Ultra-Pure System (18.2 MΩ cm). The stock solutions of Fe(III)-EDDS were a mixture of appropriate amount of newly prepared aqueous solutions of ferric perchlorate and EDDS at a stoichiometry ratio of 1:1.

5.2.2 Preparation of the synthetic SW effluent

TW80 is one of the suggested and most applied enhancing-solubility nonionic surfactants that increases the solubility of HOCs due to its notable features of lower critical micellar concentration (CMC), lower soil sorption capacity, lower toxicity, as well as higher solubilization ability and higher cost-effectiveness (Mulligan et al., 2001b). It is known that above CMC, the surface tension of HOCs varies with a much smaller slope and the solubility of HOCs is strongly improved (Trellu et al., 2016a). The CMC of TW80 is equal to 0.016 g L⁻¹ (López-Vizcaíno et al., 2012) which is much lower compared with other surfactants. Due to the above advantages, TW80 was chosen as the aiding compound and its solubilization capacity of PHE was investigated.

5.2.3 Irradiation experiments and degradation kinetics

50 mL of samples were irradiated in a jacketed cylindrical Pyrex reactor connected to water cooling system and placed in a rectangular wood box to prevent the interference from the external light sources. Four tubular lamps (Sylvania, F15W/350BL), used as irradiation sources, were fixed on the top of the wood box. The irradiation energy was determined employing an optical fiber with a charge coupled device (CCD) spectrophotometer (Ocean Optics USD 2000 + UV-vis) previously calibrated with a DH-2000-CAL reference lamp. The energy reaching the reactor determined between 300 and 400 nm (1390 μW cm⁻²) was very closed to the typical solar emission in the same wavelength range (Bianco et al., 2016).

In Figure 5-1, emission spectrum of light sources and UV-vis absorption spectra of chemical species (carried out with a Cary 300 UV-visible spectrophotometer) were presented. An overlap between the emission spectrum of the lamps and the absorption spectrum Fe(III)-EDDS complex was highlighted. PHE absorbed in the ultraviolet region with two maxima at 252 nm and 295 nm. The main absorption region was located at $\lambda < 250$ nm for PS and $\lambda < 300$ nm for PHE in TW80 solution. Fe(III)-EDDS clearly exhibited a broad but gradual decrease absorption at the region of wavelengths up to approximately 400 nm and the overlapping absorption with the lamp emission spectra from 300 nm and 400 nm as well.

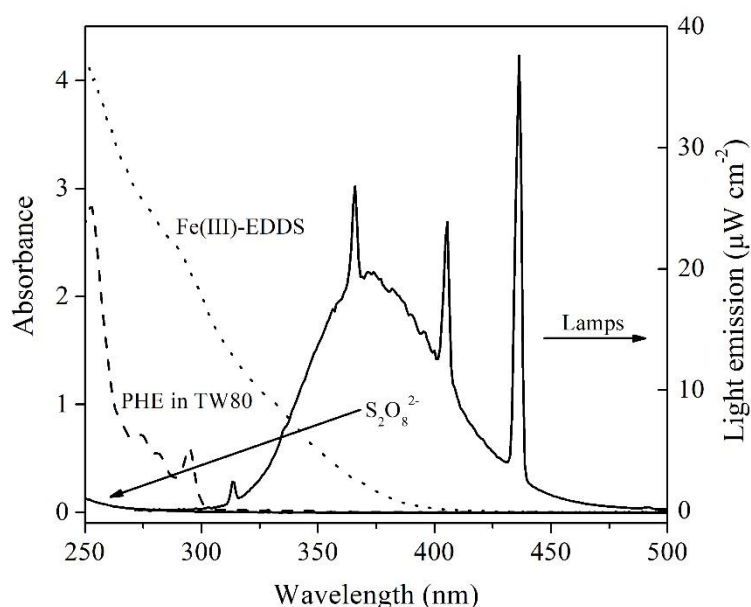


Figure 5-1 Absorption spectra of Fe(III)-EDDS (0.5 mM), $S_2O_8^{2-}$ (5 mM) and 90 μ M of PHE in 0.5 g L⁻¹ of TW80. Emission spectrum of the adopted irradiation lamps with a maximum wavelength centred at 365 nm.

All experiments were carried out at 293 ± 2 K and solutions were magnetically stirred with a magnetic bar to insure the homogenous mixture of the solution. At regular intervals, 0.5 mL of sample was withdrawn and analyzed by an UPLC-UV system (Alliance) equipped with a photodiode array detector. The eluent was a mixture of water and acetonitrile (30/70, v/v) with isocratic mode in a flow rate of 1 mL min⁻¹. The

column was a Nucleodur 100-5 C18 of 150 mm × 4.6 mm with particle size 5 μm. The degradation efficiency (DE) and pseudo-first-order decay of PHE were determinate using the following Eqs.(5-1) and (5-2):

$$DE (\%) = (1 - \frac{[PHE]}{[PHE]_0}) \times 100 \quad (5-1)$$

$$\frac{[PHE]}{[PHE]_0} = \exp (k t) \quad (5-2)$$

where $[PHE]_0$ and $[PHE]$ are the initial and residual concentrations of PHE at time 0 and t , respectively. k is the pseudo-first-order apparent rate constant (s^{-1}). The pH of the solutions was adjusted with 0.1 M of $HClO_4$ or $NaOH$ solutions.

5.2.4 Laser flash photolysis

The determination of the second order rate constants was carried out with the nanosecond laser flash photolysis (LFP) apparatus from Applied Photophysics (LKS60). A 266 nm excitation was used to generate radicals from solution and apparatus description has been reported elsewhere (Huang et al., 2018). An appropriate volume of chemical stock solutions ($TW80$, $S_2O_8^{2-}$, H_2O_2 and Cl^-) was mixed just before each experiment to obtain the desired mixtures and concentrations. All experiments were performed at ambient temperature (293 ± 2 K) and in aerated solutions. HO^\bullet reactivity was detected by employing chemical competition kinetics with thiocyanate ions (SCN^-) and dithyocianate radical anion ($SCN_2^{\bullet-}$) specie, and the determination wavelength of $SCN_2^{\bullet-}$ was at 470 nm. $SO_4^{\bullet-}$ anion decay was followed at 450 nm corresponding to the maximum absorption of this species (Hayon et al., 1972) . Dichloride radical anion ($Cl_2^{\bullet-}$) specie was generated using electron transfer reaction between photo generated $SO_4^{\bullet-}$ and Cl^- . The same method has been previously applied to generate $Cl_2^{\bullet-}$ in solution and follow their activity toward organic molecules (Wu et al., 2017). The second order rate constants between selected radicals ($SO_4^{\bullet-}$ and $Cl_2^{\bullet-}$) and $TW80$ or

PHE were determined from the regression lines of the logarithmic decays of radical transient (monitored at 450 nm and 340 nm respectively) as a function of the quencher concentration. Each value was the average of 4 consecutive laser pulses and the reported error is ± 3 , obtained from the scattering of the experimental data from the fitting line.

5.2.5 Competition kinetic

The second order rate constants for reaction of PHE with $\text{SO}_4^{\bullet-}$ and HO^\bullet were determined by competition kinetics method as described below as Eq.(5-3).

$$\ln\left(\frac{[\text{PHE}]_t}{[\text{PHE}]_0}\right) = \frac{k_{\text{HO}^\bullet/\text{SO}_4^{\bullet-}, \text{PHE}}}{k_{\text{HO}^\bullet/\text{SO}_4^{\bullet-}, \text{BPA}}} \ln\left(\frac{[\text{BPA}]_t}{[\text{BPA}]_0}\right) \quad (5-3)$$

Bisphenol A (BPA), with known rate constants with both $\text{SO}_4^{\bullet-}$ and HO^\bullet ($k_{\text{HO}^\bullet, \text{BPA}} = 4.7 \times 10^9 \text{ M}^{-1} \text{ s}^{-1}$ and $k_{\text{SO}_4^{\bullet-}, \text{BPA}} = 8.6 \times 10^9 \text{ M}^{-1} \text{ s}^{-1}$ (Huang et al., 2018) was used as reference compound in this study. The initial reaction solution contained 10 μM BPA, 2 μM PHE and 10 μM PS or H_2O_2 . Samples (0.5 mL) were withdrawn at predetermined intervals and were the analyzed via UPLC.

5.3 Results and discussion

5.3.1 PHE degradation under various systems

The solubility of PHE was tested using different concentration of TW80 in water. The results reported in Figure 5-2 indicate that PHE solubility increased with the concentration of TW80 and a maximum of PHE solubility was reached around 16 mg L^{-1} (corresponding to a concentration of 90 μM). This maximum solubility of PHE was obtained from 0.5 g L^{-1} of TW80. This concentration of TW80 was then used to prepare PHE solution for all experiments.

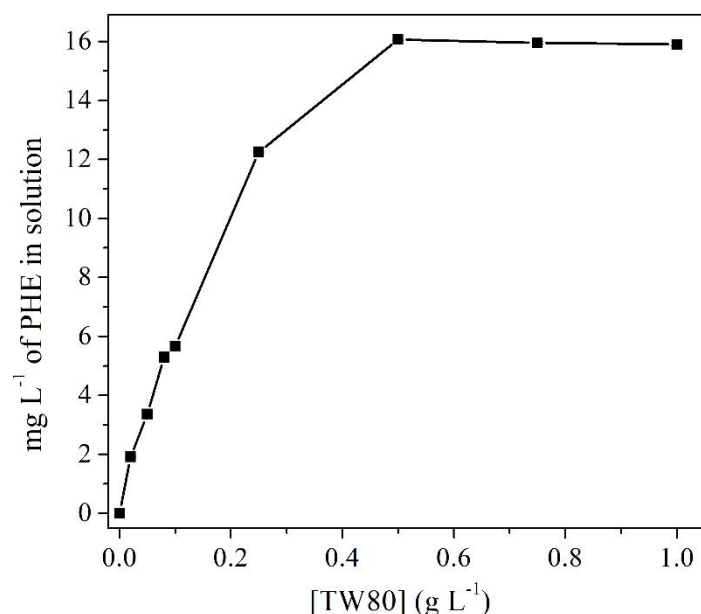
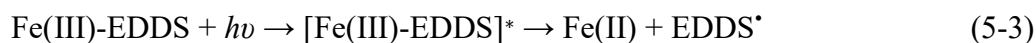


Figure 5-2 Solubility of PHE using different concentrations of TW80

The PHE degradation under simulated solar light at pH 3.5, using different mixture of Fe(III)-EDDS, Fe(III) and PS is reported in Figure 5-3a. Control experiments showed that very low degradation of PHE (less than 5%) occurred with the involvement of Fe(III)-EDDS complex and PS in the dark. Under irradiation, the direct photolysis (without PS and iron complexes) of PHE was negligible, less than 8% and the addition of Fe(III)-EDDS (0.5 mM) not significantly changed the efficiency of PHE degradation after 150 min of irradiation. As a contrary, about 30% removal of PHE was achieved in the presence of PS (5 mM) with UVA light due to the photogeneration of sulfate radicals that contributed to PHE degradation. Further addition of Fe(III) gave rise to ~35% of PHE removal. So, although Fe(III) can be photo-reduced to Fe(II) (Brand et al., 1998b) which is able to activate PS leading to the generation of sulfate radicals (Anipsitakis and Dionysiou 2004; Liang et al., 2004), only 5% of PHE degradation was achieved compared with UV/PS system. In the system with replacement of Fe(III) by Fe(III)-EDDS (0.5 mM) to PS solution, the performance was much more pronounced and PHE removal was remarkably strengthened under irradiation, especially in the first 30 minutes. This difference can be explained by the lower photoreactivity of Fe(III)

aquacomplexes in comparison with Fe(III)-EDDS at pH around 3.5 (Catastini et al., 2004; Huang 2012) since Fe(II) formation from Fe(III) aqua complexes is lower than from Fe(III)-EDDS at $\lambda > 300$ nm. Therefore, in the presence of PS, sulfate radical formation is more important with Fe(III)-EDDS (reactions 5-3 and 5-4):



Under sun-simulated irradiation in the presence of Fe(III)-EDDS, PHE exhibited two different decay steps (Figure 5-3a). In the first 30 min of irradiation, Fe(III)-EDDS was almost completely degraded at pH 3.5 (Figure 5-3b) to produce Fe(II) which represented the rate-limiting parameter for $\text{SO}_4^{\bullet-}$ formation. In the second step, after complete decomposition of Fe(III)-EDDS, iron remained in the form of Fe(III) aquacomplexes, and under the influence of UVA light, hydroxyl radical and Fe(II) could be generated as well (reaction 5-5) (Křýsová et al., 2003; Mailhot et al., 2002b). In the presence of PS, Fe(II) led to Fe(III) again (reaction 5-4) and were in the presence of the (photo)chemical cycle involving Fe(III) and Fe(II). In this system, the degradation of PHE was mainly attributed to the formation of $\text{SO}_4^{\bullet-}$ and HO^{\bullet} through analogous reactions obtained with Fe(III) aquacomplexes in solution and the subsequent cycle of Fe(III)/Fe(II). In fact, the degradation kinetic after 30 min followed the same profile compared with those obtained where PS was mixed with Fe(III) aquacomplexes.

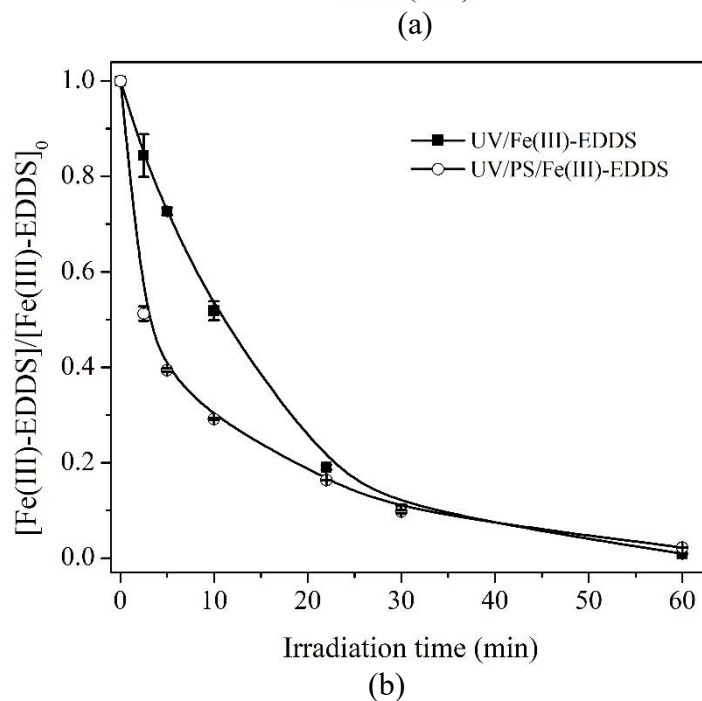
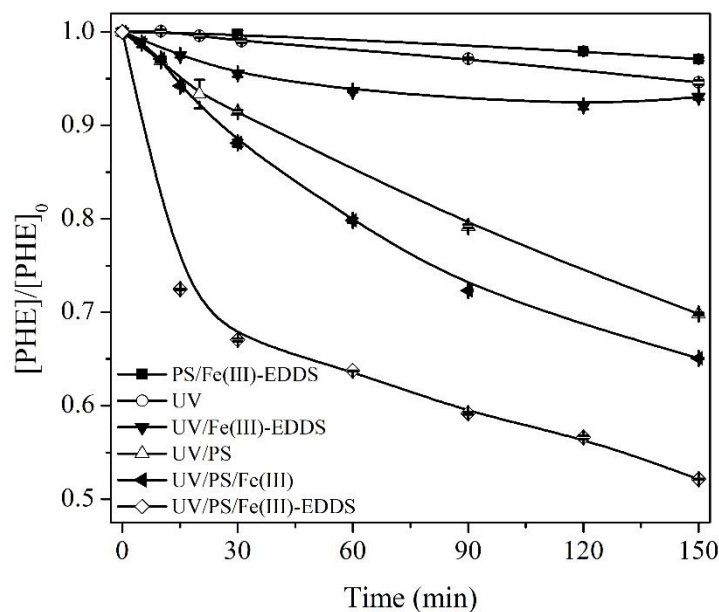
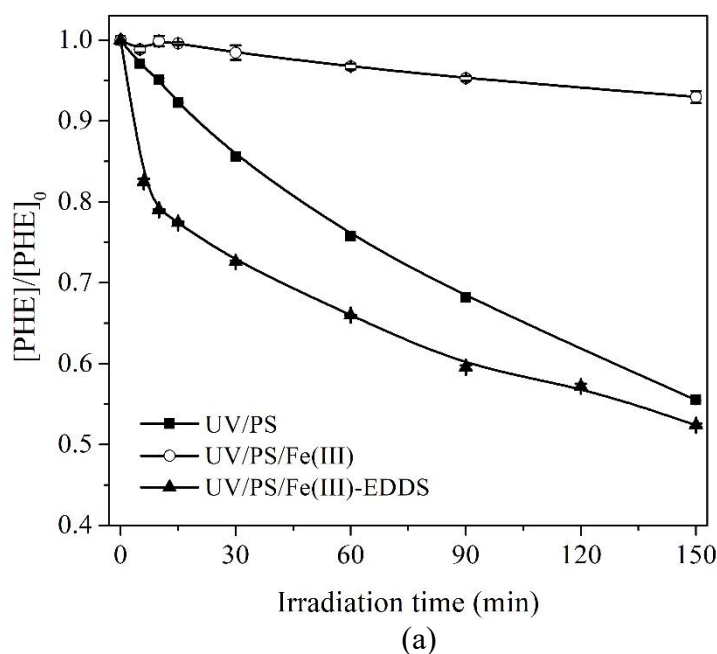


Figure 5-3 (a) Degradation of PHE and (b) degradation of Fe(III)-EDDS in different systems. Initial conditions: $[PS] = 5 \text{ mM}$, $[Fe(III)] = [Fe(III)\text{-EDDS}] = 0.5 \text{ mM}$, $[PHE] = 90 \text{ }\mu\text{M}$, $[TW80] = 0.5 \text{ g L}^{-1}$, $\text{pH} = 3.5 \pm 0.2$.

Same experiments conducted at pH 7.0 (Figure 5-4a) indicated that an enhancement of PHE degradation was still acquired with Fe(III)-EDDS, suggesting that the iron complex is photoactive also at higher pH (Wu et al., 2014). As a contrary, a strong

inhibition of PHE degradation occurred with Fe(III) aquacomplexes and PS. This effect could be ascribed to the precipitation of Fe(III) at pH > 4.0, resulting in absorption of light by iron particles and a potential screening effect for the photolysis of PS and also a very low photoreactivity of precipitated iron species.

What should be noted is on the contrary of many studies involving iron species, in our system UV/PS/Fe(III)-EDDS no significant effect of pH in the range 3.0 to 8.5 was obtained (Figure 5-4b). This observation was quite surprising, if we compare with former studies (Wu et al., 2015; Wu et al., 2014b) but was attributed to the presence of TW80 which modified the reactivity of radical species (see following results).



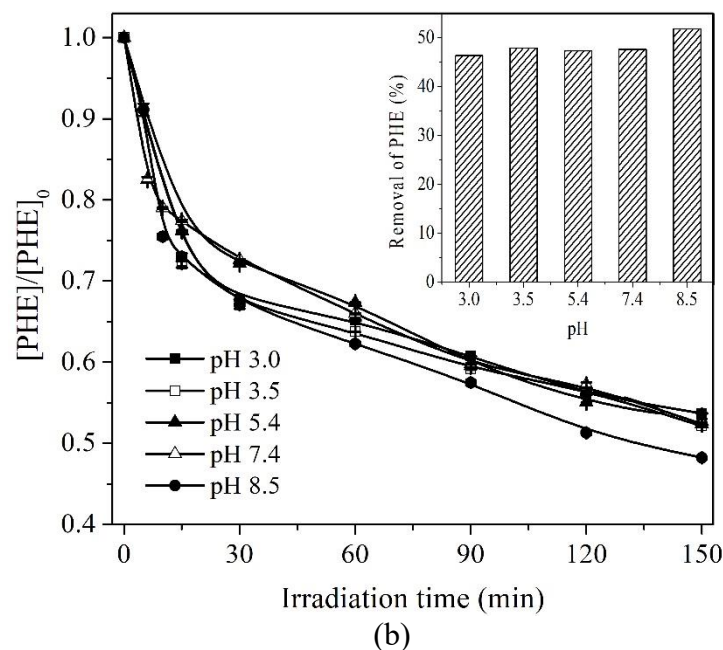


Figure 5-4 (a) Degradation of PHE in different systems at initial pH 7.0 ± 0.2 ; (b) Influence of initial pH on photo degradation of PHE in aqueous solution of TW80, insert is the removal percentage of PHE as a function of pH. Initial conditions: $[PS] = 5 \text{ mM}$, $[Fe(III)] = [Fe(III)\text{-EDDS}] = 0.5 \text{ mM}$, $[PHE] = 90 \text{ }\mu\text{M}$, $[TW80] = 0.5 \text{ g L}^{-1}$.

5.3.2 Effect of Fe(III)-EDDS

The effects of persulfate (PS) and Fe(III)-EDDS concentrations were investigated on the PHE degradation efficiency. PHE degradation involving different concentrations of Fe(III)-EDDS with 5 mM PS is reported in Figure 5-5a. After 30 min of irradiation, an enhancement of PHE degradation (more than 3 times) was achieved with the increase of Fe(III)-EDDS concentration from 0 to 0.5 mM (Figure 5-5b). However, the degradation efficiency of PHE decreased with the further increase of iron complex concentration. In fact, a scavenging effect of Fe(III)-EDDS and Fe(II) toward $SO_4^{\bullet-}$ was expected at higher concentrations (Peng et al., 2017; Yu et al., 2018b). Considering that a second order rate constant of $9.9 \times 10^9 \text{ M}^{-1} \text{ s}^{-1}$ has been determined for the reaction between $SO_4^{\bullet-}$ and Fe(II) (E. et al., 1966), it was possible to argue that scavenging effect of ferrous ions, that were more stable in solution at pH 3.5, became significant at higher

dosage of Fe(III)-EDDS. The maximum degradation of PHE (33%) after 30 min was reached using 0.5 mM Fe(III)-EDDS, while after 150 min the highest degradation efficiency (55%) was obtained with 0.25 mM of Fe(III)-EDDS (Figure 5-5b). This shift of the maximum efficiency after 30 min was attributed to the higher load of Fe(II) and EDDS at higher concentration of Fe(III)-EDDS and consequently stronger scavenging effect of sulfate radicals.

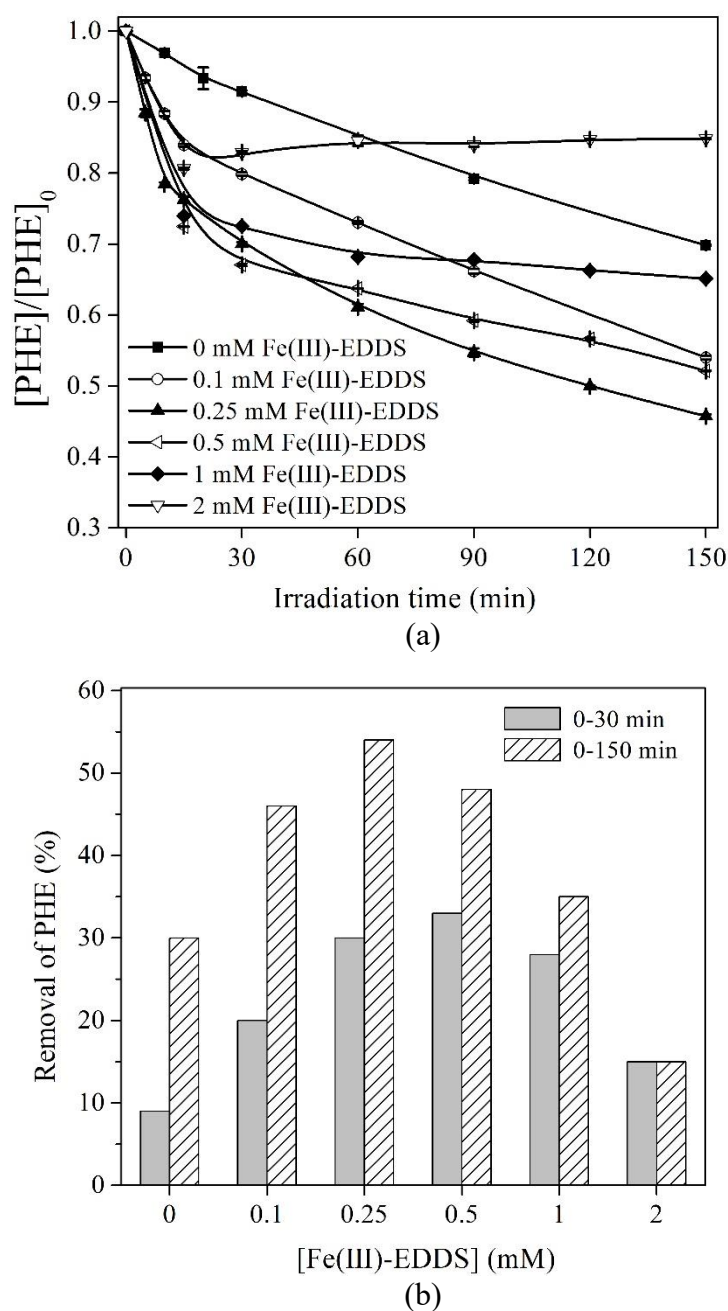


Figure 5-5 Influence of Fe(III)-EDDS concentration (a) on the degradation of PHE and

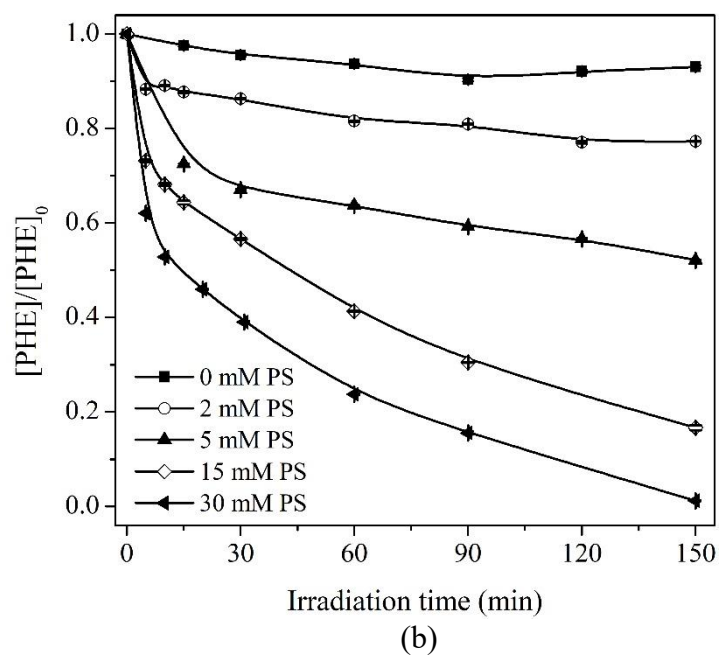
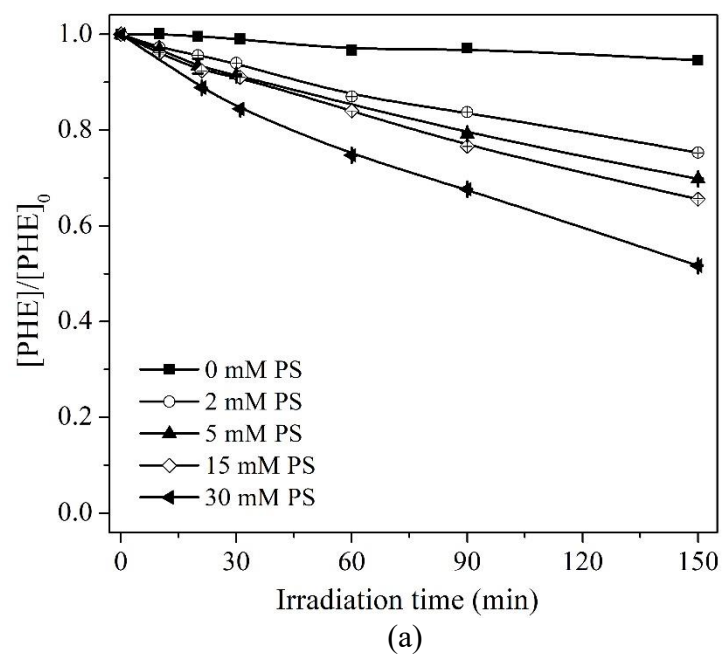
(b) removal percentages of PHE. Initial conditions: $[PS] = 5 \text{ mM}$, $[PHE] = 90 \text{ }\mu\text{M}$, $[TW80] = 0.5 \text{ g L}^{-1}$, $\text{pH} = 3.5 \pm 0.2$.

5.3.3 Effect of PS concentrations

To further explore the degradation performance of PHE in the system PS/Fe(III)-EDDS, the effect of persulfate concentration was investigated. As shown in Figure 5-6, PHE degradation efficiency was strongly promoted by increasing PS loading from 0 to 30 mM both for the photolysis of PS alone (Figure 5-6a) and in the presence of Fe(III)-EDDS (Figure 5-6b). The influence of Fe(III)-EDDS was much pronounced at higher concentration of persulfate. In the presence of Fe(III)-EDDS and after 150 min of irradiation, the enhancement of PHE degradation with 2 mM of PS was less than 2% while with 5 mM of PS the enhancement was around 18% and more than 50% with 15 and 30 mM of PS.

The effect of PS concentration on PHE removal with 150 min irradiation in the UV/PS/Fe(III)-EDDS process was also compared with that in the UV/PS process as shown in Figure 5-6c. The Fe(III)-EDDS involved processes were more efficient for PHE oxidation than the UV/PS processes with different PS concentrations. The difference of total PHE removal enlarged with PS being increased up to 30 mM. The total PHE removal doubled with addition of Fe(III)-EDDS compared with that in the UV/PS process at PS concentration of 30 mM.

These results suggested that Fe(III)-EDDS had stronger impact at higher concentration of PS showing that the generation of sulfate radical through reaction between PS and Fe(II) was the main contribution of the efficiency of the system.



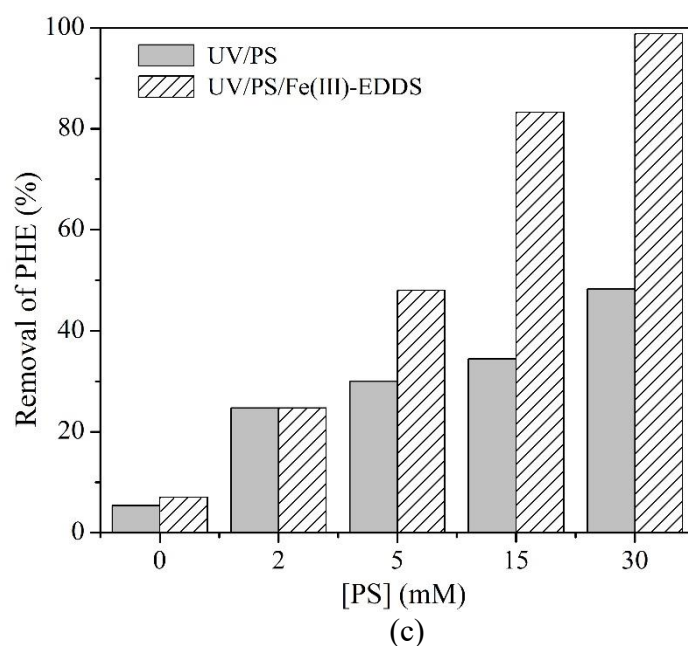


Figure 5-6 Effect of PS dose on PHE oxidation in the (a) UV/PS system; (b) UV/PS/Fe(III)-EDDS system; (c) PHE removal percentage in UV/PS and UV/PS/Fe(III)-EDDS systems. Initial conditions: $[PHE] = 90 \mu M$, $[TW80] = 0.5 g L^{-1}$, $[Fe(III)-EDDS] = 0.5 mM$, $pH = 3.5 \pm 0.2$.

5.3.4 Effect of Fe(III)/EDDS ratio

According to previously reported works; the ratio of Fe(III) and EDDS concentrations represented a key parameter for the efficiency of the pollutants removal in water (Li et al., 2010). The concentration of EDDS was kept constant at 0.5 mM while various initial loads of Fe(III) were applied. As shown in Figure 5-7, the initial degradation rate of PHE increased with a higher concentration of Fe(III). At 1 mM of Fe(III) the final elimination of PHE was higher than at 0.5 or 0.25 mM. This observation was resulted from the fact that at 1 mM of Fe(III), there were in solution 0.5 mM of Fe(III)-EDDS and 0.5 mM of Fe(III) aquacomplexes. The two iron species were photo-transformed into Fe(II) which could activate PS to generate sulfate radicals and moreover Fe(III) aquacomplexes generated photochemically also hydroxyl radicals. So in these conditions, a higher amount of sulfate and hydroxyl radicals were generated to

increase the degradation of PHE. At concentrations of Fe(III) of 0.25 or 0.5 mM, the final removal efficiencies of PHE were very close with a little higher efficiency at 0.25 mM. During the first step of reactions, Fe(III) was reduced into Fe(II) and EDDS was oxidized. However if there were some residual EDDS remaining in solution, Fe(II) species were easily re-oxidized to Fe(III) and combined with EDDS to generate Fe(III)-EDDS complex (Li et al., 2010). As a consequence, the formation of $\text{SO}_4^{\bullet-}$ and the degradation of PHE photo-induced by Fe(III)-EDDS complex could continue.

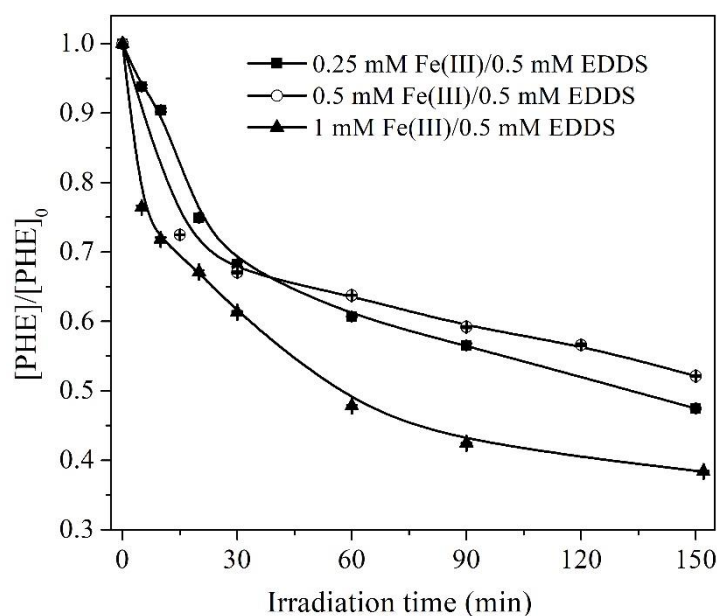


Figure 5-7 Degradation of PHE using different concentrations of Fe(III) in the presence of 0.5 mM of EDDS. Initial conditions: $[\text{PHE}] = 90 \mu\text{M}$, $[\text{TW80}] = 0.5 \text{ g L}^{-1}$, $[\text{PS}] = 5 \text{ mM}$, $\text{pH} = 3.5 \pm 0.2$

5.3.5 Effect of TW80 concentration

To better explore the role of TW80 in this system, experiments with 0.5, 0.75 and 1 g L^{-1} of TW80 were carried out. The increase of the surfactant concentration from 0.5 to 1.0 g L^{-1} inhibited significantly PHE degradation (Figure 5-8a). In fact, when TW80 concentration increased to a factor of 1.5 (0.75 g L^{-1}) and 2 (1 g L^{-1}), the apparent rate

constants of PHE degradation in the first stage were reduced to 54% and 30% of the rate constant with 0.5 g L⁻¹ TW80, respectively (Figure 5-8b). The negative effect acquired at higher TW80 concentrations could be ascribed to the competition between TW80 and PHE for the reactivity with photo generated sulfate radicals. In fact, as reported in Table 5-1, a second order rate constant between SO₄^{•-} and TW80 ($k_{TW80,SO_4^{•-}}$) of $(4.6 \pm 0.2) \times 10^9 \text{ M}^{-1} \text{ s}^{-1}$ has been determined. At 0.5 g L⁻¹ of TW80 and considering the reactivity between SO₄^{•-} and Fe(III)-EDDS and PS (Bianco et al., 2017; Neta et al., 1988) reported in literature and with TW 80 and PHE (Table 5-1), we can argue that about 33 % of photo generated SO₄^{•-} reacted with TW80 while only 7% with PHE in solution. However, increasing the concentration of TW80 to 1 g L⁻¹, the values were respectively 49% and 5%. Moreover, in previously works it has been suggested that PHE was trapped into the micelle core of the surfactant, leading to a lower availability toward oxidizing radicals (Trellu et al., 2016a; Trellu et al., 2017). The significant sulfate radical selectivity between TW80 and PHE clearly demonstrated that the concentration of TW80 was the major parameter determining the efficiency of oxidative treatment adopted for PHE removal.

Table 5-1 Second order rate constants (M⁻¹ s⁻¹) of TW80 and PHE with different radicals determined using LFP and competition kinetic method

Compounds	$k_{HO^{\bullet}}$	$k_{SO_4^{•-}}$	$k_{Cl_2^{•-}}$
TW80	$(9.9 \pm 0.1) \times 10^9$	$(4.6 \pm 0.2) \times 10^9$	$(7.1 \pm 0.1) \times 10^6$
PHE	$(6.1 \pm 0.2) \times 10^9$	$(4.3 \pm 0.4) \times 10^9$	$(4.6 \pm 0.3) \times 10^8$

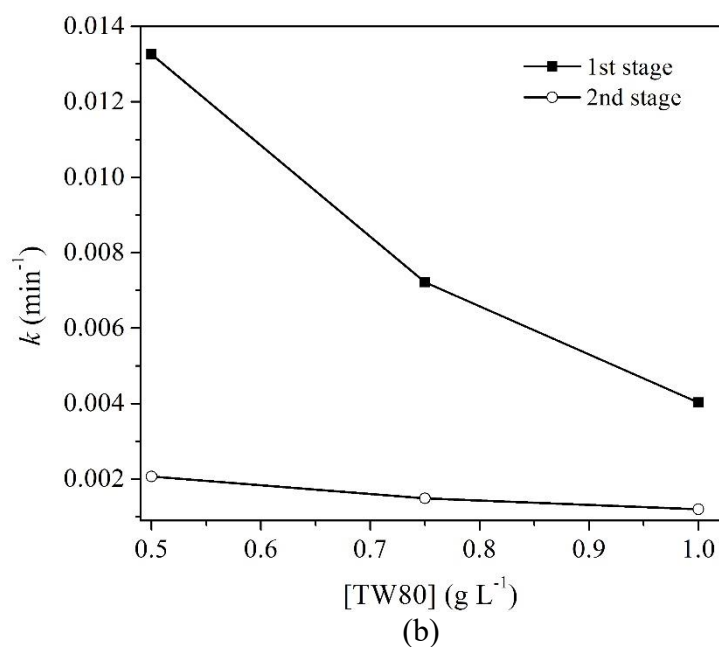
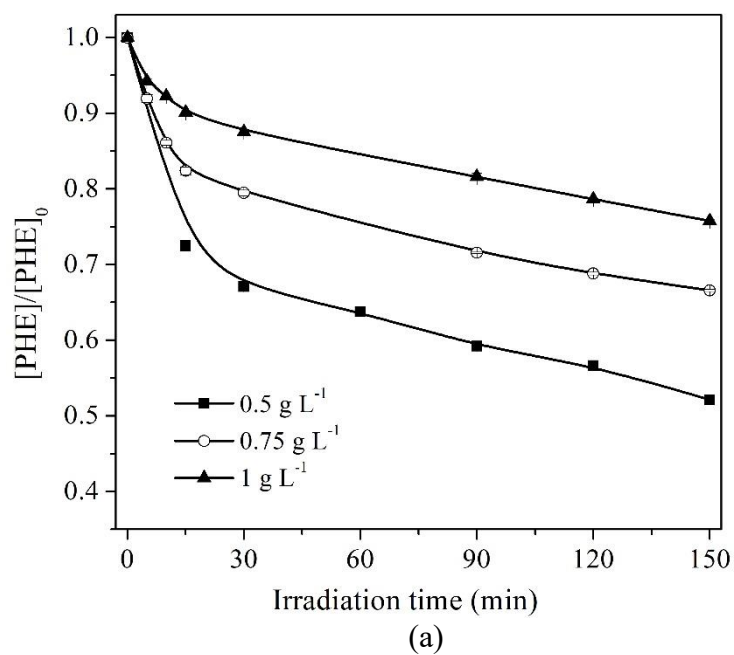


Figure 5-8 Influence of TW80 concentration (a) on photo degradation of PHE and (b) the pseudo first-order rate constants rate constants of PHE oxidation. Initial concentrations: [PHE] = 90 μ M, [PS] = 5 mM, [Fe(III)-EDDS] = 0.5 mM, pH = 3.5 \pm 0.2.

5.3.6 Effect of chloride ions addition

Inorganic species such as chloride ions are widely present in soil, resulting in the

presence of such ions into the effluent of the procedure of soil washing. However, the existence of chloride ions (Cl^-) in wastewater has been reported to affect the degradation efficiency of contaminants during the advanced oxidation processes and more particularly in PS oxidation treatments (Huang et al., 2018b; Zhang et al., 2018). Different roles of chloride ions (Cl^-) are reported in the literature on the efficiency of $\text{SO}_4^{\bullet-}$ and HO^\bullet based oxidations. Generally, it is reported that Cl^- acts as a radical scavenger that substantially inhibits the efficiency of UV based activation of H_2O_2 and $\text{S}_2\text{O}_8^{2-}$ (Tsuneda et al., 2002). However, some researchers find that reactive species produced from chloride ions, chlorine and dichloride radicals ($\text{Cl}^\bullet/\text{Cl}_2^{\bullet-}$), show high selectivity when react with organic pollutants and increase their efficiency of removal (Yang et al., 2014b). Moreover, in other investigations it is suggested that Cl^- could react with $\text{SO}_4^{\bullet-}$ to generate HO^\bullet in circumneutral and alkaline pH (Kiwi et al., 2000). In addition, the involvement of Cl^- is reported to modify the degradation mechanism using $\text{SO}_4^{\bullet-}$ based oxidation processes (Fang et al., 2012). As reported in Figure 5-9, complete removal of PHE was achieved in 150 min of irradiation with 10 mM of Cl^- , while with 50 or 100 mM of Cl^- , the same efficiency could be obtained within 60 min, demonstrating the presences of various dosages of Cl^- remarkably enhanced PHE degradation using Fe(III)-EDDS under UVA irradiation, which was totally distinguished with other studies where Cl^- acted as an inhibitor or where its effect was negligible (Yang et al., 2016). To better understand the mechanism, for the first time, we determined the second order rate constants of $\text{Cl}_2^{\bullet-}$ with PHE ($k_{\text{PHE},\text{Cl}_2^{\bullet-}}$) and TW80 ($k_{\text{TW80},\text{Cl}_2^{\bullet-}}$) respectively at $(4.6 \pm 0.3) \times 10^8 \text{ M}^{-1} \text{ s}^{-1}$ and $(7.1 \pm 0.1) \times 10^6 \text{ M}^{-1} \text{ s}^{-1}$ (Table

5-1). This results suggested that second order rate constant between PHE and dichlorine radical anion ($k_{PHE,Cl_2^{\bullet-}}$) was almost 65 times higher than the one between TW80 and the same radical ($k_{TW80,Cl_2^{\bullet-}}$). Therefore, $Cl_2^{\bullet-}$ generated by Cl^- exhibited much more selectivity to PHE in our soil washing solution. Moreover, the form of kinetics demonstrated that reactivity between $SO_4^{\bullet-}$ and Cl^- played an important role to maintain PHE degradation, especially after 30 min of irradiation.

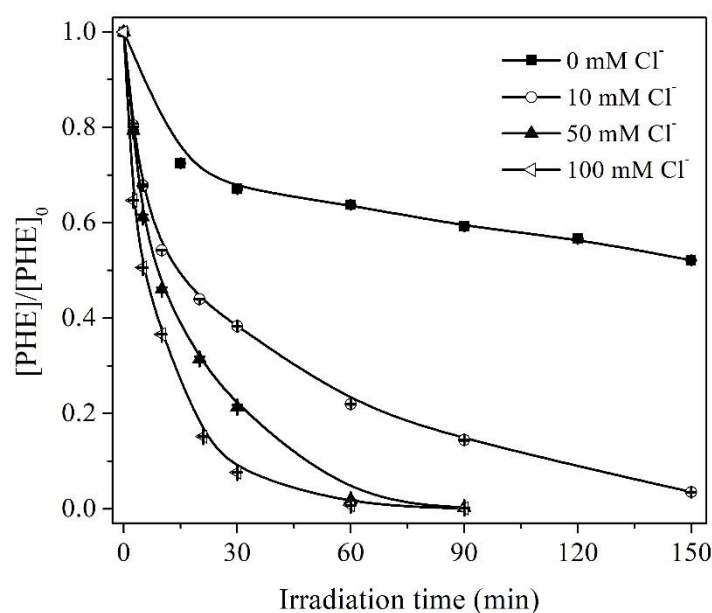


Figure 5-9 Influence of Cl^- concentration for photodegradation of PHE in TW80 aqueous solution. $[PS] = 5 \text{ mM}$, $[Fe(III)\text{-EDDS}] = 5 \text{ mM}$, $[PHE] = 90 \text{ }\mu\text{M}$, $[TW80] = 0.5 \text{ g L}^{-1}$ and $pH = 3.5 \pm 0.2$.

If we simplified our chemical system considering that generated radical species (HO^\bullet , $SO_4^{\bullet-}$, $Cl_2^{\bullet-}$) could react only with TW80 or PHE in solution, it was possible to explain, from a chemical kinetic point of view the impact of chloride on the system efficiency. In fact, in the absence of chloride ions mainly $SO_4^{\bullet-}$ was generated in solution through reaction (5-4) and photolysis of persulfate ions. Considering the concentration of chemical species (i.e. TW80 and PHE) and reactivity constant, about 82% of $SO_4^{\bullet-}$ were

trapped by TW80. However, if we considered that all $\text{SO}_4^{\bullet-}$ was significantly converted into $\text{Cl}_2^{\bullet-}$ (about 90% using 100 mM of Cl^-), in this case, the stronger reactivity between $\text{Cl}_2^{\bullet-}$ and PHE compared to those determined for TW80 suggested that only 6% of $\text{Cl}_2^{\bullet-}$ react with the surfactant and 94% with PHE.

5.3.7 Radical species involvement

In order to clearly clarify the significance of the different radicals formed during the process and their roles in this system, free radicals scavenging tests were carried out. Methanol (MeOH) was employed as scavenger for both HO^{\bullet} ($k_{\text{HO}^{\bullet},\text{MeOH}} = 9.7 \times 10^8 \text{ M}^{-1}\text{s}^{-1}$) and $\text{SO}_4^{\bullet-}$ ($k_{\text{SO}_4^{\bullet-},\text{MeOH}} = 1.0 \times 10^7 \text{ M}^{-1}\text{s}^{-1}$), and tert-butanol (t-But) has higher selectivity for reactivity with HO^{\bullet} ($k_{\text{HO}^{\bullet},\text{t-But}} = 3.1 \times 10^9 \text{ M}^{-1}\text{s}^{-1}$) than with $\text{SO}_4^{\bullet-}$ ($k_{\text{SO}_4^{\bullet-},\text{t-But}} = 8.4 \times 10^5 \text{ M}^{-1}\text{s}^{-1}$) (Buxton et al., 1988b; Neta et al., 1988). As shown in Figure 5-10, with the addition of 50 mM of t-But, PHE oxidation decreased, which revealed that HO^{\bullet} was partially responsible for PHE oxidation. PHE removal was more attenuated with methanol addition indicating that $\text{SO}_4^{\bullet-}$ was also radical species involved in the transformation of PHE. The degradation efficiency of PHE reduced from 48% (without scavenger) to 40% and 23% with t-But and MeOH, respectively.

With the different rate constants and concentrations of chemicals (TW80 and PHE) present in solution, we can deduce that, without scavengers about 18% of photogenerated $\text{SO}_4^{\bullet-}$ and 13% of HO^{\bullet} reacted with PHE. However, i) In the presence of t-But (50 mM), HO^{\bullet} radicals were almost completely trapped, only 0.3% of HO^{\bullet} still reacted on PHE. There was no effect on the percentage of $\text{SO}_4^{\bullet-}$ reacting with PHE. The

addition of t-But resulted in 40% PHE degradation instead of 48%. ii) With the addition of MeOH (50 mM), about 1% of HO[•] and 15% of SO₄^{•-} still reacted with PHE in solution. In this condition PHE concentration decreased by 25%.

As a consequence, in the presence of t-But almost no more HO[•] reacted on PHE and the percentage of PHE degradation decreased by 8%, while with addition of MeOH only 1% of HO[•] and 15% of SO₄^{•-} reacted on PHE and the percentage of PHE degradation decreased by 25%. With these data, we can evaluate that 1% of SO₄^{•-} contributed to 6% of PHE degradation and 1% of HO[•] contributed only to 0.6% of PHE degradation. In another word, SO₄^{•-} radicals contributed 10 times more than the HO[•] for the degradation of PHE in the presence of surfactant TW80. This result was not in agreement with the rate constant which was 1.4 times higher with HO[•] than with SO₄^{•-} (Table 1). Thus, this result highlighted the surrounding environment of the pollutant for the efficiency of the radical species. PHE in surfactant presented an opposite reactivity with HO[•] and SO₄^{•-} if you compared with PHE alone in aqueous solution.

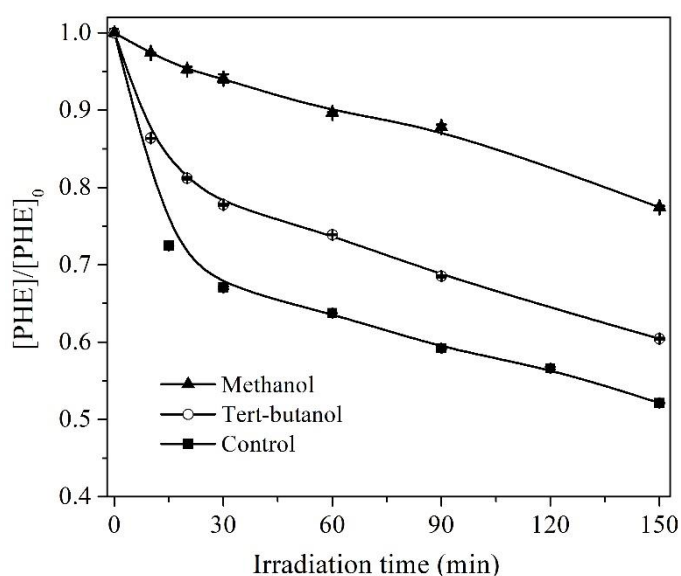


Figure 5-10 Free radical scavenging tests of photo degradation of PHE. Initial conditions: [PS] = 5mM, [Fe(III)-EDDS] = 0.5 mM. [Tert-butanol] = [Methanol] = 50

mM, pH = 3.5 ± 0.2.

5.4 Conclusions

A novel application of Fe(III) complexes was studied to improve the photochemical activation of persulfate for treatments of soil washing effluent. Experimental parameters such as Fe(III)-EDDS, PS and TW80 concentrations exhibited great effects on the PHE photodegradation in this system. The PHE degradation included two stages and the first period of Fe(III)-EDDS decomposition was the rate-limiting step. Quenching experiments proved that $\text{SO}_4^{\bullet-}$ played a more important role than HO^\bullet on PHE degradation more particularly in the presence of surfactant which completely modified the reactivity of radical species. Moreover, we provided the evidence that the presence of chloride ions could significantly improve the PHE removal in this system. The higher selectivity of $\text{Cl}_2^{\bullet-}$ between PHE and TW80 was responsible for the efficiency increase.

References

- Anipsitakis, G.P., Dionysiou, D.D., 2004. Radical generation by the interaction of transition metals with common oxidants. *Environ. Sci. Technol.* 38, 3705-3712.
- Bianco, A., Passananti, M., Deguillaume, L., Mailhot, G., Brigante, M., 2016. Tryptophan and tryptophan-like substances in cloud water: Occurrence and photochemical fate. *Atmos. Environ.* 137, 53-61.
- Bianco, A., Polo-López, M.I., Fernández-Ibáñez, P., Brigante, M., Mailhot, G., 2017. Disinfection of water inoculated with *Enterococcus faecalis* using solar/Fe(III)EDDS- H_2O_2 or $\text{S}_2\text{O}_8^{2-}$ process. *Water Res.* 118, 249-260.
- Brand, N., Mailhot, G., Bolte, M., 1998. Degradation photoinduced by Fe(III): Method of alkylphenol ethoxylates removal in water. *Environ. Sci. Technol.* 32, 2715-2720.
- Buxton, G.V., Greenstock, C.L., Helman, W.P., Ross, A.B., 1988. Critical review of rate

- constants for reactions of hydrated electrons, hydrogen atoms and hydroxyl radicals ($\cdot\text{OH}/\cdot\text{O}^-$) in aqueous solution. *J. Phys. Chem. Ref. Data* 17, 513-886.
- Catastini, C., Rafqah, S., Mailhot, G., Sarakha, M., 2004. Degradation of amitrole by excitation of iron(III) aquacomplexes in aqueous solutions. *J. Photochem. Photobiol., A* 162, 97-103.
- Chen, Y., Wu, F., Lin, Y., Deng, N., Bazhin, N., Glebov, E., 2007. Photodegradation of glyphosate in the ferrioxalate system. *J. Hazard. Mater.* 148, 360-365.
- E., H., A., H., G., B., 1966. Pulsradiolytische untersuchung des radikal anions SO_4^- . *Ber. Bunsenges. Phys. Chem.* 70, 149-154.
- Fang, G.-D., Dionysiou, D.D., Wang, Y., Al-Abed, S.R., Zhou, D.-M., 2012. Sulfate radical-based degradation of polychlorinated biphenyls: Effects of chloride ion and reaction kinetics. *J. Hazard. Mater.* 227-228, 394-401.
- Faust, B.C., Zepp, R.G., 1993. Photochemistry of aqueous iron(III)-polycarboxylate complexes: roles in the chemistry of atmospheric and surface waters. *Environ. Sci. Technol.* 27, 2517-2522.
- Hayon, E., Treinin, A., Wilf, J., 1972. Electronic spectra, photochemistry, and autoxidation mechanism of the sulfite-bisulfite-pyrosulfite systems. SO_2^- , SO_3^- , SO_4^- , and SO_5^- radicals. *Journal of the American Chemical Society* 94, 47-57.
- Huang, W., 2012. Homogeneous and heterogeneous Fenton and photo-Fenton processes : impact of iron complexing agent ethylenediamine-N,N'-disuccinic acid (EDDS). Université Blaise Pascal - Clermont-Ferrand II.
- Huang, W., Bianco, A., Brigante, M., Mailhot, G., 2018. UVA-UVB activation of hydrogen peroxide and persulfate for Advanced Oxidation Processes: Efficiency, mechanism and effect of various water constituents. *J. Hazard. Mater.* 347, 279-287.

- Kiwi, J., Lopez, A., Nadtochenko, V., 2000. Mechanism and kinetics of the OH-radical intervention during Fenton oxidation in the presence of a significant amount of radical scavenger (Cl⁻). *Environ. Sci. Technol.* 34, 2162-2168.
- Krýsová, H., Jirkovský, J.r., Krýsa, J., Mailhot, G., Bolte, M., 2003. Comparative kinetic study of atrazine photodegradation in aqueous Fe(ClO₄)₃ solutions and TiO₂ suspensions. *Applied Catalysis B: Environmental* 40, 1-12.
- Li, J., Mailhot, G., Wu, F., Deng, N., 2010. Photochemical efficiency of Fe(III)-EDDS complex: OH radical production and 17β-estradiol degradation. *J. Photochem. Photobiol., A* 212, 1-7.
- Liang, C., Bruell, C.J., Marley, M.C., Sperry, K.L., 2004. Persulfate oxidation for in situ remediation of TCE. II. Activated by chelated ferrous ion. *Chemosphere* 55, 1225-1233.
- López-Vizcaíno, R., Sáez, C., Cañizares, P., Rodrigo, M.A., 2012. The use of a combined process of surfactant-aided soil washing and coagulation for PAH-contaminated soils treatment. *Sep. Purif. Technol.* 88, 46-51.
- Mailhot, G., Sarakha, M., Lavedrine, B., Cáceres, J., Malato, S., 2002. Fe(III)-solar light induced degradation of diethyl phthalate (DEP) in aqueous solutions. *Chemosphere* 49, 525-532.
- Manenti, D.R., Soares, P.A., Módenes, A.N., Espinoza-Quiñones, F.R., Boaventura, R.A.R., Bergamasco, R., Vilar, V.J.P., 2015. Insights into solar photo-Fenton process using iron(III)–organic ligand complexes applied to real textile wastewater treatment. *Chem. Eng. J.* 266, 203-212.
- Miralles-Cuevas, S., Oller, I., Ruíz-Delgado, A., Cabrera-Reina, A., Cornejo-Ponce, L., Malato, S., 2018. EDDS as complexing agent for enhancing solar advanced oxidation processes in natural water: Effect of iron species and different oxidants.

Journal of Hazardous Materials.

- Mulligan, C.N., Yong, R.N., Gibbs, B.F., 2001. Surfactant-enhanced remediation of contaminated soil: a review. *Eng. Geol.* 60, 371-380.
- Nagaraju, V., Goje, T., Crouch, A.M., 2007. Determination of copper and iron using [S-S']-ethylenediaminedisuccinic acid as a chelating agent in wood pulp by capillary electrophoresis. *Anal. Sci.* 23, 493-496.
- Neta, P., Huie, R.E., Ross, A.B., 1988. Rate constants for reactions of inorganic radicals in aqueous solution. *J. Phys. Chem. Ref. Data* 17, 1027-1284.
- Peng, H., Zhang, W., Liu, L., Lin, K., 2017. Degradation performance and mechanism of decabromodiphenyl ether (BDE209) by ferrous-activated persulfate in spiked soil. *Chem. Eng. J.* 307, 750-755.
- Soriano-Molina, P., Plaza-Bolaños, P., Lorenzo, A., Agüera, A., García Sánchez, J.L., Malato, S., Sánchez Pérez, J.A., 2019. Assessment of solar raceway pond reactors for removal of contaminants of emerging concern by photo-Fenton at circumneutral pH from very different municipal wastewater effluents. *Chemical Engineering Journal* 366, 141-149.
- Trellu, C., Mousset, E., Pechaud, Y., Huguenot, D., van Hullebusch, E.D., Esposito, G., Oturan, M.A., 2016. Removal of hydrophobic organic pollutants from soil washing/flushing solutions: A critical review. *Journal of Hazardous Materials* 306, 149-174.
- Trellu, C., Oturan, N., Pechaud, Y., van Hullebusch, E.D., Esposito, G., Oturan, M.A., 2017. Anodic oxidation of surfactants and organic compounds entrapped in micelles – Selective degradation mechanisms and soil washing solution reuse. *Water Res.* 118, 1-11.
- Tsuneda, S., Ishihara, Y., Hamachi, M., Hirata, A., 2002. Inhibition effect of chlorine

- ion on hydroxyl radical generation in UV-H₂O₂ process. *Water Sci. Technol.* 46, 33-38.
- Usman, M., Faure, P., Hanna, K., Abdelmoula, M., Ruby, C., 2012. Application of magnetite catalyzed chemical oxidation (Fenton-like and persulfate) for the remediation of oil hydrocarbon contamination. *Fuel* 96, 270-276.
- Wacławek, S., Lutze, H.V., Grübel, K., Padil, V.V.T., Černík, M., Dionysiou, D.D., 2017. Chemistry of persulfates in water and wastewater treatment: A review. *Chem. Eng. J.* 330, 44-62.
- Wu, Y., Bianco, A., Brigante, M., Dong, W., de Sainte-Claire, P., Hanna, K., Mailhot, G., 2015. Sulfate radical photogeneration using Fe-EDDS: influence of critical parameters and naturally occurring scavengers. *Environmental science & technology* 49, 14343-14349.
- Wu, Y., Brigante, M., Dong, W., de Sainte-Claire, P., Mailhot, G., 2014. Toward a better understanding of Fe(III)–EDDS photochemistry: Theoretical stability calculation and experimental investigation of 4-tert-butylphenol degradation. *J. Phys. Chem. A* 118, 396-403.
- Wu, Y., Prulho, R., Brigante, M., Dong, W., Hanna, K., Mailhot, G., 2017. Activation of persulfate by Fe (III) species: implications for 4-tert-butylphenol degradation. *Journal of hazardous materials* 322, 380-386.
- Yang, Y., Pignatello, J.J., Ma, J., Mitch, W.A., 2014. Comparison of halide impacts on the efficiency of contaminant degradation by sulfate and hydroxyl radical-based advanced oxidation processes (AOPs). *Environ. Sci. Technol.* 48, 2344-2351.
- Yang, Y., Pignatello, J.J., Ma, J., Mitch, W.A., 2016. Effect of matrix components on UV/H₂O₂ and UV/S₂O₈²⁻ advanced oxidation processes for trace organic degradation in reverse osmosis brines from municipal wastewater reuse facilities.

Water Res. 89, 192-200.

- Yen, C.-H., Chen, K.-F., Kao, C.-M., Liang, S.-H., Chen, T.-Y., 2011. Application of persulfate to remediate petroleum hydrocarbon-contaminated soil: Feasibility and comparison with common oxidants. *J. Hazard. Mater.* 186, 2097-2102.
- Yu, S., Gu, X., Lu, S., Xue, Y., Zhang, X., Xu, M., Qiu, Z., Sui, Q., 2018. Degradation of phenanthrene in aqueous solution by a persulfate/percarbonate system activated with CA chelated-Fe(II). *Chem. Eng. J.* 333, 122-131.
- Zhang, C., Wang, L., Pan, G., Wu, F., Deng, N., Mailhot, G., Mestankova, H., Bolte, M., 2009. Degradation of atrazine photoinduced by Fe(III)–pyruvate complexes in the aqueous solution. *J. Hazard. Mater.* 169, 772-779.
- Zhang, W., Zhou, S., Sun, J., Meng, X., Luo, J., Zhou, D., Crittenden, J., 2018. Impact of chloride ions on UV/H₂O₂ and UV/persulfate advanced oxidation processes. *Environmental science & technology* 52, 7380-7389.
- Zhou, D., Wu, F., Deng, N., 2004. Fe(III)–oxalate complexes induced photooxidation of diethylstilbestrol in water. *Chemosphere* 57, 283-291.

Chapter 6 General conclusion and perspectives

6.1 General conclusion

During this work, UV/H₂O₂, UV/PS, photo-Fenton processes and PS activation using organic ligands chelated Fe(III) complexes were employed to degrade PHE from SW effluents. The results obtained during this thesis concern the degradation efficiency, the optimum operating conditions and the oxidation mechanism.

(1) The UVB based AOPs, e.g., UVB/PS and UVB/H₂O₂, are available for PHE elimination from both mimic and real SW effluents and PHE removal in different systems followed the order of UVB/PS > UVB/H₂O₂ > UVB. The photo-degradation rate and removal efficiency were affected by the concentration of oxidants, initial pH and various coexisting soil inorganic anions (Cl⁻, HCO₃⁻ and NO₃⁻). PHE removal increased almost linearly with increasing H₂O₂ concentration, and PHE decomposition was insignificantly intensified at higher PS loading. PHE degradation rate was negligibly influenced over a wide pH range. The presence of Cl⁻ inhibited PHE oxidation at alkaline pH in UVB/H₂O₂ process, while slightly promoted PHE elimination in UVB/PS process at different pH condition. The presence of HCO₃⁻ exerted negligible effect on PHE removal in the UVB/PS system but negative effect in the UVB/H₂O₂ process. The coexisting of NO₃⁻ retarded PHE degradation in both AOPs. Considering the effectiveness for PHE removal, influence of inorganic ions and energy consumption, the UVB/PS process is much more efficient and economically suitable than UVB/H₂O₂ for treatment of SW effluents.

(2) Fe(III)-CA employed photo-Fenton process strongly intensified PHE oxidation than traditional photo-Fenton for oxidizing PHE from mimic SW solution. CA ligand used for Fe(III) complexation was more efficient for PHE oxidation than EDDS, EDTA and NTA chelated complexes. Parameters of Fe(III)/CA ratio, Fe(III)-CA dose, H₂O₂ concentration exhibited different effect on PHE degradation profile and removal. The

optimal conditions to achieve best PHE degradation efficacy were Fe(III)/CA ratio of 1:1, Fe(III)-CA concentration of 0.5 mM and H₂O₂ dosage of 20 mM and pH at 4.5. The HO[•] was dominantly responsible for PHE oxidation though O₂^{•-} was also involved in the photo-Fenton processes.

(3) The Fe(III)-EDDS complex was efficient to activate PS under simulated solar light over a wide pH range from 3.0-8.5 for generation SO₄^{•-} and HO[•] for PHE decomposition in SW solutions with TW80. PHE oxidation was mainly affected by Fe(III)-EDDS concentration, PS concentration, TW80 concentration. The addition of chloride obviously enhanced PHE since the second order rate constants between corresponding Cl₂^{•-} and PHE was determined to be 65 times higher than that with TW80. Quenching experiments proved that SO₄^{•-} was more selective and played a more important role on PHE degradation than HO[•] in the presence of TW80 which was confirmed by the results of second order rate constants determination tests.

These 3 chapters demonstrated that AOP's can be use and efficient for SW effluent treatment. One important conclusion is that sulfate radicals, due to their greater selectivity towards organic compounds, are more suitable to provide effective process for the treatment of SW effluent.

6.2 Perspectives

Further studies can be developed, to complete this study, as follows:

(1) Finding out suitable methods to detect the intermediate products of PHE in the presence of surfactant and obtain the degradation pathway of PHE;

(2) The composition of SW solution is complex, except for the influence of inorganic ions, the effect of metal ion species, organic matters on PHE degradation and the interaction effects should be investigated in the future.

(3) Soil pollutants are toxic, further attention can be payed to the toxicity evolution

of SW effluents before and after treatment.

(4) Investigations are mainly focused on PHE removal for treatment of mimic SW solutions without studying the recovery of surfactant at the same time. The recovery and reuse of surfactant is important to save cost for the whole remediation processes. In the future, PHE degradation and also recovery and reusing of surfactant should be considered in actual SW effluent treatment.

Publications

- [1] **Yufang Tao**, Marcello Brigante, Hui Zhang, Gilles Mailhot, Phenanthrene degradation using Fe(III)-EDDS photoactivation under simulated solar light: A model for soil washing effluent treatment. Chemosphere, 236 (2019) 124366.
- [2] **Yufang Tao**, Olivier Monfort, Marcello Brigante, Hui Zhang, Gilles Mailhot, Phenanthrene decomposition in soil washing effluents using UVB activation of hydrogen peroxide and peroxydisulfate. Chemosphere, 263 (2021) 127996.